Abstract

Study of $p\bar{p}$ Collisions That Contain Leptons, a Photon and a b-quark Using The CDF II Detector

Ben Auerbach
2011

We present a search for anomalous production of the signature lepton + photon + b-quark + missing transverse energy ($\ell\gamma \not\!\!E_T b$) produced in $p\bar{p}$ collisions at $\sqrt{s} = 1.96$ TeV using 6.0 fb^{-1} of data taken with the CDF detector in Run II at the Tevatron. In addition to this signature-based search, we present a closely-related search for top pair production with an additional radiated photon, $t\bar{t}\gamma$. We find 85 $\ell\gamma \not\!\!E_T b$ events versus an expectation of 99.1 ± 9.3 events. High-statistics control samples are used to evaluate a low-energy photon χ^2 cut. Additionally requiring the events to contain at least three jets, have a total transverse energy of 200 GeV, and that the photon candidate passes the χ^2 cut, we observe 30 $t\bar{t}\gamma$ candidate events versus an expectation from non-top Standard Model (SM) sources of 13.0 ± 2.1 Assuming the difference between the observed number and the predicted non-top SM total is due to top production, we measure the $t\bar{t}\gamma$ cross section to be 0.18 ± 0.08 pb. We also measure the ratio of the $t\bar{t}\gamma$ cross section to the $t\bar{t}$ cross section to be 0.024 ± 0.009, which compares well with a SM prediction of 0.024 ± 0.013

Study of $p\bar{p}$ Collisions That Contain Leptons, a Photon and a b-quark Using The CDF II Detector

A Dissertation
Presented to the Faculty of the Graduate School
of
Yale University
in Candidacy for the Degree of
Doctor of Philosophy

by
Ben Auerbach

Dissertation Director: Paul Tipton

February 2011

Contents

List of Figures

List of Tables

1 Introduction and Theoretical Motivation

Nearly every object around us is made up of three basic building blocks: the proton, the neutron, and the electron. However, in the course of experimentation, it has been shown that protons and neutrons themselves are made up of even more basic components called quarks. Electrons, as far as we know, are fundamental objects. In the study of particle physics, we study the most fundamental particles and the ways in which they interact.

The interactions of all fundamental objects are mediated by particles that carry one of the four forces: gravity, electromagnetism, weak, and strong. A complete theory of particle physics would describe these forces and how the most basic objects interact with each otherup to any energy level.

Currently there is a deficiency in our theoretical understanding of particle physics. At high energies, the forces of electromagnetism and the weak force become indistinguishable, but at lower energies these two forces are distinct. The mechanism behind this higher-energy symmetry, and lower-energy broken symmetry is an open question in physics, but the standard theoretical mechanism is the Higgs field, and the resulting Higgs boson. The Higgs field couples most strongly to massive objects, so studying the properties of the most massive observed object, the top quark, can be an indirect probe of the Higgs field.

This thesis analyzes the associated production of a photon and top quarks in order to probe the mechanism by which the electroweak symmetry is broken. A significant difference between theoretical predictions of this process and those observed in data could point to a new physics mechanism.

We will discuss the above mentioned particles, symmetries, and the Higgs field in more detail in a few sections, but it is necessary to lay some groundwork before we continue. We will start by explaining the theory that explains the interactions of the most basic building blocks of matter the Standard Model of Particle Physics.

1.1 The Standard Model

Protons and neutrons are actually not fundamental. They are composed of up and down quarks, and held together by gluons.

Gluons are a force-carrier for the strong force and these objects "glue" up and down quarks together inside protons and neutrons. Through careful experimentation, scientists have found that the universe we reside in has many different particles, and that the up and down quarks have additional members in their class: the top, bottom, strange, and charm quarks [1, 2, 3, 4].

Moreover, electrons are a member of a class of object called leptons. In addition to electrons, our universe has two additional charged and more-massive leptons, the muon and the tau.

These massive leptons can interact with a $W^{\pm}$ boson, and produce a neutrino; each charged massive lepton has a corresponding neutrino. The neutrino is also a lepton, but it has no charge. There is evidence suggesting that neutrinos have a very small mass [5]. There is a boson related to the W bosons that is neutral in charge, and this is the Z boson. These bosons collectively carry the weak force. The quarks also interact with the $W^{\pm}$ and Z bosons, which play a vital role in explaining nuclear reactions.

Finally there is the photon, γ, which is required for us to see the objects around us. It interacts with all charged objects to mediate the force of electromagnetism. To complete the picture, each of the quarks and leptons has a corresponding anti-particle. This sums up all the fundamental objects in particle physics that have been observed so far, and all of their interactions, are explained by the Standard Model, except for gravity.

The ways in which each of the fundamental particles interact with each other is described to extraordinary precision by the Standard Model (SM) [6] of Particle Physics. In Figure 1.1, we can see the theoretical predictions and measurements of production cross section rates in proton antiproton collisions for many physics processes; the theory and experiment are in very good agreement.

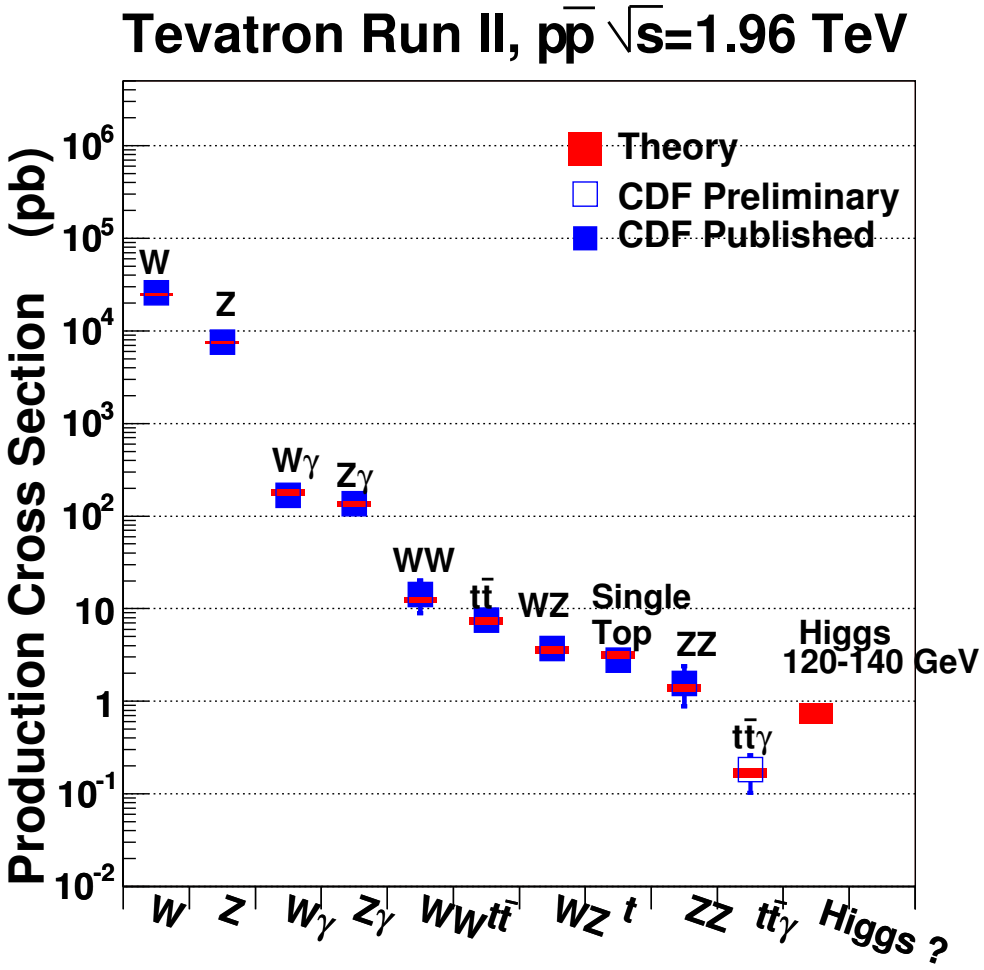

Figure 1.1: Theoretical predictions and experimental measurements of SM cross sectionss. Experimentalists have seen excellent agreement with SM theoretical predictions, through many orders of magnitude.

The SM describes interactions of fermions (spin-$\frac{1}{2}$ objects) with the force carrying bosons (integer spin). These fermions are further subdivided into two classes, leptons, and quarks. The lepton generations are grouped with a charged lepton and an uncharged neutrino. Quark generations group pairs of quarks together, up with down, charm with strange, and top with bottom. They are organized in a doublet structure:

$$\begin{pmatrix} u \\ d \end{pmatrix} \begin{pmatrix} c \\ s \end{pmatrix} \begin{pmatrix} t \\ b \end{pmatrix}$$

These quark generations have corresponding charges of $\frac{-1}{3}e$ and $\frac{2}{3}e$, where e is the charge of the electron. Both the quarks and the leptons interact with the electroweak bosons, $W^{\pm}$, Z, and γ. However to interact with the photon, the fermion must be charged, so the neutrino has no direct interaction with the photon. The quarks have an additional quantum number, called color, and their interactions are dictated by quantum-chromodynamics (QCD) [7].

The SM is built on top of a $SU(3)_c \otimes SU(2)_L \otimes U(1)_Y$ group structure. The subscripts in the group structure refer to quantum numbers of the fields, "c" is color, "L" is left-handed, and "Y" is the field's hypercharge.

One of the principles of the SM is local gauge invariance, which means an infinitesimal phase rotation with one of those group's operators should result in no change to the predictions. We also know, at higher energies the forces of electromagnetism and the weak interactions are indistinguishable. The blending of these two forces is called electroweak unification.

The SM is only validated up to the energy regime that has been probed by physicists, and nearly all of the fundamental forces are incorporated. The lone exception is the gravitational force, which does not yet have an observed force carrying boson. A complete theory of particle physics would incorporate gravity, and would explain all interactions up to any arbitrary energy.

As we increase the energies of collisions we observe, we hope to see a breakdown of the SM in the hopes of seeing a new particle, gaining a better understanding of the SM, or seeing possible extensions to it. Many corresponding discoveries of a fundamental particle have occurred at experiments performed using larger and larger amounts of energy. A heuristic for this comes from Einstein's famous $E = mc^2$ equation. Many of the objects discovered later are more massive, and thus require higher threshold energy to be created.

The symmetry of $SU(2)_L$, the group responsible for the weak-force bosons $W^{\pm}$, and Z, has been broken. In the unbroken symmetry SU(2), these bosons are required to be massless, otherwise it violates gauge invariance. However both of the bosons have been observed to be massive. This is referred to in particle physics as a broken

symmetry, and because of this there should be a massive particle responsible.

The explanation for the W and Z bosons' mass, and description of its properties have taken many shapes and sizes; perhaps the most well-known of which is the Higgs field and Higgs boson.

1.2 The Higgs Boson

To introduce the Higgs boson, we begin by supposing the electromagnetic and weak fields have retained the symmetry of $\mathrm{SU}(2) \otimes \mathrm{U}(1)$. That is to say, we are going to think of the W, Z, and the photon as inter-related massless bosons, as required by local gauge invariance.

The Lagrangian of a theory explains how the fields will interact. At this point we introduce additional field terms to the Lagrangian of this symmetric $\mathrm{SU}(2) \otimes \mathrm{U}(1)$ theory that interact with these bosons under a gauge transformation, and show it is possible to generate mass in such a way that local gauge invariance is preserved.

The Higgs field is a scalar doublet that interacts with the massless gauge bosons of the electroweak force. In addition to this SM we add a complex scalar doublet field, ϕ, that interacts with the massless bosons of the electroweak forces. The Lagrangian that describes the interactions of the field ϕ has terms that look like:

$$\mathcal{L} = (D^{\mu}\phi)^{\dagger}(D_{\mu}\phi) + \mu^2\phi^*\phi - \lambda(\phi^*\phi)^2. \tag{1.1}$$

In this equation we have the covariant derivative, D^{μ}, and the constants μ, and λ are not known, but $\mu^2 > 0$, and $\lambda > 0$. Furthermore, $D^{\mu} = \partial^{\mu} + igA^{a\mu}\tau^a + \frac{ig'}{2}B^{\mu}$. In these definitions, g is a coupling of the SU(2) gauge fields ($A^{a\mu}$) to the ϕ field and g' is the coupling of the U(1) gauge fields (B^{μ}) to the ϕ field, and τ^a is an infinitesimal generator of the SU(2) group.

With a little bit of work we can see that the minimum of Eq. 1.1 does not occur at zero, but at $|\phi| = \sqrt{\mu^2/2\lambda} \equiv v/\sqrt{2}$. Mathematically, this says that the ground state of the vacuum does not occur at $\phi = 0$, but instead is at a point $\phi = v/\sqrt{2}$; this is called the vacuum expectation value. The non-zero vacuum expectation value

means that there is always some amount of Higgs field present.

If we attempt to write out the terms around a perturbation about this minimum, with

$$\phi(x) = \begin{pmatrix} 0 \\ \frac{v}{\sqrt{2}} \end{pmatrix}$$

then there is a change in the Lagrangian in the derivative terms that looks like:

$$\Delta\mathcal{L} = \frac{1}{2}\frac{v^2}{4}\left(g^2(A_\mu^1)^2 + g^2(A_\mu^2)^2 + (g'B_\mu - gA_\mu^3)^2\right). \tag{1.2}$$

We then make the substitution that $W_\mu^\pm = \frac{1}{\sqrt{2}}(A_\mu^1 \mp iA_\mu^2)$, and $Z_\mu^0 = \frac{1}{\sqrt{g^2+g'^2}}\left(-gA_\mu^3 + g'B_\mu\right)$, and the photon field, $\tilde{A}_\mu = \frac{1}{\sqrt{g^2+g'^2}}\left(g'A_\mu^3 + gB_\mu\right)$, in Eq. 1.2. We know from field theory that when we have a term proportional to the square of the field, that this is the mass of the field. Substituting

$$M_W = g\frac{v}{2},\ M_Z = \sqrt{g^2+g'^2}\frac{v}{2}$$

into the equation above we find terms that look like $M_W^2(W^+)^2$, $M_W^2(W^-)^2$, and $M_Z^2(Z^0)^2$. This shows that assuming there is a Higgs mechanism, we are able to break the $SU(2)\otimes U(1)$ symmetry, and produce the correct masses for the photon, and the W and Z bosons, all while maintaining gauge invariance.

The values of g, g′, and v, have all been measured to spectacular precision through measurements on the muon decay lifetime, and the measurements of the mass of the W and Z bosons. These measurements directly indicate that v = 246 GeV.

The Higgs field is a complex scalar doublet, which has four degrees of freedom; two of these degrees of freedoms are required to give mass to the W bosons, and one is required to give mass to the Z boson, which leaves one degree of freedom, this is the elusive Higgs boson. Accepting the Higgs field as the explanation of electroweak symmetry breaking requires the existence of an uncharged spin-0 boson, the Higgs boson, whose existence has not yet been confirmed.

Through machinations similar to those above, the Higgs field also couples to the fields of the quarks, and leptons. The coupling strength of these fields to the Higgs field is then proportional to the observed masses of the leptons and the quarks. This explains the large difference between the masses of each of the quarks, and leptons. Moreover the coupling strengths of the Higgs field to all objects in the SM are proportional to the mass of the objects. Thus the top quark, the heaviest observed quark, should couple very strongly to the Higgs field.

It would be nice if this were the end of the story, however all is not well with this theory. If we expand about the minimum of the Higgs field, so that v$\rightarrow$ v+ h(x), where h(x) is the field of the Higgs Boson, there are terms that arise in Eq. 1.1, that are proportional to h^2, h^3, and h^4. This implies that at very high energies, the Higgs boson will interact with itself. This provides some constraints on the upper bound on the mass of the Higgs [8].

The Higgs field theory does an excellent job of explaining the breaking of the electromagnetic and weak field symmetry. Other candidate theories, with similar symmetry breaking mechanisms, are now becoming popular for their ability to explain other physical phenomena, such as dark matter.

Dark matter is invisible to the naked eye and telescopes. It does not interact with light in the universe and its presence is only known because of how its gravitational pull affects other objects. Currently there is nothing in the Standard Model that could be the fundamental particle of dark matter.

Other candidate theories for physics beyond the SM include a class of model called supersymmetry (SUSY). SUSY is an attractive theory as it encompasses the Higgs mechanism, deals with the divergences of the Higgs field, and as a bonus has objects which could explain dark matter in the universe. The structure of SUSY introduces a partner particle (super-partner) for each observed SM particle. If the SM particle was a fermion, its super-partner is a boson. The super-partner structure is able to cancel out divergences due to the Higgs field's self-interaction.

Another intriguing aspect of SUSY is that it has a Lightest Supersymmetric Particle (LSP). The LSP in SUSY is stable and does not decay to any other particle.

This particle could then be the fundamental particle that makes up dark matter in the universe.

There are particles and phenomena of the SM we can study that can yield much insight into what sort of new physics there might be. Searching for a signature that is predicted to have only a few total events could allow a window to see rare, and possibly new, physics events.

We search the SM looking for the top quark and requiring a photon. Hoping that something outside of the SM decays to these objects. The rate that these events are produced is small. The top quark may be able to shed some light on just what might be out there. Of all the observed particles it should couple the most strongly to the Higgs boson.

1.3 Top Quark Phenomenology

To date, the top quark is the most massive of all the fundamental particles, and at 173 GeV [9] is nearly as massive as a gold atom. Although it was discovered more than 15 years ago, many of its properties such as its coupling to the photon are not very well known.

The top quark is the only quark that decays before hadronization. So far, this is the only bare quark that we can study. In events with top quark pairs, each top quark decays almost exclusively to a W boson and a b quark. The W boson is capable of decaying to an electron, muon, or tau lepton and associated neutrino, or to quark pairs. The easiest events to identify are those where at least one of the W bosons decays to an electron or muon, and corresponding neutrino. When this occurs, we are able to identify the lepton, and the neutrino escapes the detector undetected.

The neutrino's presence is made known by a significant imbalance in transverse energy. From conservation of momentum, the total momentum moving perpendicular to the incoming proton-antiproton beams should be zero. If, after summing up all of the transverse momentum in the detector, there appears to be a large amount missing we are confident in saying this is due to a neutrino.

An example of a $t\bar{t}$ event is shown in Figure 1.2. It is called a semileptonic $t\bar{t}$ decay because only one of the W bosons decays leptonically. In a dileptonic decay, both W bosons decay to leptons, and in a hadronic decay both W bosons decay to pairs of quarks.

When top quark pairs are produced, many charged objects are involved such as: the incoming quarks, the top quarks themselves, the W bosons, the leptons from the W decay, and also final state quarks. Each of these objects can produce a photon that can be identified by the detector. These events are called radiative top decays, or $t\bar{t}\gamma$ events. Events from $t\bar{t}\gamma$ decays are remarkably similar to the non-radiative pair production, the exception is of course the photon. A photon in a $t\bar{t}\gamma$ event at the Tevatron is most likely to occur from one of the initial state quarks radiating off a photon.

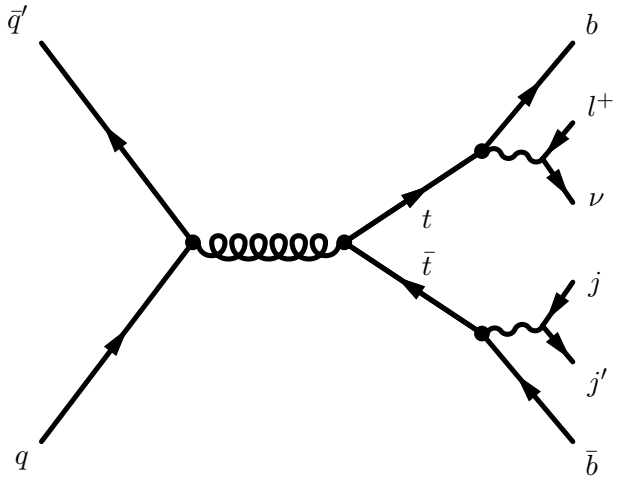

Figure 1.2: Tree level diagram for quark-antiquark annihilation producing $t\bar{t}$. In this diagram one of the W bosons decays to a lepton and a neutrino, while the other decays to a pair of jets; this is called a semileptonic decay. It is also possible for both W bosons to decay to leptons in a dileptonic decay. In a hadronic decay both W bosons decay to a pair of jets.

Production of $t\bar{t}\gamma$ could be used as a tool to further measure the $tt\gamma$ coupling [10]. The $t\bar{t}\gamma$ search will also serve as a probe of the charge of the top quark [11], and as a control sample for $t\bar{t}$+Higgs production at the LHC. The ratio between the $t\bar{t}\gamma$ production cross section, and the $t\bar{t}$ cross section will serve as a test of the SM,

and the measurement can help the LHC and their search for Higgs $\rightarrow t\bar{t}$. Furthermore the $t\bar{t}\gamma$ signature should be the first associated electroweak boson with top pair production to be observed at the LHC.

1.4 Signature-Based Searches

There are compelling arguments that there is something missing from our observed particle zoo of the SM. At this point, it is widely believed that there is some sort of physics that has not yet been observed. Unfortunately this also means that we do not know in what direction we should be looking. There are many candidate theories out there and we cannot currently test all of them so we constrain ourselves to a particular signature.

A signature-based search involves a collection of objects, and kinematic selection criteria on these objects; this group of objects makes up the signature. We predict the amount of events we should see according to the SM. We then check for consistency between what we observe in data, and our predictions.

For our search for new physics, we are using a signature-based search. Given the unknown nature of potential new physics, it is good to expect the unexpected, and look for significant deviations from the SM. We will be looking for events that should dominantly involve the top quark and a photon.

This signature is appealing because if there is something else outside the SM accessible at the Tevatron, it is likely that it will be heavier than the top quark, and might prefer to decay to this quark. Also if this object is charged, there is a possibility of a radiated photon. The top quark decays almost exclusively to a bottom quark and a W boson. The bottom quarks are very useful to particle physics searches as they will hadronize, and travel for small distances before decaying. In CDF this appears as a secondary vertex: a point with additional decays displaced from the proton antiproton interaction point. We rely on one of the W bosons to decay to leptons which will produce either an electron or muon that we can detect, and a corresponding neutrino which we detect as energy missing in the transverse direction.

The W bosons are also capable of decaying to taus as well as the previously mentioned electrons (or muons) and neutrinos, however it is very difficult to identify tau leptons at the Tevatron. As such for the remainder of this thesis when we mention identifying leptons, we are only talking about electrons and muons.

In this thesis we present a search for anomalous production of events with a high-p_T lepton (electron, e or muon, μ), photon (γ), jet tagged as containing b-meson (b-jet), and missing transverse energy ($\not\!\!E_T$), ($\ell\gamma\not\!\!E_T b$ events). We will call events satisfying these selection criteria $\ell\gamma\not\!\!E_T b$ signal events. This search is an improvement of a previous analysis, described in detail in Ref. [12].

The $\ell\gamma\not\!\!E_T b$ signature is possible [10] in different models beyond the SM, such as gauge-mediated Supersymmetry (SUSY) models [13]. The signature has known SM backgrounds.This search is related to the $\ell\gamma + X$ search [14], but with a b-tag requirement in addition to lower photon E_T, lepton p_T and $\not\!\!E_T$ requirements. Small SM backgrounds are expected in this signature which should give us a chance to see statistically anomalous events outside of the SM expectations.

The largest SM source of events in the $\ell\gamma\not\!\!E_T b$ signal sample is the production of top pairs with an additional photon, $t\bar{t}\gamma$. We focus in on $t\bar{t}\gamma$ from the $\ell\gamma\not\!\!E_T b$ signature-based search, by using additional cuts (large H_T and 3-or-more jets) so that radiative top-pair events dominate the SM predictions.

There have been previous attempts to measure the cross section of the $t\bar{t}\gamma$ process [12], however a precision measurement of both the $t\bar{t}\gamma$ cross section, and the ratio of the $t\bar{t}\gamma$ cross section to the $t\bar{t}$ cross section has not yet been performed. We attempt to be the first to measure this ratio, which should be more precise than the $t\bar{t}\gamma$ cross-section measurement, due to the cancellation of many systematic uncertainties.

1.5 Outline of the Thesis

We begin in the next section (Sec. 2) describing our detector, its geometry, and how we are able to measure and identify particles and their properties.

Sections 3.1, 3.2, 3.3, and 3.4 explain our selection criteria for muons, electrons,

photons, and jets identified as having heavy flavor, respectively. In Sections 3.5.1, and 3.5.2 we define and describe the calculation of $\not\!\!E_{\rm T}$ and the sum of the transverse energies of the leptons, photons, jets, and $\not\!\!E_{\rm T}$ ($H_{\rm T}$).

In Section 3.6 we discuss the full selection of our signal samples for our $\ell\gamma\not\!\!E_{\rm T}b$, $t\bar{t}\gamma$ and $t\bar{t}$ events, and we discuss the triggers we use to identify events we may be interested in. We further explain the datasets that we use for this analysis. Each of these types of events has a selection criteria, and those events which pass the criteria are accepted in the signal sample.

To model the SM contributions to the $\ell\gamma\not\!\!E_{\rm T}b$, $t\bar{t}\gamma$, and $t\bar{t}$ signal samples we use Monte Carlo computer simulations of SM processes. Descriptions of the samples and how we normalize them to our luminosity, are described in Section 4.

In Sections 5 and 6, we describe how we calculate the event yield from "fakes", backgrounds from SM processes which can mimic one of our signatures via one or more objects being misidentified.

To verify our object identification and to check our data-driven background measurements we examine the control samples of a lepton, photon, and $\not\!\!E_{\rm T}$ ($\ell\gamma\not\!\!E_{\rm T}$), a dilepton, and photon sample ($\ell\ell\gamma$), and a sample with a lepton, $\not\!\!E_{\rm T}$, 3-or-more jets, and significant transverse energy (pretagged $t\bar{t}$). The pretagged adjective is referring to the sample before requiring the identification of a b-tagged jet; the identification process is called "tagging." All of these samples are described in Section 7.

Using some of the control samples we mention above, we motivate an additional selection criterion to distinguish real photons from misidentified photons and describe this in Section 8.

We discuss each of the systematic uncertainties on our measurement in Section 9, and in Section 10.2 we present a diagram showing what a $t\bar{t}\gamma$ signal decay looks like in the detector.

We show in Section 10 the comparison between predicted and observed event yields in 6.0 fb^{-1}. Using these results we show the calculation of the measured $t\bar{t}\gamma$ cross section in Section 11, and present a measurement of the ratio of the production cross sections of $t\bar{t}\gamma$ and $t\bar{t}$.

2 Detector Description

One of the most important parts in the study of physics is to have a working understanding of the tools of the experiment. For particle physics experiments this includes: the accelerators, the beams, and perhaps most important of all, the detector.

We describe below how Fermilab creates and accelerates its proton and antiproton beams and collides them at a fixed point in the Collider Detector Facility detector.

2.1 The Tevatron

Fermilab uses a series of accelerators to create its 980 GeV particle beams. The beams begin as H^- ions created from the ionization of hydrogen gas, and are accelerated to 750 KeV in the Cockcroft-Walton pre-accelerator. The ions then enter a linear accelerator (LINAC) where they are accelerated up to 400 MeV. The acceleration in the LINAC occurs in a series of "kicks" from Radio Frequency (RF) cavities. The RF cavities also separate the ions into bunches. At the end of the LINAC the hydrogen ions pass through a carbon foil which strips the hydrogen ions of their electrons, leaving bare protons (p). The protons are then injected into the Booster, a circular synchrotron. The protons travel around the Booster to a final energy of 8 GeV.

Protons are then emptied from the Booster into the Main Injector, where they are further accelerated from 8 GeV to 150 GeV before being injected into the Tevatron. The Main Injector also produces 120 GeV protons which are extracted, and then sent down a transfer line until they collide with a nickel target. These collisions produce many secondary particles including antiprotons ($\bar{p}$). Studies have shown that 120 GeV is the optimal energy for antiproton production. In these collisions, about 20 $\bar{p}$ are created per one million protons.

The $\bar{p}$ are then sent to the Accumulator. The Accumulator is a long term $\bar{p}$ storage ring which is capable of storing $\bar{p}$ with minimal losses for days. When

the Accumulator reaches optimum capacity, they are sent to the Main Injector and accelerated to 150 GeV.

In the final step, the p and $\bar{p}$ are injected into the Tevatron. The Tevatron is a 1 km in radius synchrotron that accelerates both protons and antiprotons from 150 GeV to 980 GeV. Both protons and antiprotons are counter rotating in the same beam pipe; there is a large electro-static field which keeps the two beams from touching except at the collision points. The beam is steered by 774 super-conducting dipole magnets and 240 quadrupole magnets.

The Tevatron holds 36 bunches each of protons and antiprotons. The protons are added one bunch at a time, and the antiprotons are loaded 4 bunches at a time. The bunches move at 150 GeV from the Main Injector into the Tevatron. RF cavities then accelerate the bunches to 980 GeV. The bunches are now beams of protons and antiprotons, and then some electrostatic fields are reversed causing the protons and antiprotons to collide at two points. Each interaction point lies at the heart of the two particle detectors, D0 (named for the position in the Tevatron ring) and the Collider Detector Facility (CDF). A cartoon of the entire process can be seen in Figure 2.1.

2.2 The Collider Detector at Fermilab and its Geometry

The Collider Detector at Fermilab (CDF) is a cylindrically-symmetric detector designed to study a wide range of physics at the Tevatron. The detector is made up of layers of sub-detectors, with silicon layers near the collision point, and additional detector subsystems layered on top of one another with increasing radial distances.

CDF uses a right-handed coordinate system, with the z-axis pointing in a tangent to the ring of the Tevatron, and aligned with the direction of the proton beam trajectory. The x-axis points out along a radius of the Tevatron; it is parallel to the ground and it is perpendicular to the z-axis. The y-axis is the final component in the right handed coordinate system, and points up. The polar angle, θ = arccos(z/r), where r = $\sqrt{x^2 + y^2}$. The azimuthal angle, ϕ = arctan(y/x), and the pseudo-rapidity, η, is defined as, η = - log [tan ($\frac{\theta}{2}$)]. When we speak of the transverse direc-

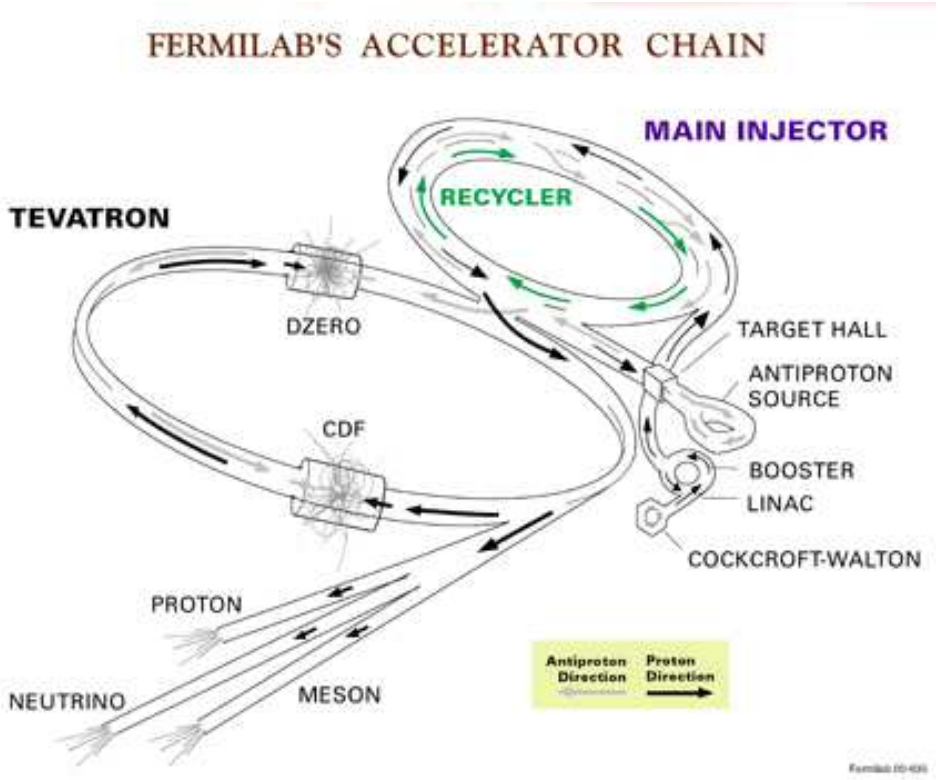

Figure 2.1: Cartoon of Fermilab's proton and antiproton accelerators

tion, we are describing a vector which points in the local r-direction. Occasionally, we will mention using cones of a certain radius, R. The value $R = \sqrt{(\Delta\eta)^2 + (\Delta\phi)^2}$, and the cone is defined by R and the origin of the coordinate system.

The identification of particles, and the resolution of the detector are two critical aspects for our detector. For identifying electrons, muons, and photons, we must understand both their efficiencies and fake-rates. For these objects, in the central region, tracking is essential. For charged electrons, and muons, we expect to see tracks associated with these objects, and we also expect no track for a photon. Along with being able to correctly identify particles, we must also understand their kinematics.

To accurately measure the momentum and energy of the particles we need to have good timing and position resolution throughout the detector. Interactions in the detector are timed from the collision point up to each detector interaction point. Each interaction in the detector yields a position measurement as well. Putting these

pieces of data together and we can reconstruct a particle's momentum and energy.

The energy scale and its resolution is well understood in the calorimeters. Resolving the different tracks from many different objects in the detector is important in the identification of secondary vertices which tend to occur in the decays of B hadrons. Understanding the energy scale gives us a higher confidence in measuring the kinematic properties of the identified particles.

The following sections describe the subsystems used to identify particles.

2.3 Tracking System

The tracking system of CDF is used to reconstruct the trajectory of charged particles. The trajectory of charged particles moving through the detector gives valuable information about the decay products from a collision. The tracking system is very close to the interaction point to help distinguish many different particles.

A secondary vertex comes from B hadrons, which while not stable, can travel on average several millimeters before decaying, and the tracking system is able to measured this displacement. CDF has two tracking systems: an open-cell wire drift chamber, and the silicon systems.

Both systems are located in a 1.4 Tesla uniform magnetic field pointing along the z-axis, created by a superconducting solenoid 5 m in length, and a radius of 1.5 m. Charged particles in a magnetic field will follow a helical trajectory; the curvature of these tracks are used for charge identification, and for transverse momentum (p_T) measurements.

The silicon system, is made of three subcomponents. From smallest radius to largest they are: Layer 00 (L00), the Silicon Vertex Detector (SVX), and the Intermediate Silicon Layer (ISL). The silicon systems are one-, or two-sided semiconductors with p-strips mounted in n bulk material. As charged objects move through the detector, ionization occurs and the charge can be read out from the strips.

L00 [15] is a single layer of radiation-hard silicon mounted directly on the beam pipe (r = 1.6 cm) see Figure 2.2, and provides only axial tracking information

only. It was largely designed to help recover impact parameter functionality due to degradations in the SVX detector. The systems have an implant pitch of 25 μm, and the strips are each 8 μm wide.

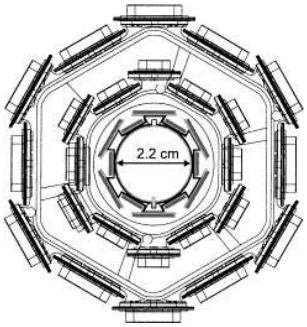

Figure 2.2: An artist's rendition of L00 and SVX. We can see that L00 is mounted directly on the beam pipe. The outer two layers of silicon detectors are part of SVX

The second subsystem, SVX [16], contains 5 layers of double-sided silicon. It reaches from r = 2.44 cm to r =10.6 cm away from the beamline. One side of each wafer of silicon in the SVX is able to make measurements in the r-ϕ plane. The other side of the wafers in the first, third, and fifth layer, make stereo measurements in the z-ϕ plane, and the second and fourth layers contain small stereo angle strips pitched 1.2° away from the strips to make axial measurements. The SVX is divided into 12 identical wedges equally spaced in ϕ, and three barrel shaped segments in z. The strip pitch is 60-65 μm for axial strips, 58-60 μm for the small stereo angle strips, and 125-145 μm for 90° stereo angle strips. Figure 2.3 is an artist's rendition of the SVX system.

The ISL [17] is divided into 5 barrel-shaped segments and has two double-sided layers and is located at radii 20-29 cm. One side of the ISL contains strips making axial measurements, while the opposite sides make small angle (1.2°) stereo measurements. Both sides have a pitch of 112 μm.

The Central Outer Tracker (COT) [18] is an open-cell drift chamber with 2520 cells organized into eight superlayers, lying outside of the silicon systems and with a radius extending to 137 cm. A superlayer is a group of cells which are all at the same radius in the COT. Each cell has a total of 12 sense wires and 13 potential

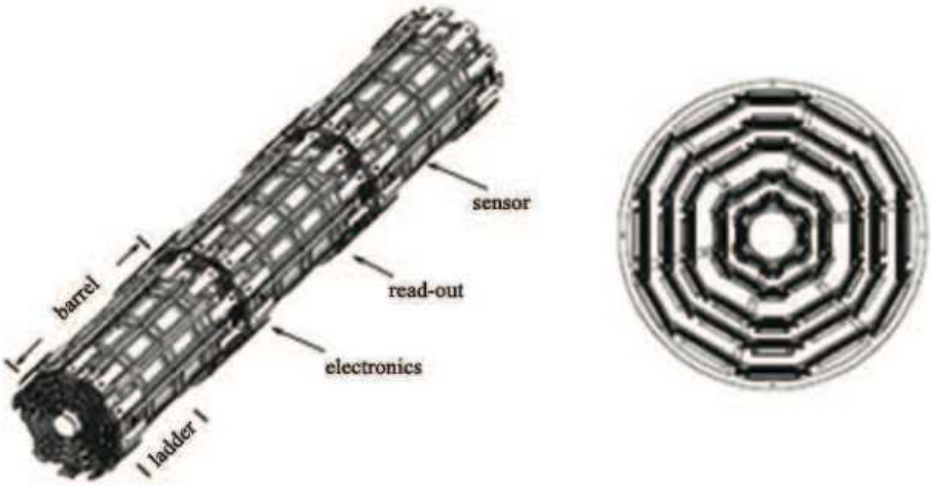

Figure 2.3: An artist's rendition of SVX, left side view, right end on view.

wires; the even layered superlayers have wires oriented axially, and the odd layers' wires are oriented with an angle offset $\pm$ 2° for stereo measurements.

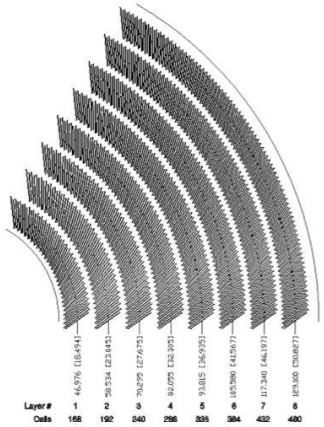

Figure 2.4: A section (1/6 of the total) of the Central Outer Tracker

The COT is filled with a mixture of equal parts of ethane and argon. The drift time for electrons produced from passing particles is designed to be less than 100 ns. As a charged particle travels through the COT, it produces ionization electrons. These electrons drift toward the sense wires in the electric field produced by the potential wires, and the cathode field panels. The drift electrons will move in a

direction perpendicular to the magnetic field, at an angle α with respect to the electric field lines. In the COT the drift angle, α is about 35°.

The optimal resolution for a track occurs when the trajectory of the drift electrons is perpendicular to the track going through the COT. Most high-p_T tracks will be nearly radial, thus each of the COT cells are tilted by 35° with respect to the radial, to compensate for the drift angle. A schematic diagram of a portion of the COT can be seen in Figure 2.4. The transverse momentum resolution is $\sigma_{PT}/p_T = 0.15\ \% \times p_T$.

When an electron gets near a sense wire, the wire's local 1/r field accelerates the electron, which in turn causes more ionization. The resulting ionization forms an "avalanche" and we measure this as a signal (hit) on the sense wire. The location of the hit can be found by finding the time of the hit, and the time of the collision. We determine the distance using the two time measurements.

2.4 Calorimetry

The measurement of energy is done by sampling calorimeters. The calorimeter is located outside of the solenoid and consists of alternate layers of scintillator and absorbing material. It is designed to absorb and measure the energy of the photons, electrons and hadrons. The calorimeter is split into two layers, the electromagnetic calorimeter, and the hadronic calorimeter. The innermost layer is the electromagnetic calorimeter. It is designed to stop electrons and photons and uses lead as its absorbing material and polystyrene as its scintillator material. The hadronic calorimeter is designed to measure charged and neutral hadrons and uses steel as its absorbing material and acrylic as its scintillating material. The calorimeter is split into two regions, one covering the positive η region, the other the negative η region.

A high energy electron or photon passing through the EM calorimeter will undergo pair production ($\gamma \rightarrow e^+e^-$) or bremsstrahlung ($e^\pm \rightarrow \gamma e^\pm$). This particle multiplication is called a shower. In each transition the energy per particle will drop until there is not enough energy to allow farther travel or create more particles. The point where the largest number of particles occur is called the shower maximum.

Beyond the shower maximum, the particles slowly lose their energy through either Compton scattering for photons or ionization losses for electrons and positrons. The EM calorimeter measures the energy from each of the particles in the shower, and the calorimeter is designed to fully contain showers from electrons and photons.

Both the central ($|\eta| < 1.1$) and plug ($1.1 < |\eta| < 3.6$) electromagnetic (EM) calorimeters have fine grained shower profile detectors at electron shower maximum, and preshower pulse height detectors at approximately 1 radiation length (X_0) depth. Electrons are identified by E/p (Energy divided by momentum, energy measured in the calorimeter, momentum measured in the tracking) measurements in the EM calorimeter, HAD/EM (Hadronic energy divided by EM energy) measurements being nearly 0, and using shower shape and position matching in the shower max detectors.

Hadrons lose their energy through nuclear interaction cascades which have pions, protons, kaons, muons, photons, etc. These reactions do not occur as rapidly as the showers in the EM calorimeter, and with fewer showers there is a larger fluctuation in the energy resolution.

2.4.1 Central Calorimeters

The central calorimeters consist of the central electromagnetic calorimeter (CEM) and the central hadronic calorimeter (CHA), and the end wall hadronic calorimeter (WHA).

The CEM and CHA are constructed in wedges of about 15° in azimuth, and extend 250 cm in the positive and negative z direction. There are 24 such wedges in each of the positive and negative z sides. Each wedge contains 10 towers each covering a range 0.11 in pseudorapidity. The WHA has 48 modules segmented into 12 polar towers and each module has 15 sampling layers.

The CEM covers $|\eta| < 1.1$ and contains 31 layers made up of lead layers and polystyrene scintillator layers. The calorimetry is segmented in "towers" in a projective geometry in η and ϕ pointing towards the center of the detector, with 10 groups in η, and 24 wedges in ϕ. Two photomultiplier tubes are used to read out

the light from the scintillators for each tower. A schematic diagram is shown in Figure 2.5. There is an energy resolution of $13.5\%/\sqrt{(E_T)} \oplus 2\%$. [1]

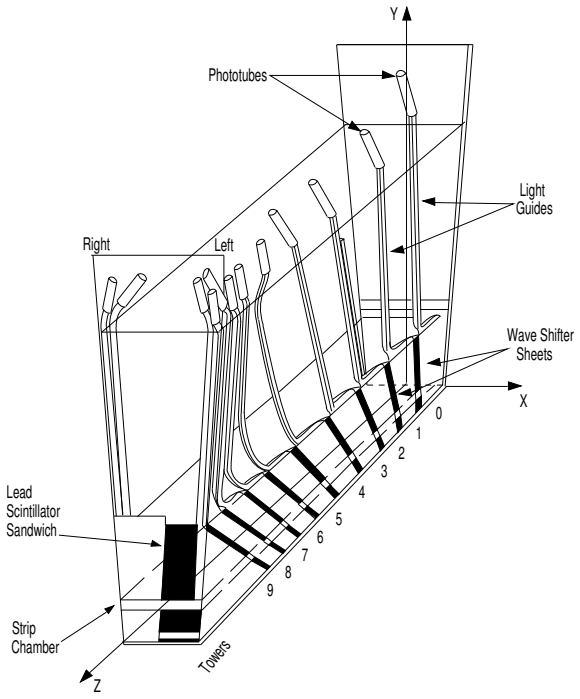

Figure 2.5: A schematic diagram of the Central Electromagnetic Calorimeter (CEM) detector. The absorbing layers and active layers are parallel to the base in the diagram. As the electromagnetic particles interact in the active layers light is produced. The light goes through the wave shifter sheets, into the light guides, and finally into the phototubes. The signal we observe in the phototubes is used to measure the amount of energy of the object.

The Central Electromagnetic Shower (CES) detector is embedded inside the CEM at the shower maximum, at a depth of about 6 radiation lengths. The CES detector is made up of a strip and wire chamber located at a radius of 184 cm from the beamline. Cathode strips measure the z-position, and the anode wires measure the ϕ position, a schematic diagram is shown in Figure 2.6. The CES is capable of distinguishing a single shower from a prompt photon and two showers from a decay of a neutral meson to two photons (i.e. $\pi^0 \rightarrow \gamma\gamma$), with a resolution of 2 mm at 50 GeV.

The Central Preradiator Detector (CPR) is located at the front of each calorime-

[1] The symbol $\oplus$ means added in quadrature.

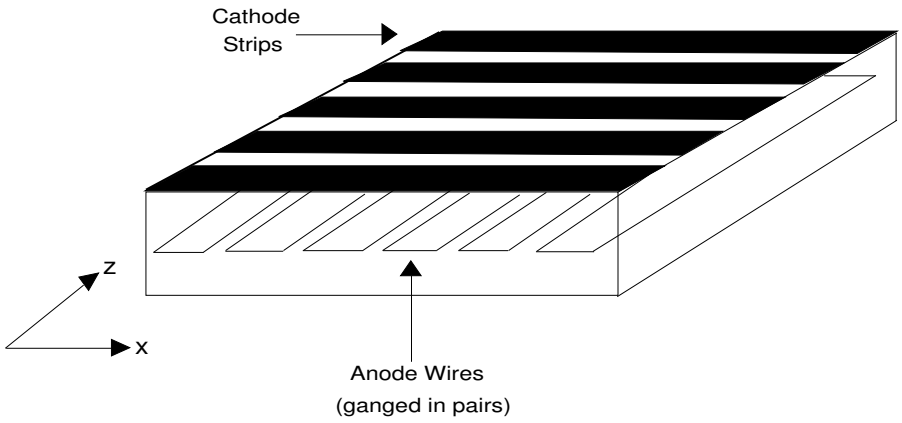

Figure 2.6: A schematic diagram of the Central Electromagnetic Shower (CES) detector. The CES detector is capable of making two measurements of the electromagnetic shower, one alone the strip directions, and another along the wire directions. Measurements of the shower shape are compared to shower shapes measured on test-beam data using a χ^2 fit.

ter wedge, and it uses the solenoid and tracking detectors as a radiator. It uses proportional chambers to sample the early development of the shower to measure conversions in the coil. A prompt photon has a 60% chance of converting, while the chance of at least one photon from a π^0 decay is about 80% [19].

Outside of the CEM, is the central hadronic calorimeter, CHA, and WHA. The CHA covers the region $|\eta| < 0.6$ and the WHA [20] covers the region $0.7 < |\eta| < 1.2$. They use steel as the absorbing material for the hadrons to interact with. When the hadrons interact with the steel they create showers of lighter hadrons, such as pions, kaons, and protons. In each of these showers the hadronic particles lose energy to the calorimeter which can be measured in towers just like in the CEM. The scintillator material in the CHA and WHA is acrylic. Figure 2.7 shows a picture of a CHA wedge. The active and absorbing layers can be seen. The energy resolution of the CHA and WHA is $75\%/\sqrt{\mathrm{E_T}} \oplus 3\%$, as measured on the test beam for single pions.

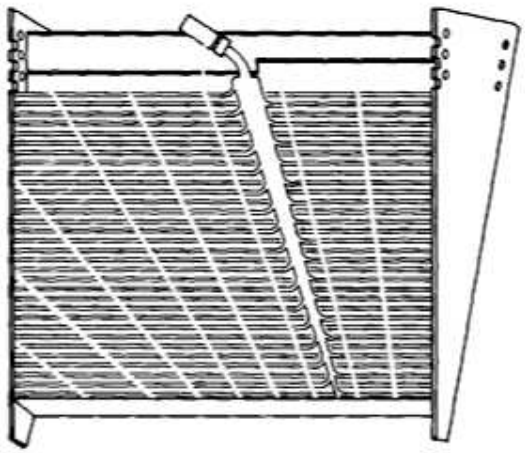

Figure 2.7: A section of the Central Hadronic Calorimeter. The absorbing layers of steel, and active layers of acrylic can be seen. When the shower products interact with the acrylic the light is guided to a photomultiplier tube.

2.4.2 Plug Calorimeters

The plug calorimeters consist of the plug electromagnetic calorimeter (PEM) and the plug hadronic calorimeter (PHA). In order to fit into the end of the central region of CDF it is shaped like a giant plug, hence the name. The plug calorimeters' layers are oriented perpendicular to the beam, and allow measurement of the energy of particles with a pseudorapidity of $1.1 < |\eta| < 3.6$.

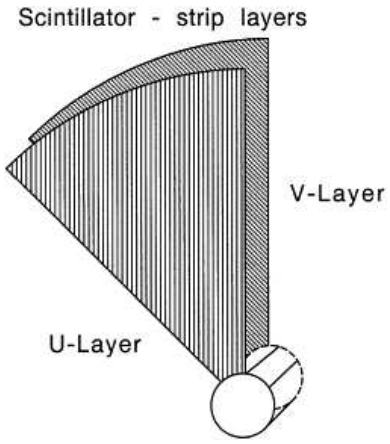

Figure 2.8: View of U and V layers of Plug Shower Max Detectors

Wedges in the plug calorimeter span 15° in azimuth for $2.1 < |\eta| < 3.6$, and

7.5° in azimuth for $1.1 < |\eta| < 2.1$. The PEM is a series of 22 alternating layers of lead and scintillator, and has the same structure as CEM. The transverse energy resolution of the PEM is $16\%/\sqrt{E} \oplus 1\%$.

The plug shower max (PES) detector is located at about 6 X_0 in depth in the PEM. The PES is segmented into U and V layers which are offset from the radial direction by +22.5° and -22.5° respectively, leading to a resolution of about 1 mm, and can be seen in Figure 2.8.

PHA is located behind the PEM, and has the same tower segmentation. As in the CHA, there is a 23 layer steel scintillator sampling calorimeter and the resolution is about $80\%\sqrt{E} \oplus 5\%$ [21]. A schematic of how the plug calorimeter is put together is shown in Figure 2.9.

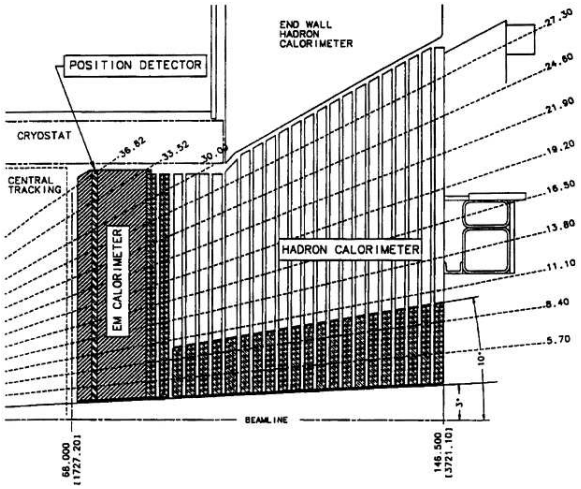

Figure 2.9: Longitudinal view of the CDF Plug Calorimeter and the Wall Hadronic Calorimeter.

2.5 Muon Detectors

Muons will pass through the calorimeter leaving behind only ionization energy. Because muons are 210 heavier than electrons, they are able to pass through the electromagnetic calorimeter without being stopped. Muons do not interact hadronically; so they escape the hadronic calorimeter.

The previously described calorimeter is unable to reliably detect muons because

nearly all muons make it through the calorimeter without being stopped, leaving behind only ionization energy.

The muon detectors are located behind the calorimeters and are covered with large amounts of steel shielding to stop remnant hadronic particles escaping the calorimeter. The return yoke of the solenoid magnet provides shielding from hadrons punching through the calorimeter. The shielding does not stop the muons, which pass through leaving behind hits in the muon detectors, which are four layers of single-wire drift cells four layers deep. Behind the CHA and the steel shielding is the central muon detector (CMU), which covers $|\eta| < 0.6$. After the CMU there is the central muon upgrade (CMP). The CMP covers the same η range as the CMU. Muons that are detected in this region are required to have at least three hits in both the CMU and CMP subsystems, and are called CMUP muons, and the group of three such hits is called a "stub".

The central muon extension, CMX covers $0.6 < |\eta| < 1.0$, and like the CMU and CMP subsystems has four layers of drift tubes. However due to the floor, in the bottom quadrant the drift tubes take a fan shape referred to as the "miniskirt" [22]. Similar to the CMUP muons, CMX muons require the presence of a stub in the CMX detector.

The maximum drift time of the CMU is greater than the bunch crossing time and this can cause discrepancies in the Level 1 trigger (discussed in Sec. 2.8). There are scintillation counters To resolve this discrepancy.

2.6 Time of Flight System

The Time of Flight (TOF) [23] system is meant to precisely measure the time between a collision and when objects reach the TOF. The design resolution of the TOF is 100 ps and this provides differentiation between decays of kaons and pions. The TOF is also used to differentiate muons from the collisions from those due to cosmic rays, and while the TOF is not explicitly used in this analysis, the rejection of muons from cosmic rays is.

The TOF has a radius of 140 cm, which corresponds to a flight time of about

5 ns for the fastest particles. It is located between the COT and the solenoid.

The TOF is constructed of 216 scintillator bars each with dimensions 4x4x279 cm; each bar covers 1.7° in azimuth. Each scintillator has a photomultiplier tube (PMT) attached at each end. The signal from the PMTs provide information on integrated charge as well as timing.

2.7 Luminosity Counters

Most measurements at CDF will require good knowledge of the integrated luminosity for normalization, and to estimate the magnitudes of Monte Carlo driven backgrounds. Luminosity is a measure of particle interactions; at the Tevatron, it is a measure of the chance that a proton will collide with an antiproton. The rate of inelastic scattering of $p\bar{p}$ can be used to determine the luminosity.

The luminosity of CDF is calculated using Čerenkov Luminosity Counters (CLC) [24]. The CLC are located in the very forward regions of the detector, $3.7 < |\eta| < 4.7$. The luminosity is measured based on the numbers of proton antiproton interactions, and this is converted to a luminosity amount.

The luminosity of a $p\bar{p}$ collider can be estimated using the following equation:

$$\mathcal{L} = \frac{f \times \mu}{\sigma}. \tag{2.1}$$

where f is the frequency of beam crossing, μ is the average number of interactions per beam crossing, and σ is the inelastic cross section of $p\bar{p}$ scattering.

2.8 Trigger and Data Acquisition

Physical processes of interest to us occur at rates many orders of magnitude below the total $p\bar{p}$ inelastic cross section. Furthermore, the rate of collisions at the Tevatron is much too rapid to possibly save all events; so it is necessary to have a system which saves events which could be interesting to physicists at CDF, and to reject events which are not interesting.

The CDF trigger system does exactly this. It uses a three level architecture

to accept or reject events: Level 1 (L1), Level 2 (L2), and Level 3 (L3). At each increase in level, the data volume is further reduced.

At L1 the trigger must make its decisions within 5 μs of each collision. Collisions occur at a rate of 1.7 MHz, and the L1 triggers system lowers the acceptance rate to about 40 kHz. L1 can make its decision based on axial layers of the COT which are used by the eXtreme Fast Tracker (XFT) to reconstruct ϕ and p_T of tracks left by charged objects. L1 can look at the ratio of hadronic to electromagnetic energy in calorimeter towers and identify electrons and photons, and differentiate them from jets. Muons can be reconstructed using XFT and hits made in the muon subsystems. $\not\!\!E_T$ and $\sum E_T$ (a scalar sum of the transverse energy of all of the calorimeter towers) are also reconstructed at L1. Events which pass L1 acceptance are then passed to the L2 hardware.

At L2 the event selection is further refined, and decisions are made within 30 μs. L2 uses information from layers 0-3 of SVX, and combines this information with the XFT tracks. At L2 there is a more careful clustering in the calorimeter including information from the CES. The SVX data is processed by the Silicon Vertex Tracker (SVT), and this system looks for a displaced vertex. An event at the L2 trigger system is asynchronous (i.e. an event does not need to be finished by a fixed time after the collision occurred). The acceptance rate of L2 is about 400 Hz.

All accepted L2 events are sent to the highest level trigger which is implemented in software on a farm of several hundred computers, L3. At L3, each event is sent to the event builder, which fully reconstructs and analyzes the event using the latest calibrations of the detector. Events which pass L3 are now ready to be saved; the L3 accept rate is about 100 Hz [25]. We show a block diagram of the trigger decision used by CDF in Figure 2.10.

There are a variety of triggers available to CDF users, and these triggers correspond to various physics processes. It is important to be cognizant of the choice of trigger one makes.

The events are separated according to which triggers were fired in the event. Since we will be searching for events with high-p_T leptons, our datasets are those

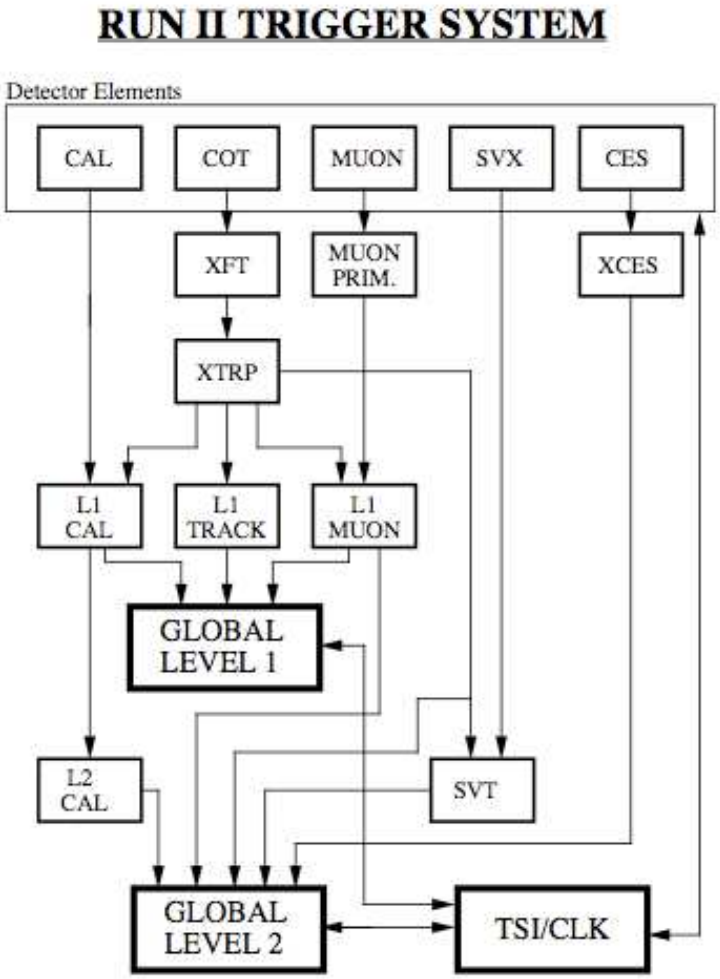

Figure 2.10: Block Diagram of CDF's Trigger System. Flow of data through the L1 and L2 of trigger system. The SVT information, based on the track impact parameter of displaced tracks is used by L2. At each progressive level the volume of data is reduced. The L3 trigger is completely software based, and is run on a computer farm.

which have had a high-p_T lepton trigger fired. These events are further separated by which lepton triggers were fired, either electron or muon.

3 Object Identification

In this section we describe the selection criteria used to identify the objects that make up our signatures, including: photons, muons, electrons, and jets. Many of our cuts are similar to the standard identification cuts used at CDF, however some of our selection criteria are largely historic. This analysis inherits the object selection from previous analyses [12, 26].

There are a few differences in how some of the event kinematics and features are calculated between the previous analysis and this current analysis. One of the differences is the method of how the primary vertex is chosen [27].

Our data format, the StNtuple, identifies the primary vertex (the point where the collisions between the proton and anti-proton occurred) is the point with the highest total p_T of objects coming from it.

This choice of primary vertex directly affects the E_T of all of our reconstructed objects, and we see slightly different kinematics in events that we use as control samples. However, the differences were very minimal.

In the next subsections we describe how we identify: muons, electrons, photons, jets, $\not\!\!E_T$, and H_T.

3.1 Lepton Selection: Muons

For muon signal events we require at least one "tight central muon" to be identified in the event. Furthermore we identify objects as "loose central muons", which are less restrictive than tight central muons, but are treated as muons. Both of these cuts are described below.

3.1.1 Muon Selection Criteria

The selection criteria we use are identical to the standard criteria [28, 29], with the exceptions that we have not applied the impact parameter cut and we do not use cuts on fiducial distance (x-fid, z-fid).

Tight central muons should make their way through the detector leaving hits

Variable	Tight	Loose	Stubless
Track p_T	$> 20\ GeV$	$> 12\ GeV$	$> 12\ GeV$
Track quality cuts	3 Ax 3 St SLx5 hits	3 Ax 2 St SLx5 hits	3 Ax 3 St SLx5 hits
Track $\|z0\|$	$< 60\ cm$	$< 60\ cm$	$< 60\ cm$
Calorimeter Energy (Em)	< 2 + sliding	< 2 + sliding	< 2 + sliding
Calorimeter Energy (Had)	< 6 + sliding	< 6 + sliding	< 6 + sliding
Fractional Calorimeter Isolation E_T	< 0.1	< 0.1	< 0.1
Cosmic	False	False	False
Chi2/(N of COT hits-5)	-	-	< 3
Cal.Energy (EM+Had)	-	-	> 0.1
CMUP muons cuts(*)	yes	yes	no
CMX muons cuts(**)	yes	yes	no

Table 3.1: Muon identification criteria and isolation cuts used in this analysis.
(*)CMUP muons cuts: $|\Delta X(CMU)| < 3$ cm, $|\Delta X(CMP)| < 5$ cm
No muons from CMP bluebeam section for run<154449
(**)CMX muons cuts: $|\Delta X(CMX)| < 6$ cm, COT exit radius > 140 cm
No muons from the CMX keystone or miniskirt before October 2004 shutdown (run 186598)
The sliding cut refers to a different cut if the muon has $p_T > 100$ GeV. The track quality cuts require at least 5 hits in 3 axial (ax) and 2 or 3 stereo (st) layers.

and tracks through the silicon, and COT systems. Muons should leave clusters of hits in the CMX, CMU, and or CMP muon detectors. We call a group of three or more such hits a stub.

Muons are classified according to the position of the stubs in the detector. Classification of muons according to [28, 29] goes as follows: first we check for tight muons with stubs in both the CMU and CMP (CMUP muons) or a stub in the CMX (CMX muons), and then we check for loose muons (either CMUP, CMX, or muons without a stub in the CMU and CMP (stubless muons)).

Muon tracks are extrapolated from hits in the COT through the calorimeters and out to the muon detectors. Tight central muons are required to have the distance between track extrapolation to the radius of the muon detector and the stub position in the muon detector differ by less than 3 cm for CMU, 5 cm for CMP, and 6 cm for CMX.

During the course of running the CDF detector there have been small problems with the muon detectors. Muon candidates observed during these data-taking periods are not accepted as muons. This is encoded in our data as a "Region is OK"

variable.

The "Region is OK" cut for CMUP muons requires no muons from CMP blue-beam section for run<154449, and for CMX muons that the COT exit radius > 140 cm, and no muons from the CMX keystone, or miniskirt before October 2004 shutdown (run 186598). The bluebeam was a section of data-taking where there were beam-related problems. The miniskirt and keystone region requirements are due to issues with the CMX detector.

The muon tracks used in the initial selection for this analysis are beam-constrained COT-only, as is done by the muon group in their efficiency studies [28]. For default muon tracks that contain silicon we link backwards to the COT-only parent track and use that track for all subsequent analysis.

For tracks that are COT-only beam-constrained tracks, we also apply a curvature correction [30] for the track p_T in data before applying kinematic selection criteria and calculating additional kinematic variables. The form of the curvature correction is shown in Equation 3.1 where Q is the charge of a track (+1 for positive charge and -1 for tracks negative charge):

$$
\begin{aligned}
c_1 &= Q/\mathrm{p_T} \\
c_2 &= c_1 + 0.00020 * sin(\phi + 3.4) \\
c_3 &= c_2 + 0.00022 * sin(3 * \phi + 0.9) \\
c_4 &= c_3 - (0.000026 + 0.000072 * cot(\theta) - 0.00024 * cot(\theta) * cot(\theta)) \\
c_5 &= c_4 - 0.0002 * cot(\theta) * sin(\phi - 0.9) - 0.0002 * cot(\theta) * cot(\theta) * sin(\phi - 4.1) \\
\mathrm{p_T} &= \mathrm{Q}/\mathrm{c_5}
\end{aligned}
\tag{3.1}
$$

In the above set of equations we define the value c_1, to be the inverse of the transverse momentum multiplied by the charge of the track. The track's charge can be inferred by the path it takes in the magnetic field. Using this equation we are correcting the p_T of the track.

All central muons are required to have $|z_0| < 60$ cm so that the collision is

well-contained within the CDF detector. The value z_0 is the initial displacement in the z-direction of the muon. In order to be well-measured, the muon track is required to have a minimum of 3 axial and 3 stereo superlayers with at least 5 hits in each superlayer of the COT.

High-energy muons are typically isolated "minimum-ionizing" particles that have limited calorimeter energy. A muon traversing the central electromagnetic calorimeter (CEM) deposits an average energy of about 0.3 GeV. Therefore we require muon candidates to deposit less than 2 GeV total in the CEM towers (we take into account two towers in the CEM) the muon track intersects. Similarly, muons transversing the central hadronic calorimeter (CHA) deposit an average energy of about 2 GeV; we consequently require muon candidates to deposit a total energy less than about 6 GeV, also increasing with muon momentum, in the CHA towers intersected by the track extrapolation. To take into account the (slow) growth of energy loss with momentum, for very high energy muons (momentum (p) greater than 100 GeV) we require the measured CEM energy to be less than $2.0 + 0.0115 *$ (p$-$100) GeV and CHA energy to be less than $6.0 + 0.028 *$ (p$-$100) GeV. These are the sliding cuts mentioned in Table 3.1

To suppress hadrons and decay muons created from hadrons in jets, we require the total transverse energy deposited in the calorimeters in a cone of R=0.4 around the muon track direction (known as the fractional calorimeter isolation E_T) to be less than 0.1 of the muon track p_T.

Cosmic rays can show up in the detector as muons, and thus we must make sure we do not accept these muons as arriving from the collision. Fortunately the COT cosmic finder by itself is essentially fully efficient. So to suppress cosmic rays we use the COT-based cosmic rejection from the CosmicFinderModule [31, 32] and reject events which it tagged as containing Cosmic Ray muons.

3.1.2 Loose Central CMUP and CMX Muons

Each high-p_T muon signal event in this analysis, contains at least one tight CMUP or CMX muon, all of our signal events additionally identify high-p_T muons that could

come from the decays of heavy particles, and thus may not be as well reconstructed in the detectors. There are two types of secondary muons we accept: "Loose" CMUP and CMX muons, described here, and stubless muons (see Section 3.1.3).

Loose muons are muon objects with either CMUP or CMX stubs, but with looser COT cuts than the tight CMUP or CMX muons (see Table 3.1). We require 3 axial and 2 stereo COT superlayers with at least 5 hits each for loose CMUP and CMX muons.

3.1.3 Loose Central Muons: Stubless

The cuts for Stubless muons are looser than the tight cuts, and in particular do not require a stub in the muon chambers.

There are three types of "Stubless" muons:

- CMU muons (muon track matches the CMU stub only),
- CMP muons (muon track matches a stub in the CMP only),
- CMIO muons (muon track not matched to a stub in the CMU, CMP or CMX).

A pattern-finding algorithm is used to help identify muons, and can often remove a stereo layer in the COT to get a good fit. This results in a badly reconstructed polar angle, and the appearance that a muon left no energy in the extrapolated traversed calorimeter towers [33].

To better identify stubless muons we have requirements to address this issue. The fitted tracks' reduced χ^2 (χ^2/(N of COT hits - 5)), must be less than 3, and it must be extrapolated to calorimeter towers with at least 0.1 GeV of deposited energy [28, 33]. These cuts help reject charged kaons that decay as they pass through the COT. These decays are called "decays in flight" and a muon from these decays form a "seagull" pattern which is reconstructed as a single high-momentum track.

3.2 Lepton Selection: Electrons

We require at least one "tight central electron" in each of our signal events to be counted in the electron channel. Additionally we also search for "loose" electrons

in the CEM and PEM which are still electrons but are reconstructed less well. The loose electrons are identifed as electrons and will not identified as any other object, such as a jet.

The tight central, loose central, and plug electron cuts are listed below in Tables 3.2 and 3.3. The loose and plug electrons are treated as electrons. However for each of our signal events we must have a tight central electron; plug electrons (even tight plug electrons) and loose electrons do not satisfy this requirement.

3.2.1 Electron Selection Criteria

Variable	Tight	Tight100	Loose
E_T	> 20 GeV	> 100 GeV	> 12 GeV
Track p_T	> 10 GeV	> 25 GeV	> 10 GeV
Track $\|z0\|$	< 60 cm	< 60 cm	< 60 cm
Had/Em	$< 0.055 + 0.00045 \times E$	$< 0.055 + 0.00045 \times E$	$< 0.055 + 0.00045 \times E$
E/P	< 2.0	-	-
L_{shr}	< 0.2	-	-
χ^2 CES Strips	< 10	-	-
$\Delta X(CES)$	-3.0 cm $< Q_{trk} \times \Delta X <$ 1.5 cm	$\|\Delta X\| < 3.0$ cm	-
$\|\Delta Z\|$ (CES)	< 3.0 cm	< 5.0 cm	-
Fractional Calorimeter Isolation E_T	< 0.1	< 0.1	< 0.1
Track quality cuts	3 Ax, 2 St SL x 5 hits	3 Ax, 2 St SL x 5 hits	3 Ax, 2 St SL x 5 hits

Table 3.2: Central electron identification and isolation cuts.

Our selection criteria for electrons is based on an old standard [34]. However we apply neither the fiducial requirement nor the conversion cut. Both of these requirements attempt to identify fake electrons, or objects less likely to be real electrons. The acceptance gain by removing the fiduciality requirement is approximately 14% [35]. This was the same selection criteria in Ref. [35]. We have kept the cuts as they are to provide a consistency check with an older analysis [36] which used the same selection criteria for electrons.

3.2.2 Tight Central Electrons

Electrons are identified by selecting high-momentum tracks measured in the detector that point toward high-energy clusters in the CEM. The electron track is the highest-momentum track intersecting two towers in the CEM cluster. As with the muons,

Variable	Tight	Phoenix Tight
E_T	> 15 GeV	> 15 GeV
Had/Em	< 0.05	< 0.05
Fractional Calorimeter Isolation E_T	< 0.1	< 0.1
PEM χ^2	< 10	< 10
Delta R	< 3.0 cm	< 3.0 cm
PES 5by9 U and V	> 0.65	> 0.65
PEM $\|\eta\|$	$1.2 < \|\eta\| < 2.0$	$1.2 < \|\eta\| < 2.0$
PhxMatch	-	TRUE
Number of Silicon Hits	-	≥ 3
|Z(Phoenix)|	-	< 60 cm

Table 3.3: Plug electron identification and isolation cuts. We are using the "Phoenix Tight" selection [37, 38].

we use beam-constrained COT-only tracks and apply the same correction found in Eq. 3.1.

An EM cluster in the central region is made up of towers in the CEM. A tower is called a seed tower if its measured energy > 3 GeV; it is a shoulder tower if its measured energy was greater than 0.1 GeV. An EM cluster is formed by incorporating adjacent towers with a seed tower and continues until no more adjacent towers can be added, or the maximum cluster size is reached. In the central region the maximum cluster size is 3 towers in η and 1 tower in ϕ [39].

To be classified as an electron, a candidate is required to have its calorimeter energy (E) be less than two times the tracking momentum (P). The track of the electron must have at least 5 hits in each of 3 axial and 2 stereo super-layer segments. To improve acceptance of very-high-energy electrons with E_T greater than 100 GeV, the E/P cut is not longer applied, but the reconstructed track of the electron must be greater than 25 GeV. The electron's track is also required to have the track extrapolate back to $|z_0| < 60$ cm so the collision is well-contained in the CDF detector.

A track extrapolated to the CES radius must satisfy the following position requirements: it must be within the charge-signed CES shower position of the cluster in the r-ϕ view, -3.0 cm $< Q_{trk} \times \Delta X < 1.5$ cm and it must be within 3 cm of the CES shower in the z-direction (ΔZ).

We require the shape of the electron's shower in the CEM be consistent with

expectations of a single charged particle. The ratio of the hadronic energy (measured in the CHA towers behind the CEM towers in the electron cluster) to the energy measured in the CEM towers of electron cluster itself must be less than 0.055+0.00045×E GeV.

The amount of lateral shower sharing with adjacent towers in the CEM cluster is compared to test-beam data and a dimensionless quantity Ł$_{shr}$ parameterizes this. The value of Ł$_{shr}$ is required to be less than 0.2.

The electron candidate's shower shape in the strips of the CES is compared to that measured from test-beam data. The χ^2 of the fit between the shape of the test-beam data and the candidate's shower shape is required to be less than 10. No cut is applied on the shape observed in the wires of the CES.

To ensure the electrons are well isolated, the total transverse energy deposited in the calorimeter in a cone R=0.4 around the electron track is required to be less than 10% of the E_T of the electron. The isolation value is corrected for leakage via a standard algorithm [40], but it is not corrected for the number of vertices.

3.2.3 Loose Central Electrons

While each of our high-p_T electron signal events must contain at least one tight electron, all events are searched for additional high-P_T electrons that are less well reconstructed than tight electrons. We still want to identify these objects as electrons, so that they will not be misidentified as a photon, or a jet. The cuts for these additional electrons are looser than the tight cuts, and in particular do not require any of the CES variables, i.e. no track-cluster match in ΔX or ΔZ, no cut on strip χ^2, and no cut on Ł$_{shr}$.

3.2.4 Plug Electrons

Additional isolated electrons in the plug calorimeter with $E_T > 15$ GeV are identified for measured PEM rapidities of $1.2 < |\eta| < 2.0$. We expect electrons even in the plug to have very minimal energy leaving the PEM, and so we require minimal leakage or activity in the hadron calorimeter; the hadronic energy divided by the

electromagnetic energy (Had/Em) must be less than 0.05.

Like the central electrons, the fractional isolation (isolation energy over the electron energy) must be less than 0.1. The electron energy collected in a group of 9 (three by three) towers (PEM 3x3) must have χ^2 less than 10 compared to the expectation shape as measured by test-beam data.

The ratio of the shower measured in the PES by 5 strips compared to that measured in 9 strips (PES 5by9) must be greater than 0.65. We require this for both the U and V directions, and this ensures that our electron has a shower shape we expect.

These criteria for plug electrons are similar to the standard selection [34] with the exception that we use PEM-based η instead of PES-based η.

Finally, we apply face corrections to the PEM energy of the plug electron candidate, add the PPR energy and scale resulting number by 1.0315, as shown in Equation 3.2.

$$E_{\text{plug electron}} = (E_{pem}^{cor} + E_{ppr}) \times 1.0315 \tag{3.2}$$

3.3 Photon Selection

The photon selection criteria are identical for photons in both the muon and electron samples, and are described below. The photon selection criteria we use is standard for the CDF experiment. The photons must be central with a $|\eta| < 1.1$.

3.3.1 Photon Selection Criteria

To be identified as a photon, a photon candidate is required to have a minimum corrected transverse energy (E_T^{corr}) of 10 GeV. For both photons and electrons, the CES shower position is determined by the energy-weighted centroid of the highest-energy clusters of the strips and wires in the CES which correspond to a seed tower. The direction of the photon candidate is found by connecting the primary interaction vertex to the shower position in the CES.

Variable	Cut
E_T^{corr}	> 10 GeV
Had/Em	< 0.125 or $< 0.055 + 0.00045 \times E^{corr}$
$(\chi^2_{Strips} + \chi^2_{Wires})/2.0$	< 20
N Tracks	≤ 1
Track P_T	$< 1 + 0.005 \times E_T^{corr}$ GeV
Cone R=0.4 $IsoE_T^{corr}$	$< 2.0 + 0.02 \times E_T^{corr} - 20)$ GeV
Cone R=0.4 TrackIso	$< 2.0 + 0.005 \times E_T^{corr}$ GeV
2nd CES Cluster (Strip and Wire)	$< 2.4 + 0.01 \times E_T^{corr}$ GeV
Fiducial	CES $\lvert X \rvert < 21$ cm, 9 cm $<$ CES $\lvert Z \rvert < 230$ cm

Table 3.4: Selection Criteria used for Photon Identification

To ensure that events are well-measured, the shower position of the photon is required to fall within the fiducial region of the CES so that the shower is fully contained in the active region.

The photon candidate's shower shape in the CES is compared to that measured from a single particle test-beam. The shapes are compared with a χ^2 fit along two directions in the CES, along the strips direction, and along the wires direction. The χ^2 values from both of these measurements is then averaged, and we refer to this average as the photon's χ^2.

We found in the $t\bar{t}\gamma$ analysis that making an additional χ^2 cut on low energy photons retains much of the purity of the $t\bar{t}\gamma$ sample and excludes a good portion of the background due to jets being misidentified as photons. This cut and the methods are explained in detail in Section 8.

Photon candidates are required to have characteristics consistent with those of a neutral electromagnetically-interacting particle. No COT track with $p_T > 1$ GeV may point at the photon cluster; however we allow at most one track with $p_T < 1$ GeV to point at the cluster.

The variable "$IsoE_T^{corr}$" is the amount of transverse energy in the cone of R=0.4 less the amount of energy from the EM cluster. The isolation energy has been corrected due to phi-crack leakage [40]. We refer to "$IsoE_T^{corr}$" as E_T^{iso} for the remainder of this dissertation. The tracking isolation variable "TrackIso" is the sum of the p_T of tracks in a cone of R=0.4 surrounding the photon, measured in GeV.

3.4 B-Tag Identification

The jets used in this analysis are reconstructed from calorimeter towers using a cone algorithm with a radius R $\leq$ 0.4. The E_T in each tower in the cone is calculated with respect to the z coordinate of the event. The calorimeter towers belonging to any electron candidate are not used by the jet clustering algorithm. The energy of the jet is corrected for the pseudo-rapidity dependence of the calorimeter response, the calorimeter time dependence, and extra E_T from any multiple interactions.

When identifying jets we check that the jet object does not have any of the objects identified in the current analysis close to it (within $\Delta R < 0.5$).

The E_T of potential jets are corrected with Level 5 [41] corrections, and they are accepted as jets if $E_T^{corr} > 15$ GeV and detector rapidity $|\eta| < 2$.

The b-jet selection criteria are identical for b-jets in both the muon and electron samples and described below. For a jet to be identified as a b-jet, we require it be identified as a b quark candidate through the presence of a displaced vertex within the jet, arising from the decay of a long-lived bottom hadron (b-tag).

The SecVtx algorithm uses a two pass approach for identifying secondary vertices. In the first pass the algorithm applies a loose track selection and it attempts to identify a secondary vertex with at least three tracks coming from it. If this fails, the algorithm then uses a tighter track requirement and looks for a secondary vertex with at least two tracks coming from it.

One a secondary vertex is found a 2 dimensional decay length, L_{xy}, the distance the secondary vertex traveled from the primary interaction point before decaying. The value L_{xy} is the projection, onto the jet axis in the r-ϕ view, of the vector pointing from the primary vertex to the secondary vertex. The sign of L_{xy} is defined by the absolute difference in phi between the secondary vertex vector and the jet vector. If $\phi < 90^\circ$ then the sign is positive, otherwise it is negative. A large positive L_{xy} is consistent with a jet decaying from a heavy flavor hadron, while those due to mismeasured tracks should be small or negative [42].

We use the "loose" SecVtx [42] tagging method for b-tag identification[2]. There are additional categories of tagging one could use such as "tight" or "ultra-tight" however we are trying to keep our acceptance high, and "tight" or "ultra-tight" are too restrictive.

The benefits of "tight" and "ultra-tight" b-tagging is that they both have very little misidentifications (mistags), and the problem is they will reject looser tags. We already expect a very low event yield from the $t\bar{t}\gamma$ search [12], and so we attempt to maximize acceptance of potential b-tags.

3.5 Calculating the Missing Transverse Energy and H_T

3.5.1 Calculating the $\not\!\!E_T$

Missing E_T ($\not\!\!E_T$) is the signature of neutrinos, or possible new non-interacting particles such as the gravitino or LSP. It can also come from mismeasurement of the true E_T of objects, or from backgrounds such as cosmic rays or beam halo.

Missing transverse energy is calculated from the calorimeter tower energies in the region $|\eta| < 3.6$. Corrections are then made to the $\not\!\!E_T$ for non-uniform calorimeter response [41] for jets with uncorrected $E_T > 15$ GeV and $|\eta| < 2.0$, and for muons with $p_T > 12$ GeV:

- Muons: correct for $E_T - p_T$, where E_T is the transverse energy deposited in electromagnetic and hadron calorimeters, and p_T is the transverse momentum of a muon track. We correct $\not\!\!E_T$ for all muons with $E_T > 20$ GeV.
- Jets: correct for $E_T - E_T^{corr}$, where E_T is the transverse energy of an uncorrected jet, and E_T^{corr} is the transverse energy of a jet, corrected for non-uniform calorimeter response [41]. We correct for jets with $E_T^{corr} > 15$ GeV.

3.5.2 Calculating the H_T

H_T is a sum of E_T's and p_T's of all objects in the event (leptons, photons, $\not\!\!E_T$, jets). To calculate H_T we use Tight and Loose Central Electrons (Table 3.2), Tight

[2]We are using the b-tagging collection "PROD@SecVtxModule-JetClu-cone0.4-loose".

Phoenix Electrons (Table 3.3), Tight and Loose CMUP and CMX muons, Stubless muons (Table 3.1), $\not\!\!E_T$, and jets in the event with $|\eta| < 2$ and $E_T^{corr} > 15$ GeV.

3.6 Defining the Event Categories by Topology

In this thesis, we are primarily concerned with three signatures: $t\bar{t}\gamma$, $\ell\gamma\not\!\!E_T b$, and $t\bar{t}$. The dominant contribution to all of these signatures comes from top quarks. The top quarks we are interested in will decay immediately to bottom quarks and W bosons. We search for events involving leptonic decays of the W bosons by requiring high-p_T leptons, and large $\not\!\!E_T$. The cut on $\not\!\!E_T$ also allows us to suppress events from QCD contributions. These signatures share common features enumerated in Table 3.5.

Selection Criteria for lepton, jets, and $\not\!\!E_T$ channel	
Variable	**Selection Critera**
lepton track isolation	≤ 4.0 GeV
Jet E_T	≥ 15 GeV
Jet $\|\eta\|$	≤ 2.0
Lepton E_T	≥ 20 GeV
Lepton type	1 CEM electron or CMUP muon or CMX muon
$\not\!\!E_T$	> 20 GeV

Table 3.5: Basic selection criteria of lepton, jets, and $\not\!\!E_T$ events. The full requirements of muons, electrons, and $\not\!\!E_T$ can be found in Secs. 3.1, 3.2 and 3.5.1 respectively. CEM electrons, CMX muons and CMUP muons refer to the type of leptons and their selection criteria.

QCD contributions are able to mimic this signature when a jet is misidentified as a lepton, and a mismeasurement of jet energies occur. The mismeasurement of jet energies can make it look like there is $\not\!\!E_T$.

By requiring a larger cut on $\not\!\!E_T$ we are able to reduce the amount of QCD contributions, while keeping acceptance of signal events high. In Sec. 6.2 we describe the procedure for calculating the amount of QCD events for the $t\bar{t}$ sample. The distribution of data events in the $t\bar{t}$ sample without a $\not\!\!E_T$ cut is shown in Figure 6.1; it can be seen that most of the QCD contribution is in the low $\not\!\!E_T$ range.

Each of our samples further requires identification of a b-tagged jet. A small

yield is expected based on previous analyses of the $\ell\gamma\not\!\!E_{\rm T}b$ and $t\bar{t}\gamma$ signatures [12]. Identification of b-tagged jets is made using SecVtx [42] "loose"-tagged jets.

The CDF top-quark group typically uses "tight" tagging for their signals involving $t\bar{t}$ to minimize mistags. Since we eventually want to compare $t\bar{t}\gamma$ and $t\bar{t}$ events using similar selections, we will use the "loose" b-tags for both.

Selection Criteria for the $\ell\gamma\not\!\!E_{\rm T}b$ Signal Sample	
Variable	**Selection Critera**
Jet $E_{\rm T}$	$\geq$ 15 GeV
Jet $\lvert\eta\rvert$	$\leq$ 2.0
Lepton $E_{\rm T}$	$\geq$ 20 GeV
Lepton type	1 CEM electron or CMUP muon or CMX muon
$\not\!\!E_{\rm T}$	$>$ 20 GeV
N_{b-tag}	$\geq$ 1
Photon type	1 Central Photon
Photon $E_{\rm T}$	$\geq$ 10 GeV

Table 3.6: This is the full list of requirements for the $\ell\gamma\not\!\!E_{\rm T}b$ event selection. The event must also satisfy the requirements shown in Table 3.5.

Both the $\ell\gamma\not\!\!E_{\rm T}b$ and $t\bar{t}\gamma$ signals require the identification of a tight photon, and a tight lepton. The full requirements of muons, electrons, and $\not\!\!E_{\rm T}$ can be found in Secs. 3.1, 3.2 and 3.5.1 respectively. All photon cuts are enumerated in Table 3.3. The full list of cuts required for $\ell\gamma\not\!\!E_{\rm T}b$ is shown in Table 3.6.

To better distinguish signal processes from background processes in the $t\bar{t}\gamma$ sample, an additional requirement is placed on a photon's χ^2 value of the reconstructed shower profile in the CES compared to that from test-beam data (this is explained in greater detail in Sec. 8).

Because our search for $\ell\gamma\not\!\!E_{\rm T}b$ is a signature-based search for signs of possible new physics, we want to keep the photon selection looser. If some heavy object decays to a photon, there is a possibility it will not be as clean in the CES detector, so the χ^2 cut is not applied in this case.

In events involving $t\bar{t}$ production, we expect to have a higher jet multiplicity than events coming from W decays with QCD contributions. To reduce the amount of these backgrounds we can require a higher $H_{\rm T}$ for the event. So, to differentiate

Selection Criteria for the $t\bar{t}$ Signal Sample	
Variable	**Selection Critera**
N_{b-tag}	≥ 1
Jet E_T	≥ 15 GeV
Jet $\|\eta\|$	≤ 2.0
N_{Jets}	≥ 3
Lepton E_T	≥ 20 GeV
Lepton type	1 CEM Electron or CMUP muon or CMX muon
$\not\!\!E_T$	> 20 GeV
H_T	> 200 GeV
M_T	< 20 GeV (electrons) < 10 GeV (muons)

Table 3.7: In addition to the cuts shown in Table 3.5, this is the full list of requirements for the $t\bar{t}$ event selection

$t\bar{t}$ and $t\bar{t}\gamma$ signals from their backgrounds, an additional requirement of $H_T > 200$ GeV is required for both of these event selections.

It is necessary to require the transverse mass (M_T) of the lepton and $\not\!\!E_T$ object to be greater than 20 GeV for electrons and greater than 10 GeV for muons, to better model the QCD contamination of the $t\bar{t}$ sample. Removing these regions allows for a much better kinematic fit of the data. This was not required for $\ell\gamma\not\!\!E_T b$ or $t\bar{t}\gamma$ due to very low statistics when modeling the QCD contribution, and for consistency with the previous $t\bar{t}\gamma$ search [12].

In Tables 3.7, and 3.8 we show the full selection requirements for both the $t\bar{t}$ and $t\bar{t}\gamma$ signals. Care was taken to make the selections as similar as possible.

For all of our samples, we require that the event be triggered with a high-p_T lepton trigger in order to be selected, and we discuss this further in the next section.

3.7 Triggers Used in this Analysis

There are a variety of triggers available to CDF users, and these triggers correspond to various physics processes. It is important to be cognizant of the choice of trigger one makes.

For our analysis we are using triggers corresponding to high-p_T leptons; these are standard triggers used by the CDF top-quark research group. This is a useful

Selection Criteria for the $t\bar{t}\gamma$ Signal Sample	
Variable	**Selection Critera**
N_{b-tag}	≥ 1
Jet E_T	≥ 15 GeV
Jet $\|\eta\|$	≤ 2.0
N_{Jets}	≥ 3
Lepton E_T	≥ 20 GeV
Lepton type	1 CEM Electron or CMUP muon or CMX muon
$\not\!\!E_T$	> 20 GeV
H_T	> 200 GeV
Photon type	1 Central Photon
Photon E_T	> 10 GeV
Photon χ^2	< 6; if $E_T(\gamma) < 25$ GeV < 20; otherwise

Table 3.8: In addition to the cuts shown in Table 3.5, this is the full list of requirements for the $t\bar{t}\gamma$ event selection.

choice for a couple of reasons. First, we want to measure the ratio of production cross sections of $t\bar{t}\gamma$ and $t\bar{t}$, and using a photon trigger to select addition $t\bar{t}\gamma$ events would include a systematic error that would not cancel out in the ratio. Second, these triggers allow us to make a good comparison between our measurement of the $t\bar{t}$ cross section and previous measurements of the $t\bar{t}$ cross section made by other members of the CDF collaboration [43].

The trigger paths used in this analysis can be found in Table 3.9; these are the same trigger requirements used by CDF's top quark research group uses.

In order to validate the stability of the trigger paths we are using, we ran over the first 4.8 fb^{-1} of data and looked for lepton + $\not\!\!E_T$ events (W), dilepton events (Z), dilepton + photon ($\ell\ell\gamma$), and lepton + photon + $\not\!\!E_T$ ($\ell\gamma\not\!\!E_T$) events.

3.8 Datasets

The data presented in the analysis represent 6.0 fb^{-1} for which the silicon detector and all three central muon systems (CMP, CMU and CMX) were operational.

Data at CDF are divided based on the type of trigger one uses for an analysis, and what time period the data comes from. The data are divided into periods based

Trigger Path Used	Run Range (inclusive)
MUON_CMX18	138425 - 200272
MUON_CMX18_L2_PT15	138425 - 226194
MUON_CMX18_L2_PT15_LUMI_200	200273 - 226194
MUON_CMX18_&_JET10	226195 - 257201
MUON_CMX18_&_JET10_LUMI_270	226195 - 257201
MUON_CMX18_&_JET10_DPS	226195 - 257201
MUON_CMX18	257201 - and up
MUON_CMUP18	ALL
MUON_CMUP18_L2_PT15	138425 - 229763
MUON_CMUP18_L2_LOOSE_DPS_V	Broken Runs
ELECTRON_CENTRAL_18	ALL

Table 3.9: List of triggers used by the CDF Top Group, and this analysis. The Broken Runs are: 262603, 262602, 262780, 262550, 262652, 262619, 262565, 262671, 262823, 262618, 262670, 262807, 262806, 262564, 262673, 262548, 262759, 262653, 262604, 262668, 262776, 262687, 262808

	W	Z	$\ell\gamma\not{E}_T$	$\ell\ell\gamma$
0d	742.24 ± 1.54	33.91 ± 0.33	0.87 ± 0.053	0.37 ± 0.034
0h	754.89 ± 1.46	33.46 ± 0.31	0.88 ± 0.050	0.30 ± 0.029
0i	716.47 ± 1.12	32.84 ± 0.24	0.86 ± 0.039	0.27 ± 0.022
0j	674.73 ± 0.85	31.21 ± 0.18	0.79 ± 0.029	0.22 ± 0.015
0k	676.81 ± 1.19	31.59 ± 0.26	0.69 ± 0.038	0.21 ± 0.021
0m	636.22 ± 0.74	29.12 ± 0.16	0.67 ± 0.024	0.21 ± 0.013
0mn	645.79 ± 0.84	29.43 ± 0.18	0.68 ± 0.027	0.20 ± 0.015

Table 3.10: Results using top triggers, as shown in Table 3.9. which is independent of run number. This table only shows results for Electrons. Each category has been normalized by the integrated luminosity in the sample. The 0m dataset (Sec. 3.8) was split into two groups, the first half is denoted 0m, and the second half is denoted 0mn.

on when the data is collected, and the periods are grouped into a larger data set stored on a server. The server's files are labeled as: 0d, 0h, 0i, 0j, 0k, 0m, and 0p.

Our data involving muons come from the inclusive high-p_T muon samples: bhmu0d, bhmu0h, bhmu0i, bhmu0j, bhmu0k, bhmu0m, and bhmu0p. The data involving electrons come from the inclusive high-p_T electron samples: bhel0d, bhel0h, bhel0i, bhel0j, bhel0k, bhel0m, and bhel0p.

In these cases the last two characters state which server has the data, and the first four characters identify the data as being from the high-p_T electron (bhel) or

muon (bhmu) data samples.

The data format we use is called an ntuple. We process each of the basic data structures used by CDF and turn it into an ntuple using the TTGNtupler package (Appendix B.1). The TTGNtupler package strips the size of the raw StNtuple data format by only saving a subset of the data in the StNtuple, and identifying at least one loose electron, one loose muon, or an antielectron (the selection criteria are shown in Table 5.1).

3.9 Selecting Candidate Events from Data

The bhel, and bhmu datasets are exceptionally large. Furthermore in the StNtuple data format that the data are preserved in, there is more information than we need. We look in the large streams of data for events that match our signal criteria, or events we use for control samples. Then in these events, we save only the information that we need for the analysis.

To reduce processing time, we took a few steps to select events. At the first step (StNtuple $\rightarrow$ TTGNtuple) we required an event to contain at least one loose electron (Table 3.2, we required $E_T^e > 12$ GeV cut), or at least one loose muon (Table 3.1, we required $p_T^\mu > 12$ GeV cut), or an antielectron (Table 5.1). For the events that match these criteria, we only save information about the event that we need for our analysis. We performed this step on CDF CAFs (a large network of computers), and output TTGNtuples were saved on the University of Chicago (UC) disk space (Appendix B.1).

At the second step we have selected events needed for signal and background studies, and also for cross-checks from the data-taking periods such as: lepton and significant $\not\!\!E_T$, dilepton, $\ell\gamma\not\!\!E_T$ and $\ell\ell\gamma$ event yields. We performed this step on the University of Chicago batch system and output TTGNtuples were saved on the Yale disk space (Appendix B.1) for further analysis. In Table B.1, we list the raw number of events in the datasets, the run ranges for the datasets as well as the number of events selected the datasets.

Selecting the data like this allows us to keep a copy of the data we use locally

and we can run over it more quickly.

4 Standard Model Predictions

The dominant sources of events in the $\ell\gamma\not{E}_{\rm T}b$ and $t\bar{t}\gamma$ signal sample come from leptonic W decays with associated heavy flavor production from gluon-splitting, or radiative $t\bar{t}$ events. The number of events from these types of decays are calculated using Monte Carlo (MC) event generator programs. To model the SM processes in the $\ell\gamma\not{E}_{\rm T}b$ signal sample events, we mostly use the MadGraph [44] event generation software.

The dominant sources of events passing the $t\bar{t}$ selection criteria come from $t\bar{t}$ decays. This process is generated using the Pythia generator. Large SM contributions to the $t\bar{t}$ signature also come from W decays with associated production of $b\bar{b}$, $c\bar{c}$, and a charm quark; these processes are modeled using Alpgen and Pythia.

The samples generated with MadGraph are not used by a large portion of the CDF experiment, and we describe below the parameters that we used for generating these samples. We explain how we input the decay simulations through a computer simulation of the detector, and finally how we calculate the event yields for each of these processes.

4.1 New MadGraph Samples

4.1.1 Introduction: The Matrix Element Generators

The dominant sources of events in the $t\bar{t}\gamma$ and $\ell\gamma\not{E}_{\rm T}b$ signal sample comes from $t\bar{t}\gamma$ decays, and $W\gamma$ decays with associated heavy flavor quarks. To study a large sample of these decays, and many others, we use computer simulations of the decays of the particles called MC.

The number of events in the $\ell\gamma\not{E}_{\rm T}b$ and $t\bar{t}\gamma$ signal sample due to $t\bar{t}\gamma$ production is estimated using the leading-order (LO) MC event generator program MadGraph. The resulting number of events and the samples' cross sections are listed in Table 4.1.

This program outputs 4-vectors and helicities of particles emanating from a diboson production event in an ASCII format. In addition, the information on how the particles are produced ("mother" and "daughter") is recorded, including the

energy scale and other parameters used for the matrix element calculation.

These files are then fed into the LesHouchesModule [45], which runs PYTHIA [46] to add parton fragmentation, final-state radiation and initial-state radiation (both QED and QCD). It then writes out the events in CDF HEPG[3] format. The CDF HEPG format is a code that is used to identify all of the event parameters, including kinematics and identification of objects.

These files are used as input to the CDF detector simulation program. Each of the objects from the event interacts in a computer simulation of the detector. This program outputs simulated data in a format identical to that of an actual CDF Run II event. Simulated $\ell\gamma\not{E}_{\mathrm{T}}b$ event rates can then be estimated in a manner identical to that of CDF data.

We perform an additional check of MADGRAPH MC, by generating $t\bar{t}$ MC with MADGRAPH. We then compare the generated cross sections to those measured by the CDF Top group, and see consistency.

4.1.2 $t\bar{t}\gamma$ MC Samples

We generate radiative top quark events in which the top quark decays to a W boson and b quark. The W boson then decays to a charged lepton and corresponding neutrino. In the processes either the initial quarks of the collision or charged decay products radiate a photon.

Samples are generated separately for semileptonic and dileptonic $t\bar{t}\gamma$ decays. Semileptonic means exactly one W boson decays to a charged lepton and corresponding neutrino, and dileptonic means both W bosons decays to a charged lepton and corresponding neutrino. Table 4.1 shows the amount of $t\bar{t}\gamma$ decays we have simulated for this analysis.

In a similar manner we also used MADGRAPH to simulate associated production of a W boson, a photon, and heavy flavor quark decays including: $c\bar{c}$, $b\bar{b}$, and c-quark.

[3]HEPG is a system of particle identifications contained in MC samples that allows us to know what type of processes are occurring in the computer simulation.

MadGraph allows the user to change kinematic requirements of the generated particles to match requirements for the detector, and the full list of requirements for our generated particles is shown in Appendix D.

DataSet Name	Events	Crossection (pb)
Mad_$t\bar{t}\gamma$ semileptonic	43724	0.0726349
Mad_$t\bar{t}\gamma$ dileptonic	33801	0.0216773

Table 4.1: The $t\bar{t}\gamma$ MadGraph datasets.

4.2 The other SM Processes as Sources of $\ell\gamma \not{E}_{\rm T} b$ and $t\bar{t}\gamma$ Events

We consider WW, WZ, W$c\bar{c}\gamma$, W$b\bar{b}\gamma$ and W$c\gamma$ as the other sources for $\ell\gamma \not{E}_{\rm T} b$ and $t\bar{t}\gamma$ events.

The samples we use are described below. Those listed with parentheses are common names of MC samples used by working groups at CDF. Those without the parentheses are samples which we have generated using MadGraph.

When possible we use MC samples that are in use by a large portion of the CDF experiment. We use the WW sample (ihhs1a) which is an inclusive WW decay sample used by both the Higgs group and Top group at CDF.

The generator-level MC events were run through Pythia. They were then run through the full CDF detector simulation and 5.3.3 Production, and then ntupled [27]; a tabulation of the datasets is given in Ref. [47].

The description of these MC Samples is given in Table 4.2.

DataSet Name	Events	Crossection (pb)
WZ	409648	3.65
W$\gamma b\bar{b}$	12279	0.03737
W$\gamma c\bar{c}$	14152	0.06910
Wγc	48261	0.29904
$t\bar{t}$ (ttopel)	1146088	6.1
WW (ihhs1a)	4880529	12.4

Table 4.2: SM Backgrounds to the $t\bar{t}\gamma$ Sample.

4.3 SM Processes as Sources of $t\bar{t}$ Events

The dominant source of events with a lepton, true $\not\!\!E_{\mathrm{T}}$, significant transverse energy, and 3 or more jets with at least one originating from a b-hadron is $t\bar{t}$, and W decays with associated heavy flavor decays (W+HF). The full list of MC simulations that are used for this signature, including the samples' cross sections, and their common names are listed in the Appendix in Table E.1.

4.3.1 Discussion of k-factors for MC processes

There are numerous ways in which a MC cross section may not adequately represent the SM process observed in data. In some cases, MC samples are generated solely at tree level. As a result the higher order processes which will affect a data sample's cross section are not adequately calculated in the MC. We adjust the cross section by using a multiplicative constant (k-factor) to account for the difference between the cross section at tree-level, and those from higher orders. This is the case for the W plus heavy flavor (W+HF) samples, and for Z decays. An additional multiplicative factor of 2.04 is used for W decays require, whereas the Z decays require a factor of 2 [48][4].

4.4 Calculating Event Yields of Monte Carlo Based Backgrounds

The rates of the backgrounds for our samples, as well as our signatures' acceptances, are calculated using a MC-based approach. Several electroweak processes can contribute to the $t\bar{t}\gamma$, and $\ell\gamma\not\!\!E_{\mathrm{T}}b$ samples including, WW, WZ, ZZ, as well as W$\gamma b\bar{b}$, W$\gamma c\bar{c}$, and Wγc decays. Similarly for the $t\bar{t}$ sample we use MC to model the backgrounds: W$b\bar{b}$, W$c\bar{c}$, and Wc decays, as well as diboson, and single top production.

The expected event yield to our sample is calculated using the formula:

[4]The factor 2.04 comes from the multiplication of 1.36×1.5, in accordance with [48, 49]

$$N_{\mathrm{p\bar{p}\to X}} = \sigma_{\mathrm{p\bar{p}\to X}} \cdot A \times \epsilon \cdot \int dt \cdot \mathcal{L} \tag{4.1}$$

where $\sigma_{\mathrm{p\bar{p}\to X}}$ is the theoretical cross section, of $\mathrm{p\bar{p}}$ going to a specific process X. The value $\int dt \cdot \mathcal{L}$ is the total integrated luminosity, and $A \times \epsilon$ is the acceptance of the signal times the selection efficiency. Many of the MC samples used were generated with 1 fb^{-1} statistics, so we must normalize these samples to our total integrated luminosity. The value ϵ is based on object identification and trigger efficiencies which differ between data and MC. These efficiencies are calculated from available data periods, and averaged by luminosity in the data samples, and vary by lepton type.

Furthermore for the W decay MC (W+HF, Wγ+HF) used for background predictions, there are two k-factors required to account for differences between generated MC and what is observed in the detector (Sec 4.3.1).

5 Backgrounds: Object Misidentification in the $\ell\gamma\not{E}_{\mathrm{T}}b$, and $t\bar{t}\gamma$ Signal Samples

In addition to the expectations from SM processes that produce $\ell\gamma\not{E}_{\mathrm{T}}b$ and $t\bar{t}\gamma$ events described in Section 4.1, there are backgrounds where SM processes have misidentified leptons, photons and b-tags, and/or incorrectly calculated $\not{E}_{\mathrm{T}}$. We generically call these misidentifications "fakes". To estimate the following backgrounds as precisely as possible, we use data-driven methods.

The data-driven methods are preferable because we use data taken from the detector to help us interpolate the rates at which fakes occur. Data-driven methods for fakes are preferable to MC-based background prediction as the MC does not well model the rates at which objects will be misidentified.

5.1 Misidentified Photons

Three sources of fake photons are considered: QCD jets in which a neutral hadron or photon from hadron decay mimics a direct photon, electron bremsstrahlung, and photons from tau decays where $\tau \rightarrow$ hadron $\rightarrow \gamma$. The bremsstrahlung process occurs when a high energy photon is radiated off of an electron. The electron then has much lower energy and curls away from the photon, so only the photon is detected.

5.1.1 Jets Misidentified as Photons

High-$\mathrm{p_T}$ photons are created from hadron decays in jets initiated by a scattered quark or gluon. In particular, mesons such as the π^0 or η decay to photons which may satisfy the photon selection criteria. The number of events in which a jet is misidentified as a photon expected in the $\ell\gamma\not{E}_{\mathrm{T}}b$ and $t\bar{t}\gamma$ samples are determined by measuring energy in the calorimeter nearby the photon candidate.

Photons should deposit their energy in the calorimeter in a manner similar to electrons. As photons and electrons interact in the electromagnetic calorimeter, both pair production ($\gamma \rightarrow e^+e^-$) and bremsstrahlung ($e^{\pm} \rightarrow \gamma e^{\pm}$) reactions occur

repeatedly forming a shower of particles in the calorimeter. We use the calorimeter isolation shape from electrons to model the isolation shape we expect from photons.

We construct a sample of pure electrons by looking for $Z^0 \rightarrow e^+e^-$ decays. The electrons we select have passed the electron selection cuts, and the reconstructed Z^0 mass is close to the measured Z^0 mass between 86 and 96 GeV, and the two leptons are of opposite charge. Furthermore, there is very little $\not\!\!E_T$ in the event.

To identify the shape in calorimeter isolation, we construct a sample of fake photons. An enriched fake photon sample is created with the object selection of the $\ell\gamma\not\!\!E_T b$ signature, but we reverse a quality cut on the photon candidates, requiring $\chi^2 > 20$. This rejects real photons. Furthermore we do not use isolation requirements on the photon candidates so that we can see the distribution of E_T^{iso}. The distribution in E_T^{iso}, in a cone with R=0.4 in η-ϕ space around the fake photon candidate, is shown in Fig. 5.1. We approximate this shape with a linear shape.

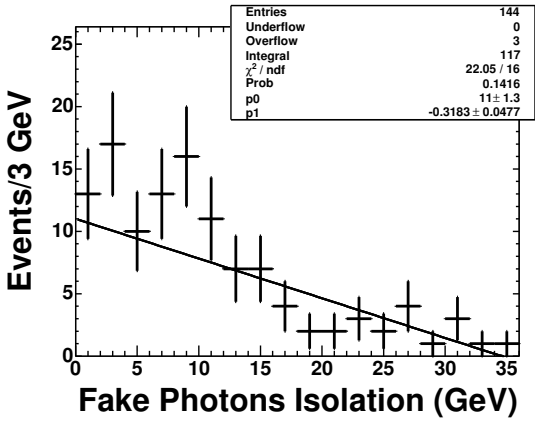

Figure 5.1: The distribution in the total calorimeter energy, E_T^{iso}, in a cone in η-ϕ space around the fake photon candidate in lepton, $\not\!\!E_T > 20$ GeV, fake photon candidate, and b-jet events. This distribution is then fit with a linear function.

Our event selection for the fake photon candidate requires the same event selections as $\ell\gamma\not\!\!E_T b$ and $t\bar{t}\gamma$, and requires the photon to pass all selection criteria except isolation requirements. Figure 5.2 shows the distribution in the total (electromagnetic plus hadronic) transverse energy isolation measured in the calorimeter, E_T^{iso}, in a cone of radius $R = 0.4$ in η-ϕ space around the photon candidate, for four samples: $e\gamma\not\!\!E_T b$, $\mu\gamma\not\!\!E_T b$, $t\bar{t}\gamma$ (e and μ channel).

These distributions are then fit to the isolation shape measured for electrons from $Z^0 \to e^+e^-$ decays plus a linear background function. Using these two templates we are able to estimate the number of events in which a jet is misidentified as a photon we have accepted.

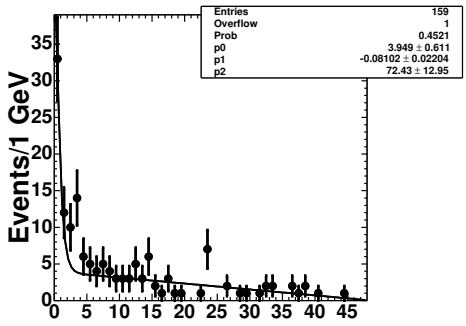

(a) Calorimeter Isolation of Photons Candidates ($e\gamma \not\!\!E_T b$)

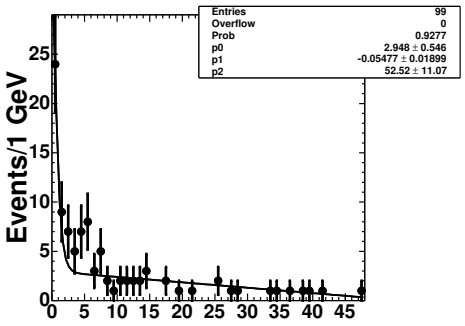

(b) Calorimeter Isolation of Photons Candidates ($\mu\gamma \not\!\!E_T b$)

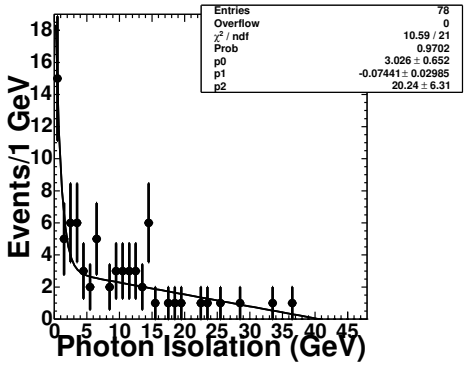

(c) Calorimeter Isolation of Photons Candidates ($t\bar{t}\gamma$ (e))

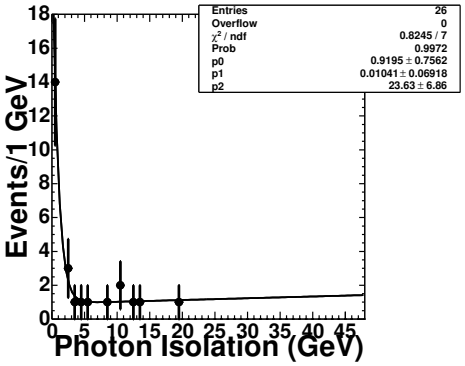

(d) Calorimeter Isolation of Photons Candidates ($t\bar{t}\gamma$ (μ))

Figure 5.2: The method and data used to estimate the number of background events from jets misidentified as photons. For each of the four samples, $e\gamma \not\!\!E_T b$ (left top), $t\bar{t}\gamma$ (e channel, right top), $\mu\gamma \not\!\!E_T b$ (left bottom), and $t\bar{t}\gamma$ (μ channel, right bottom), the number of events is plotted versus the total (electromagnetic plus hadronic) calorimeter energy, E_T^{iso}, in a cone with R=0.4 in η-ϕ space around the photon. This distribution is then fit to the shape measured for electrons from $Z^0 \to e^+e^-$ decays plus a linear background.

The number of events in which a jet is misidentified as a photon is calculated by finding the number of background events in our photon selection region. We estimate this by finding the area under the straight line in the 0-2 GeV region of isolation for each of our selections. The 0-2 GeV region is chosen because it contains nearly the entire selection region of photons.

The systematic uncertainty for this misidentification is estimated using a $\ell\gamma\not\!\!E_{\rm T}$ sample, where we select events with: a tight lepton, a photon, and substantial $\not\!\!E_{\rm T}$ (Section 7). This sample is not limited by statistics, so the uncertainty we find should be dominated by the systematic uncertainty. Using the $\ell\gamma\not\!\!E_{\rm T}$ control sample (Section 7.2), we find the value of the uncertainty by: varying our fit parameters within their uncertainties, using a quadratic background shape, and by changing the range of $E_{\rm T}^{\rm iso}$ isolation energy over which the fit is made. To be conservative, we select the largest deviation from the central value and use this as our uncertainty. We find there is about a 20% uncertainty in this method.

The predicted number of events with jets misidentified as photons is 17.07 ± 3.85 for the $\ell\gamma\not\!\!E_{\rm T}b$ signature and 7.76 ± 2.53 for the $t\bar{t}\gamma$ events.

5.1.2 Electrons Misidentified as Photons

To determine the rate at which an electron is misidentified as a photon ($e \rightarrow \gamma$) in the central EM Calorimeter (CEM) we use Method-B [50]. The method calculates the probability for an electron passing the standard electron cuts to fake a photon by extracting the ratio of the number of $Z^0 \rightarrow$ e+"γ" events relative to $Z^0 \rightarrow e^+e^-$ events [51].

A $Z^0 \rightarrow$ e+"γ" event occurs when a Z^0 decays to two electrons and one of them radiates off a photon. The electron that radiated off the photon loses its energy, and is not detected. The ratio of $Z^0 \rightarrow$ e+"γ" events to $Z^0 \rightarrow e^+e^-$ events gives a probability for an electron to fake a photon.

This is further refined by comparing the photon's $E_{\rm T}$ to similar $E_{\rm T}$'s of electrons. The probability of an electron to fake a photon is parameterized as a function of the electron's $E_{\rm T}$.

The number of events in which an electron is misidentified as a photon from the $\ell\gamma\not\!\!E_{\rm T}b$ sample is found by selecting events with: a b-jet, substantial $\not\!\!E_{\rm T}$, a tight lepton, and an electron capable of being misidentified as photons. Electrons capable of being misidentified as photons include all tight, and loose electrons with $E_{\rm T}$ greater than 10 GeV. For the $t\bar{t}\gamma$ sample, the event selection is further refined

to include more than 2 jets, and H_T greater than 200 GeV.

Each event is weighted by the probability of the electron to be misidentified as a photon divided by the number of possible combinations of electrons capable of being misidentified as a photon in the event.

The predicted number of events with electrons misidentified as photons is 6.36± 0.58 for the $\ell\gamma \not\!\!E_T b$ signature and 1.47 ± 0.25 for the $t\bar{t}\gamma$ events.

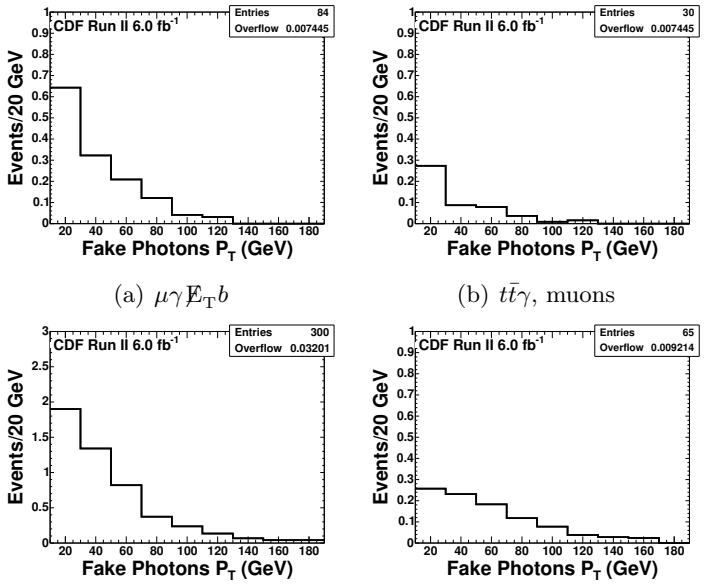

(a) $\mu\gamma \not\!\!E_T b$ (b) $t\bar{t}\gamma$, muons

(c) $e\gamma \not\!\!E_T b$ (d) $t\bar{t}\gamma$, electrons

Figure 5.3: Spectrum of electrons capable of being misidentified as a photon. For a) we selected $\mu e \not\!\!E_T b$ events, and then applied $e \to \gamma$ fake rate [50], and for b) we further required $H_T > 200$ GeV, and $N_{jets} > 2$. For c) we selected $ee \not\!\!E_T b$ events, and then applied $e \to \gamma$ fake rate [50], and for d) we further required $H_T > 200$ GeV, and $N_{jets} > 2$.

5.1.3 $\tau \to \gamma$ Fake Rate

In addition to estimating the number of $\ell\gamma \not\!\!E_T b$ and $t\bar{t}\gamma$ events that arise from a jet being misidentified as a photon ($j \to \gamma$), we also estimate the number of events in which a tau could be misidentified as a photon ($\tau \to \gamma$).

The fake rate of a ($j \to \gamma$) as a photon is on the order of 10^{-4} or smaller [52]. The rate for taus to fake photons is expected to be on the order of 10^{-2} which is two orders of magnitude larger. Due to the way jets fragment, it is much harder for

a jet to produce a single isolated (high p_T) π^0 compared to a tau.

We evaluate the $\tau \to \gamma$ misidentification rate from the $t\bar{t}$ Monte Carlo sample (ttopel sample). In the first step we select events on HEPG level with of the W's going to $\tau\nu$, $\tau \to$ hadron $\to \gamma$. Then we apply our analysis cuts to the stripped sample.

In total for $\ell\gamma\not{E}_T b$ category we observe 0.74 ± 0.098 $\tau \to \gamma$ events, and for the $t\bar{t}\gamma$ category we observe 0.31 ± 0.098 $\tau \to \gamma$ events.

5.2 Misreconstructed b-jets (Mistags)

B hadrons have a long lifetime and, on average, are able to travel about 450 μm before decaying. After this distance, the hadron decays, and the displaced vertex can be measured. A secondary vertex can also be identified when poorly reconstructed tracks seem to cross each other near the origin. Identifying jets which come from B hadrons is called "tagging". A secondary vertex that does not originate from a heavy flavor (HF) quark decay and results in a light flavored jet being b-tagged is called a mistag.

The performance of b-tagging algorithms is typically characterized by the efficiency for identifying real b-jets and the rate at which jets are mistakenly tagged. The mistag rate is determined in a data-driven fashion, using a parametrized tag rate measured in generic jet events. We are looking for the rate at which a jet which does not arise from a b quark is identified as being a heavy flavored jet. The term taggable means that the jet has more than one SecVtx track coming from it. SecVtx is the name of the algorithm we use to tag our jets. Both of these conditions are common for jets occurring from B hadron decay.

Positive and negative tags for jets are accounted for separately, with the negative tag rate being used to model the mistag rate. The positive tag rate is the rate where a potential secondary vertex appears in front of a primary vertex. Furthermore the tracks coming from the secondary vertex move in the correct direction as a heavy flavor decay. The negative tag rate is the rate at which potential secondary vertices appear behind the interaction point. The tracks coming from a negative tag appear

to be coming from the wrong direction relative to that of a heavy flavor decay. These secondary vertices are inconsistent with those jets from heavy flavor decays.

The negative tag rate is found to be well parameterized by five jet parameters: jet E_T, number of good SVX tracks, the sum of all jet E_T in the event, jet η, and jet ϕ. To calculate the negative tag rate we follow the procedure described in Ref. [53], which is called the "mistag matrix" method.

The mistag matrix parameterizes the rate at which a jets is misidentified as a heavy flavor jet as a function of many variables such as: the jet's E_T, η, ϕ. The mistag matrix finds the negative and positive tag rates for each jet, and then we are able to use them to estimate the likelihood of an event to have a jet wrongly tagged as a heavy flavor jet.

In an event loop, first we cache all of the jets with $E_T > 10$ GeV, $|\eta| < 2.4$, so the mistag matrix knows the event Sum of E_T of the jets, and all of the jet information it requires.

The mistag matrix identifies the parameters α and β. The former accounts for the number of of heavy flavor events in the negative-tagged sample, and the latter accounts for the heavy flavor content of the pretag sample [54]. The average per-jet mistag probability, R^-_{mistag}, α, and β are defined as:

$$\mathrm{R}^-_{\mathrm{mistag}} = \frac{N^-_{light} + N^-_{heavy}}{N^{pre}_{light} + N^{pre}_{heavy}}$$

$$\alpha = \frac{N^+_{light}}{N^-_{light} + N^-_{heavy}}$$

$$\beta = \frac{N^{pre}_{light} + N^{pre}_{heavy}}{N^{pre}_{light}}$$

$$\alpha\beta\mathrm{R}^-_{\mathrm{mistag}} = \frac{N^+_{light}}{N^{pre}_{light}}$$

The positive and negative signs show whether a jet was tagged as a b-jet (+) or was not tagged as a b-jet (-). The pre superscript, dictates the number of objects in the sample before the tagging value was applied. The subscript heavy denotes either

b or c flavor jets. The parameters α, β, and R^{-}_{mistag} were determined using Monte Carlo and parton to observed jet matching. The results are then compared to data for inclusive jets samples, and corrected with an overall scale factor.

After the jet information is cached, we loop over the identified jets again and get the predicted tag rates and errors for the event. We use the per-jet mistag rate for the event and find the probability for a taggable jet to be mistagged.

The total number of mistagged events, N_{-} for a signature is:

$$N_{-} = \sum \left(1 - \prod_{j}^{N_{jets}} \bar{P}_j \right) \tag{5.1}$$

where $\bar{P}_j$ is the probability that the jet in question, j, was tagged correctly (the complement of the probability of a jet being mistagged). The mistag probability for the event is the complement of the event having no mistagged jets. The mistagged probability for each event is summed over all events matching the criteria of a signature without requiring the b-tagged jet. The product runs over all jets in the event, and the sum runs over all events matching the event selection for a mistagged event; the $\ell\gamma \not{E}_{\mathrm{T}} b$ and the $t\bar{t}\gamma$ event selection is the same but there is no requirement of a b-tag.

The number of non heavy flavor jets which are mistagged as heavy flavor jets is overestimated by this procedure. We compensate for this by finding the number of events without heavy flavor relative to the total number of events.

We isolate in data a sample of $\ell\gamma \not{E}_{\mathrm{T}} b$ and $t\bar{t}\gamma$ events without requiring a b-tagged jet; these are the pretagged samples. We subtract off the contribution to this pretagged sample the number of events that contain true heavy flavor contributions: $t\bar{t}\gamma$, Wγ + HF, QCD events that have objects misidentified as leptons and $\not{E}_{\mathrm{T}}$ reconstructed in the signal range, etc.

$$N_{pretagged}^{W\gamma+LF} = N_{pretagged}^{data} - N_{pretagged}^{QCD} - N_{pretagged}^{t\bar{t}\gamma} - N_{pretagged}^{diboson} - N_{pretagged}^{W\gamma+HF} \quad (5.2)$$

Diboson includes the contribution from WW and WZ decays. This procedure is described more fully in Ref. [55].

We then normalize the original overestimate by the fraction $\frac{N_{pretagged}^{W\gamma+LF}}{N_{pretagged}^{data}}$. This is the number of mistagged events due to events without a HF quark.

The total number of mistagged events in the $\ell\gamma\not{E}_{\mathrm{T}}b$ signal is 32.56 ± 2.75, and in the $t\bar{t}\gamma$ sample it is 2.74 ± 0.51 events.

5.3 QCD (Jets Misidentified as Leptons and $\not{E}_{\mathrm{T}}$)

The QCD contribution to our signal occurs when we have events that look like our signature, however the leptons have come from neither a W nor Z boson source. In this case, the lepton has likely come from a jet. We generically call these events in which a jet is misidentified as a lepton and $\not{E}_{\mathrm{T}}$, QCD fakes.

In each event, after leptons and jets have been identified, we correct the jet $\mathrm{E_T}$ based on calorimeter response, and after correcting jet $\mathrm{E_T}$ [41], we recalculate the $\not{E}_{\mathrm{T}}$ based on the new jet $\mathrm{E_T}$ values (as discussed in Section 3.5.1).

A lepton which comes from a jet should be identified as a jet. When we instead identify this jet as a lepton, we do not correct the jet's $\mathrm{E_T}$, so "non-W/Z" leptons can cause a mismeasurement of $\not{E}_{\mathrm{T}}$.

To estimate the contribution of our signal due to QCD fakes, we follow the lead of B. Cooper and A. Messina [56] using the antielectron method. Antielectrons are jets which pass the kinematic requirements of electrons, but which fail two or more quality cuts. These objects are kinematically similar to electrons and we use them to mimic non-W/Z leptons. The full selection criteria of antielectrons can be seen in Table 5.1.

Calculating the QCD background to the $\ell\gamma\not{E}_{\mathrm{T}}b$ sample takes a couple of steps. First, we plot the spectrum of $\not{E}_{\mathrm{T}}$ of events in data that have: an identified lepton,

Antielectron Must Pass all of these	
Variable	AntiElectron
E_T	> 20 GeV
Track $\|z0\|$	< 60 cm
Fractional Calorimeter Isolation E_T	< 0.1
E/P	< 2.0
Track quality cuts	3 Ax, 2 St SL x 5 hits
Antielectron Must FAIL at least two of these	
Had/Em	$< 0.055 + 0.00045 \times E$
L_{shr}	< 0.2
χ^2_{Strips}	< 10
ΔX	$\|\Delta X\| > 3.0$ cm; if $E_T > 100$ GeV -3.0 cm $> Q_{trk} \times \Delta X$ or $Q_{trk} \times \Delta X > 1.5$ cm
$\|\Delta Z\|$	> 5.0 cm; if $E_T > 100$ GeV > 3.0 cm; otherwise

Table 5.1: Cuts required for antielectrons. Antielectrons are chosen in such a way that all kinematic variables, and variables which are strongly correlated to kinematic variables, must be passed. This makes the objects kinematically very similar to electrons. The antielectrons are required to fail at least two quality cuts which identify that this object is not an electron.

an identified photon, and a b-tagged jet. We keep separate the yields from electron and muons. Next we compare the spectrum of $\not\!\!E_T$ observed in data to what we observe from MC processes (normalized by cross sections and luminosity, etc.), again requiring an identified lepton, a b-tagged jet, and a photon. Then we compare the 0-20 GeV region of the $\not\!\!E_T$ distribution from data and the the sum of all of our MC processes. The difference between these distributions should be due to QCD contributions.

We expect the dominant contribution of QCD to be in the low-$\not\!\!E_T$ region, below 20 GeV of $\not\!\!E_T$. The difference between data and MC with $\not\!\!E_T$ below 20 GeV is fit using the antielectron sample: a b-tagged jet, a photon, and an antielectron. The antielectron sample is scaled to minimize a χ^2 fit between the antielectron sample and the difference between data and MC samples in the 0-20 GeV $\not\!\!E_T$ region. The QCD contribution is estimated from this scaled antielectron distribution by summing the antielectron $\not\!\!E_T$ distribution from 20 GeV and higher.

The distributions used to find this background are shown in Figure 5.4. The

uncertainty on these measurements comes from the statistical uncertainty on the number of events, as well as the systematic uncertainty due to the χ^2 fit. We use the authors' quoted systematic uncertainty of 8%.

To calculate the number of QCD events for the $t\bar{t}\gamma$ signatures, we repeat this process requiring the samples to pass our selection criteria. The $t\bar{t}\gamma$ samples require $H_T > 200$ GeV, and at least three jets. Using this prescription, the total number of QCD events in the $\ell\gamma\not{E}_T b$ sample is 15.92 ± 7.38, and in the $t\bar{t}\gamma$ sample there are 0.40 ± 0.38 events.

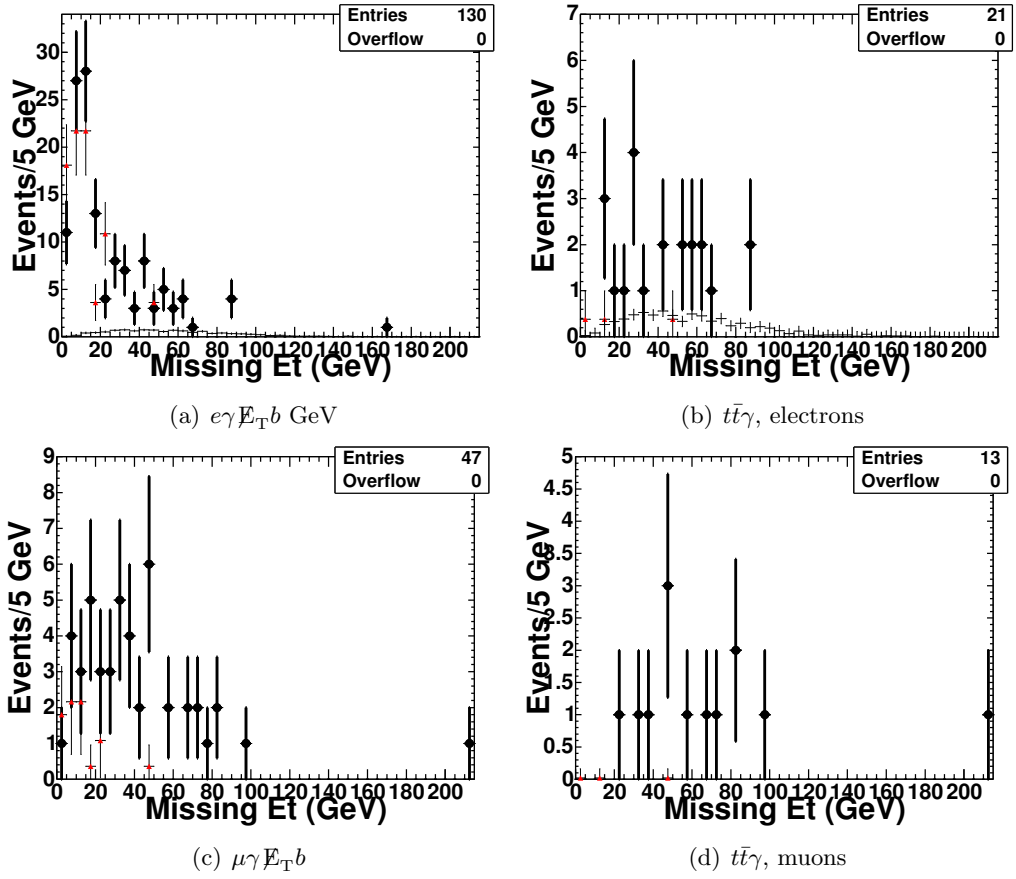

(a) $e\gamma\not{E}_T b$ GeV

(b) $t\bar{t}\gamma$, electrons

(c) $\mu\gamma\not{E}_T b$

(d) $t\bar{t}\gamma$, muons

Figure 5.4: Spectrum of antielectrons used to calculate QCD fakes (red triangles). We selected events with a bjet, a photon, and an antielectron, and then scaled its $\not{E}_T$ distribution below 20 GeV to those distributions from data of $\ell\gamma\not{E}_T b$ without a $\not{E}_T$ cut (black points). The process was repeated analogously for the $t\bar{t}\gamma$ samples.

5.4 Double Counting of Fake Events

We know in the case of data-driven backgrounds there is a possibility that events used to calculate a given background may have an overlap with events used to calculate a second background. When this situation occurs, it results in an overestimate of background events because we have double counted.

We describe an example procedure of how we estimate and remove double counting from a pair of our background estimates:

1. consider $e \to \gamma$ background. It is obtained by selecting $e\ell b\not{E}_{\mathrm{T}} + \mathrm{N_{jets}}$ events, and each event is then multiplied by the fake rate of an electron being misidentified as a photon ($f.r.(e \to \gamma)$). We get the expected number of events with an electron misidentified as a photon:

   $\mathrm{N1} = (\mathrm{e} \to \gamma)\ell \mathrm{b}\not{E}_{\mathrm{T}} + \mathrm{N_{jets}}$

2. Now let's estimate the number of events with a mistagged jet, $j \to b$. We start from $\gamma\ell j\not{E}_{\mathrm{T}} + N_{jets}$, and each event is then multiplied by the possibility of mistagged jet ($f.r.(j \to b)$). We get the expected number of mistagged events

   $\mathrm{N2} = \gamma\ell(\mathrm{j} \to \mathrm{b})\not{E}_{\mathrm{T}} + \mathrm{N_{jets}}$

3. Some of the events with a fake photon ($e \to \gamma$) also have a mistagged jet ($j \to b$), so if we just take the total N1+N2, then we will overestimate our backgrounds. We need to subtract the overlap between the two, which is

   $\mathrm{N1N2} = (\mathrm{e} \to \gamma)\ell(\mathrm{j} \to \mathrm{b})\not{E}_{\mathrm{T}} + \mathrm{N_{jets}}$

   and therefore

   $\mathrm{N} = \mathrm{N1} + \mathrm{N2} - \mathrm{N1N2}$

4. To get this, we should apply step **2** to the events from which we obtain ($e \to \gamma$) background. Therefore, we take events with $e\ell j\not{E}_{\mathrm{T}} + \mathrm{N_{jets}}$ and multiply each of them by $f.r.(e \to \gamma) \times f.r.(j \to b)$

In the next six subsections we describe the exact procedures we use for finding the overlap between each of our four data-driven background models.

5.4.1 Double Counting of Events in Which a Jet is Misidentified as a Photon, and an Electron is Misidentified as a Photon

To measure the number of overlap of events with both jets capable of being misidentified as a photon and electrons capable of being misidentified as a photon, the event selection requires both a jet capable of being misidentified as a photon, and an electron capable of being misidentified as a photon.

To find this number of double counting in $\ell\gamma\not{E}_{\mathrm{T}}b$ signature we require: substantial $\not{E}_{\mathrm{T}}$, a b-tagged jet, a tight lepton, an electron capable of being misidentified as a photon, and a jet capable of being misidentified as a photon.

The roughly linear behavior in isolation for photon candidates with χ^2 greater than 20 was shown in Section 5.1.1. Further requiring the isolation on these objects be less than 2.0 GeV we have an object which is not a photon, but is kinematically very similar. We will assume the fake rate of these objects being misidentified as a photon is unity.

The event also has an electron capable of being misidentified as a photon. In Section 5.1.2, we explained that there is a probability of the electron being misidentified as a photon, and how it is calculated.

The events which have both an electron capable of being misidentified as a photon and a jet being misidentified as a photon are weighted by the probability of an electron in the event being misidentified as a photon.

This process is done in an analogous way for the $t\bar{t}\gamma$ selection. We use the same event selection but require the total number of jets in the event be more than 2, and the $\mathrm{H_T} > 200$ GeV. However, the jet that could be misidentified as a photon must have $\mathrm{E_T}$ above 25 GeV in this case. We apply a tighter χ^2 for low $\mathrm{E_T}$ photons and assume that there are no low $\mathrm{E_T}$ jets which could be misidentified as photons. This does imply we will be slightly underestimating the number of double counted events.

5.4.2 Double Counting of Events Where a Jet is Capable of being Misidentified as a Photon, and Jets Mistagged as b-jets

The overlap of backgrounds of a jet capable of being misidentified as a photon, and a jet misidentified as a b-jet occurs when there is jet in the event which is kinematically similar to a photon, and a jet which could be incorrectly tagged as a b-jet.

For the $\ell\gamma\not\!\!E_{\rm T}b$ event selection, we require: a tight central lepton, $\not\!\!E_{\rm T}$, a taggable jet, and a jet capable of being misidentified as a photon.

Recall we showed in Section 5.1.1 the roughly linear behavior of jets capable of being misidentified as a photon by requiring the $\chi^2_{\rm CES} > 20$. If we further require the isolation on these objects be less than 2.0 GeV we have an object which is not a photon, but is kinematically very similar. We will assume the fake rate of these objects being misidentified as a photon is unity.

We find the probability for the event to have a mistagged jet as in Section 5.2. The events with both a jet capable of being misidentified as a photon, and a potentially mistagged jet are weighted by the mistag probability and all such events are summed over. This sum is the double counting of jets capable of being misidentified as photons, and a potentially mistagged jet.

An analogous procedure is done for those events in the $t\bar{t}\gamma$ sample, where we further require three or more jets, and $\rm H_T > 200$ GeV. However, the jet capable of being misidentified as the photon must have $\rm E_T$ above 25 GeV in this case. We apply a tighter χ^2 for low $\rm E_T$ photons and assume that there are no such fake photons. This does imply we will be slightly underestimating the number of double counted events.

5.4.3 Double Counting of Electrons Capable of Being Misidentified as Photons, and Jets Mistagged as b-jets

The overlap of of jets mistagged as b-jets and those events with electrons capable of being misidentified as a photon in the $\ell\gamma\not\!\!E_{\rm T}b$ sample must have both a taggable

jet, and an electron capable of being misidentified as a photon.

To find the number of double counted events in the $\ell\gamma\not\!\!E_{\rm T}b$ signature we require: a tight central electron, substantial $\not\!\!E_{\rm T}$, an electron capable of being misidentified as a photon, and a taggable jet.

The procedure for this case of double counting is to: find the probability the electron will fake a photon, find the mistag probability, and multiply these two probabilities together, then sum this probability for all such events.

The mistag probability is found in the same manner as described in Section 5.2. The probability of an electron being misidentified as a photon is found in the same way as described in Section 5.1.2

The product of the two probabilities is the probability of both the electron being misidentified as a photon, and the event having a mistagged jet. We weight all events in our selection with the probability product, and sum over all such events. The sum is the total number of double counted events for the $\ell\gamma\not\!\!E_{\rm T}b$ sample.

For the $t\bar{t}\gamma$ sample, the event must have $\rm H_T > 200$ GeV and more than 2 jets, and the procedure is repeated analogously.

5.4.4 Double Counting of QCD Misidentifications, and Jets Mistagged as b-jets

The overlap of events due to QCD fakes and mistagged events occurs when an event has a jet being misidentified as a lepton and a jet which could have been mistagged as a b-jet.

The double counting of events in the $\ell\gamma\not\!\!E_{\rm T}b$ signature will require: a central photon, a lepton which appears to have come from a jet, a jet which may have been mistagged, and substantial $\not\!\!E_{\rm T}$.

We will use an antielectron to play the role of the lepton which appears to come from a jet, and we require the lepton have track isolation less than 4 GeV. We weight the event by the probability that the antielectron event will be misidentified as a lepton in this case we assume that probability to be unity.

We further weight the event by the probability that the event was mistagged,

following the same procedure as in Section 5.2. We sum over all such weighted events, and the resulting sum is the number of double counted QCD fakes, and mistagged events for the $\ell\gamma\not{E}_{\rm T}b$ sample.

This procedure is repeated analogously for the $t\bar{t}\gamma$ event selection. We require $H_{\rm T} > 200$ GeV, three or more jets, and the photon must pass the χ^2 cut.

5.4.5 Double Counting of QCD fakes, and Jets Capable of Being Misidentified as Photons

To find the number of double counted events with QCD fakes, and jets misidentified as photons events for the $\ell\gamma\not{E}_{\rm T}b$ signal, we require an antielectron, a b-tagged jet, and substantial $\not{E}_{\rm T}$ uncorrected due to the antielectron. The reasoning for this is described in Sec. 5.4.4. For these events the lepton is an antielectron, and the photon is a fake photon candidate. The fake photon candidate passes the photon cuts except we require $\chi^2_{\rm CES} > 20$, and require the isolation to be less than 2.0 GeV. The antielectron must have a track isolation less than 4 GeV to enter our selection criteria for $\ell\gamma\not{E}_{\rm T}b$. This event looks like a jet misidentified as a photon event, and like a QCD event for the $\ell\gamma\not{E}_{\rm T}b$ signal. For the $t\bar{t}\gamma$ event selection, we further require $H_{\rm T}$ greater than 200 GeV and three or more jets, and the $E_{\rm T}$ of the photon must be greater than 25 GeV. We are assuming that with the tight χ^2 cut there are no fake photons; this is a conservative estimate.

5.4.6 Double Counting of QCD fakes, and Electrons Misidentified as Photons

There is a potential for overlap in the $\ell\gamma\not{E}_{\rm T}b$ sample where there could be a lepton which came from a jet decay, and also an electron misidentified as a photon. To find events that will be double counted in these backgrounds in the $\ell\gamma\not{E}_{\rm T}b$ sample we require: a central photon, substantial $\not{E}_{\rm T}$, a b-tagged jet, an electron capable of being misidentified as a photon, and a lepton due to a QCD fake.

For the lepton due to a QCD fake we use an antielectron, and we require the antielectron to have a track with isolation less than 4.0 GeV. We assume the

probability for this antielectron to fake a lepton to be unity.

We then further weight the event by the probability that the electron is misidentified as a photon (as described in Section 5.1.2). We sum over all such weighted events, and the resulting sum is the number of double counted events for the $\ell\gamma\not{E}_{\mathrm{T}}b$ sample.

We further require $\mathrm{H_T}$ greater than 200 GeV and three or more jets (not including the antielectron), and the photon χ^2 requirement to pass the $t\bar{t}\gamma$ selection criteria. Then the double counting is calculated in an analogous way.

6 Fakes of the $t\bar{t}$ signature

The $t\bar{t}$ signature has only two sources of objects being misidentified, mistagged jets, and QCD contamination. When computing the yields of fakes for the $t\bar{t}$ signature, the methods are kept very close to the $t\bar{t}\gamma$ and $\ell\gamma\not{E}_{\mathrm{T}}b$. However, there are some differences and we explain those in the sections that follow.

6.1 Mistag estimate

To find the number of events with light flavor jets misidentified as b-jets, the same prescription in Section 5.2 is followed for caching jet information from our events. For the $t\bar{t}$ sample, we require a lepton, $\not{E}_{\mathrm{T}} > 20$ GeV, $\mathrm{H_T} > 200$ GeV, three or more jets, and $\mathrm{M_T}$ must be greater than 10 GeV for muons or 20 GeV for electrons. As in Section 5.2, at least one of these jets must be taggable. The event is then weighted by the probability of at least one of the jets being mistagged. A mistag estimate is then the summation of all such weighted events.

As was the case in Section 5.2, some events that identified as mistagged in the $t\bar{t}$ signature will have had true heavy flavor quarks in the event. We correct the original estimate based on our understanding of events that pass our cuts. We isolate in data a sample of events with the $t\bar{t}$ event selection, but we do not require a b-tagged jet. This sample is called the pretagged $t\bar{t}$ sample and has: one tight lepton, three or more jets, $\mathrm{H_T} > 200$ GeV, $\not{E}_{\mathrm{T}} > 20$ GeV, and the $\mathrm{M_T}$ selection.

From the pretagged sample, we subtract off the contribution of events that contain true heavy flavor contributions: $t\bar{t}$, QCD, single-top, W+HF, etc.

$$N^{W+LF}_{pretagged} = N^{data}_{pretagged} - N^{QCD}_{pretagged} - N^{t\bar{t}}_{pretagged} - N^{diboson}_{pretagged} - N^{singletop}_{pretagged} - N^{W+HF}_{pretagged} \tag{6.1}$$

Where diboson includes: WW, WZ, and ZZ contributions.

The original prediction is scaled by the ratio of $\frac{N^{W+LF}_{pretagged}}{N^{data}_{pretagged}}$. This fraction is the number of mistagged events due to events with a tight lepton, $\not\!\!E_T > 20$ GeV, $H_T > 200$ GeV, satisfying the M_T cuts, but with no true heavy flavor contribution. The scaled result is called the Method 2 mistag estimate. The total prediction for the number of events with misidentified b-tagged events in the $t\bar{t}$ sample is 572 ± 46 events.

6.2 QCD estimate

The estimate for the number of QCD events which pass our selection cuts for the $t\bar{t}$ signature is calculated as outlined by B .Cooper, A .Messina [56] (and in Section 5.3 however we have dropped the requirement for a tight photon). We begin by taking the total yield of events from data with a tight lepton, a b-jet, $H_T > 200$ GeV, no $\not\!\!E_T$ cut, and the M_T is greater than 20 GeV for electrons and 10 GeV for muons. The QCD yield is calculated for electron and muon channels separately. The events in data are plotted as a function of the $\not\!\!E_T$ for the event. The $\not\!\!E_T$ distribution due to mistagged events without a $\not\!\!E_T$ cut is estimated using a Method 2 estimate as described in Section 6.1. We then add to the mistagged distribution the MC distributions of events from $t\bar{t}$, diboson (WW, WZ, and ZZ), W plus heavy flavor distributions, etc. In the 0-20 GeV of $\not\!\!E_T$ the yield from data is greater than that expected from the combination of MC samples and mistagged events. These surplus events are due to QCD events, and we use antielectron events to estimate the number of events due to QCD processes.

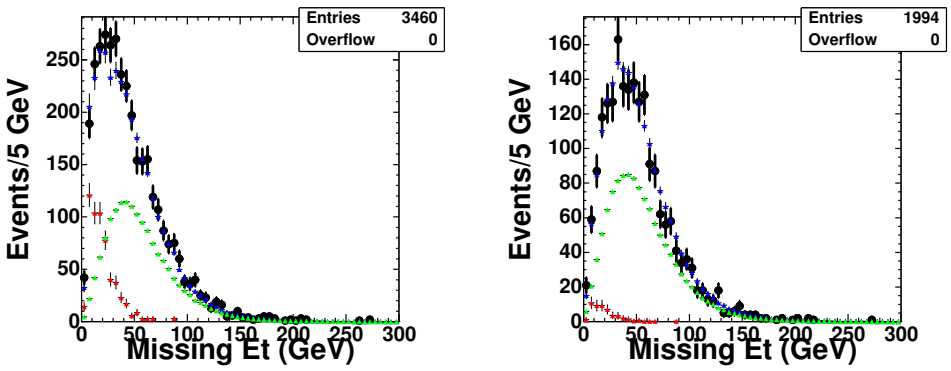

(a) $t\bar{t}(e)$ (b) $t\bar{t}(\mu)$

Figure 6.1: Antielectron and data distribution for the $t\bar{t}$ signature. The red points are scaled antielectrons, green points are from the $t\bar{t}$ MC, and blue is all MC, as well as the distribution of mistags and the antielectrons summed together. We see good agreement in the 0-20 GeV region which determines the scale factor of the antielectrons, and the 20-∞ GeV Region shows good agreement as well. The antielectrons' distributions show that the majority of the QCD signal is in the low $\not\!\!E_{\mathrm{T}}$ range.

The antielectron distribution comes from the high-p_{T} electron stream data. The antielectron events require: an antielectron a b-tagged jet, three jets or more, $H_{\mathrm{T}} >$ 200 GeV, and satisfy the M_{T} cut. We plot the $\not\!\!E_{\mathrm{T}}$ from these events, and scale the antielectron distribution to match the difference between the yields from data and MC and mistag sum in the 0-20 GeV $\not\!\!E_{\mathrm{T}}$ distribution.

The total amont of QCD events in our signal region is the sum of the scaled number of antielectron events which have $\not\!\!E_{\mathrm{T}}$ in the signal region. For the systematic uncertainty, we use the same fraction as quoted by the authors of this method, 8%. We find the total number of QCD background events in the $t\bar{t}$ sample to be 240 ± 40 events.

6.3 Double Counting of QCD fakes and Jet Mistagged as b-jets

In Section 5.4.4 we described the procedure for measuring the number of double counting we had between events that are likely due to QCD and events that are likely due to light jets being misidentified as heavy flavor jets. However because we use the Method 2 estimate, there is no longer double counting to measure. Our

mistagging estimate in Eq. 6.1 shows the removal of background due to mistagged QCD events. Furthermore, in our QCD estimate, we account for events that are due to mistagged b-jets.

An iterative process is used to find the number of events with mistags or due to QCD contribution in the $t\bar{t}$ signal. We begin by estimating the number of Method 2 mistags assuming no QCD events. Using the Method 2 estimate of mistags for this sample, we then calculate the number of events due to QCD using the antielectron method described above.

Using this information we find N_{QCD} in Eq. 6.1. We recalculate the number of mistagged events again with the new N_{QCD} value, and use the number of mistagged events in the antielectron method, to find N_{QCD} again.

We repeat this process until we see no changes in the QCD or mistag estimates. This takes two or three iterations depending on the lepton channel.

7 Control Samples

Several control samples such as a dileptonic and photon ($Z\gamma$) sample, a lepton, photon and $\not\!\!E_{\rm T} > 20$ GeV ($\ell\gamma\not\!\!E_{\rm T}$) sample, and a lepton, $\not\!\!E_{\rm T} > 20$ GeV, and more than two jets, and transverse mass cut (pretagged $t\bar{t}$) sample, were used to validate our data-driven backgrounds and understanding of our signals.

These samples were constructed to be very similar to signatures we are looking for and/or involve many of the same objects. All of the samples have large statistics which provides a nice workbench for both our understanding of the individual objects, as well as the background methods that we use for our main analysis.

The samples we are primarily interested in are subsets of these control samples. However we still consider these control regions since, in the $\ell\gamma\not\!\!E_{\rm T}b$ sample there are 85 signal events in the $\ell\gamma\not\!\!E_{\rm T}$ control region of 8276 events. In the $t\bar{t}$ sample there are 4429 signal events compared to the 18987 events in the pretagged $t\bar{t}$ sample.

7.1 The $Z\gamma$ Control Sample

We construct a $Z\gamma$ sample requiring events which have two opposite-signed same-flavor leptons, and a photon, and the invariant mass of the two leptons and photon must be between 86 and 96 GeV.

This event selection selects only $Z\gamma$ events with a minuscule component due to jets misidentified as photons. We use this event selection to measure the cross section of $Z\gamma$ in a sample-rich environment. We find the cross section for $Z\gamma$ to be about 6.3 pb for our object selection. Here we are using merely standard lepton and photon selection cuts found in Tables 3.1, 3.2, and 3.4.

For the sum of the $ee\gamma$ and $\mu\mu\gamma$ samples, Figure 7.1 shows the observed distributions of: a) the three-body mass of $\ell\ell\gamma$ system, b) the missing transverse energy, $\not\!\!E_{\rm T}$, c) the $\rm E_T$ of the leptons of the event, and d) the $\rm E_T$ of the photon. We see very good agreement between the data and the MC simulation.

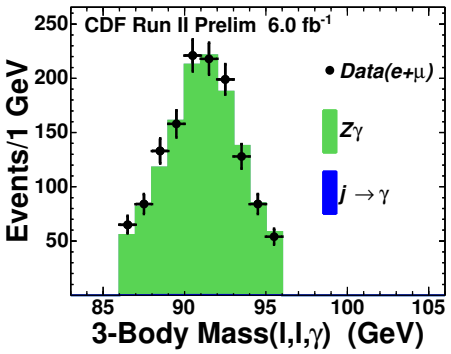

(a) Invariant mass of the two leptons and photon in $Z\gamma$ events

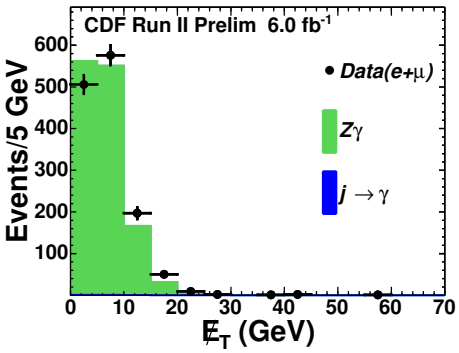

(b) $\not\!\!E_T$ from $Z\gamma$ events

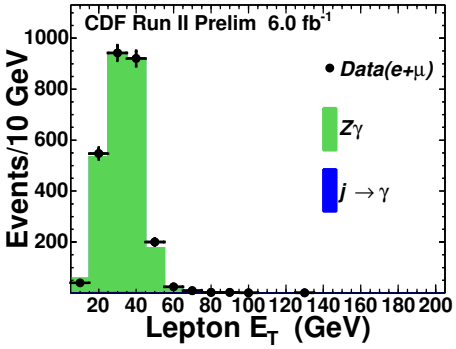

(c) E_T of electrons and p_T of muons from $Z\gamma$ events

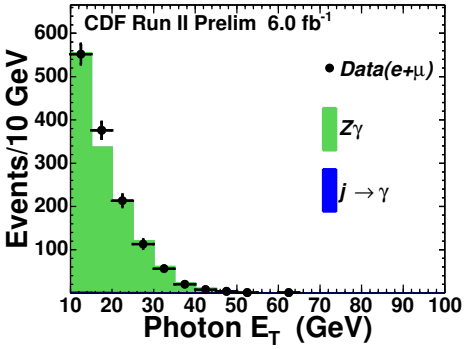

(d) E_T of photons from $Z\gamma$ events

Figure 7.1: Kinematic distributions for $Z\gamma$ events showing a) the three-body mass of $\ell\ell\gamma$ system, b) the missing transverse energy, $\not\!\!E_T$, c) the E_T of the leptons of the event, and d) the E_T of the photon.

7.2 The $\ell\gamma\not\!\!E_T$ Control Sample

The $\ell\gamma\not\!\!E_T$ sample is chosen to be similar to the $\ell\gamma\not\!\!E_T b$ sample. We looked for high-p_T electrons or muons, $\not\!\!E_T > 20$ GeV, and a photon with $E_T > 10$ GeV. This sample has 4462 $e\gamma\not\!\!E_T$ events, and 3814 $\mu\gamma\not\!\!E_T$ events. This signal is dominated by $W\gamma$ events, and events where jets are misidentified as photons.

We are following the background prescriptions of $\ell\gamma\not\!\!E_T b$ and $t\bar{t}\gamma$ for the $\ell\gamma\not\!\!E_T$ sample. The $\ell\gamma\not\!\!E_T$ sample is constructed to better understand some of our data-driven backgrounds: jets misidentified as photons, electrons misidentified as photons, and QCD. The prescriptions are discussed in greater detail in Secs. 5.1.1, 5.1.2, and 5.3 respectively.

Unlike the $\ell\gamma\not{E}_{\rm T}b$ and $t\bar{t}\gamma$ samples, we are not statistics limited when we find the number of events with jets misidentified as photons in this sample, and this helps us to calculate the systematic uncertainty on the number of events of jets misidentified as a photon background measurement.

The electrons misidentified as photons background is small, relative to $W\gamma$ and events where a jet is misidentified as a photon, in this sample. However, it is still an important measurement, and the $\ell\gamma\not{E}_{\rm T}$ sample allows a large-scale check of our method.

The QCD background measurement is a large background in the $\ell\gamma\not{E}_{\rm T}$ sample and is estimated as mentioned above, and allows us to check the systematic errors on the measurement. We use the $Z\gamma$ cross section we measured in the previous section to scale the $Z\gamma$ sample. We present the total event yields and SM prediction for our $\ell\gamma\not{E}_{\rm T}$ control sample in Table 7.1.

The backgrounds due to misidentifications for the $\ell\gamma\not{E}_{\rm T}$ sample included: jets misidentified as a photon, electrons misidentified as a photon, and leptons and $\not{E}_{\rm T}$ from QCD events. Double counting in these three categories is very small and was neglected from the calculations. We show kinematic distributions of this control sample in Figure 7.2.

For the $\ell\gamma\not{E}_{\rm T}$ events we show in Figure 7.2 we show kinematic distributions for: a) the three-body transverse mass of $\ell\gamma\not{E}_{\rm T}$ system, b) the $\rm E_T$ of the leptons of the event, c) the $\rm E_T$ of the photon, and d) the missing transverse energy, $\not{E}_{\rm T}$. In Figure 7.3 we show the same kinematic distributions but on a logarithmic scale to show features in the tails of the distributions more clearly. We show the muon-channel and electron channel in Figure 7.4 and Figure 7.5 respectively. We show the same kinematic distributions as in Figure 7.2.

7.3 The Pretagged $t\bar{t}$ Control Sample

For a control sample to $t\bar{t}$, we constructed a pretagged sample of $t\bar{t}$ where we dropped our requirement for a tagged b-jet from the $t\bar{t}$ sample. The sample has only one data-driven background in this case, and that is leptons and $\not{E}_{\rm T}$ from QCD events.

CDF Run II Preliminary, 6.0 fb^{-1}			
$\ell\gamma\not\!\!E_{\rm T}$, Isolated Lepton			
Standard Model Source	$e\gamma\ \not\!\!E_{\rm T}$	$\mu\gamma\not\!\!E_{\rm T}$	$(e+\mu)\gamma\not\!\!E_{\rm T}$
$W\gamma$	2900 ± 400	2200 ± 300	5100 ± 700
$Z\gamma$	97 ± 13	370 ± 49	470 ± 61
QCD (j$\rightarrow l$ and $\not\!\!E_{\rm T}$)	135 ± 20	7.2 ± 1.1	142 ± 21
$\ell j\not\!\!E_{\rm T}(j \rightarrow \gamma)$	1660 ± 300	870 ± 100	2500 ± 400
$le\not\!\!E_{\rm T}$ (e$\rightarrow\gamma$)	40.5 ± 5.2	18.0 ± 2.3	58.5 ± 1.9
Total SM Prediction	4800 ± 500	3500 ± 300	8300 ± 800
Observed in Data	4462	3814	8276

Table 7.1: A comparison of the numbers of events predicted by the standard model (SM) and the observations for the $\ell\gamma\not\!\!E_{\rm T}$ search. The SM predictions for this search are dominated by the $W\gamma$, and $Z\gamma$ production, particularly when we miss a muon. Other contributions come from misidentified leptons, photons, or $\not\!\!E_{\rm T}$. MC samples have been scaled to 6.0 fb^{-1}. All other data-driven numbers have been measured in the manner described in earlier sections.

This sample requires: a tight central lepton, $\not\!\!E_{\rm T}$ greater than 20 GeV, 3 or more jets, the $M_{\rm T}$ of the lepton, $\not\!\!E_{\rm T}$ system must be greater than 20 GeV for the electron channel, and 10 GeV for the muon channel.

The pretagged $t\bar{t}$ sample is an ideal control sample for $t\bar{t}$ because the only non-MC background is the QCD sample. This provides a great cross-check on our QCD measurement technique for $t\bar{t}$, and allows us to check on k-factors that W+HF MC samples require.

We find 11616 pretagged $t\bar{t}(e)$ events and 7371 pretagged $t\bar{t}(\mu)$ events. This sample is dominated by a W+LF background. The k-factors due to heavy flavor content have a large uncertainty associated with them, and this drives the uncertainty on the histograms as shown in Figure 7.7. The measured cross section of $t\bar{t}$ (7.6 pb) is used in the plots.

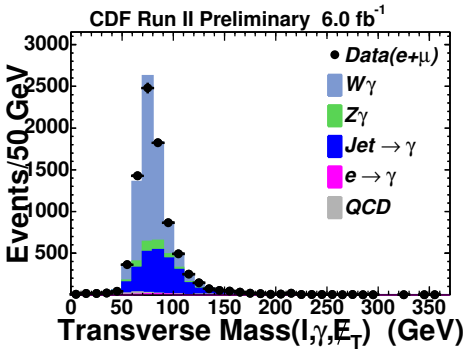

(a) Transverse Mass of the Lepton, Photon, and $\not\!\!E_T$ object from $\ell\gamma\not\!\!E_T$ events

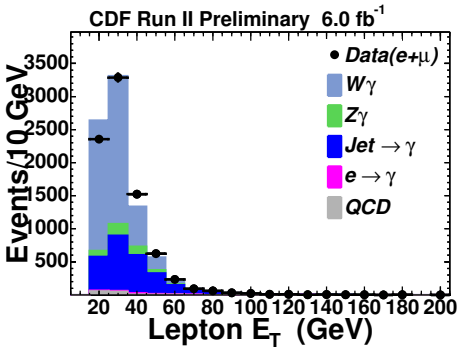

(b) The E_T of electrons and p_T of muons from $\ell\gamma\not\!\!E_T$ events

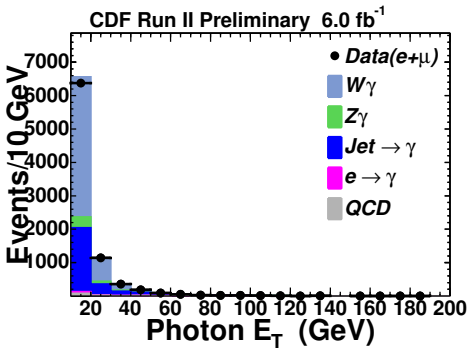

(c) E_T of the photons from $\ell\gamma\not\!\!E_T$ events

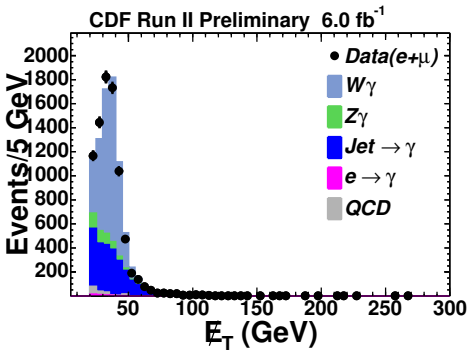

(d) $\not\!\!E_T$ of events in the $\ell\gamma\not\!\!E_T$ sample

Figure 7.2: Kinematic distributions for $\ell\gamma\not\!\!E_T$ events a) the three-body transverse mass of $\ell\gamma\not\!\!E_T$ system, b) the E_T of the leptons of the event, c) the E_T of the photon, and d) the missing transverse energy, $\not\!\!E_T$.

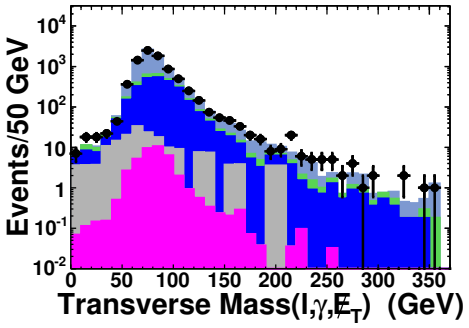

(a) Transverse Mass of the Lepton, Photon, and $\not\!\!E_{\rm T}$ object from $\ell\gamma\not\!\!E_{\rm T}$ events

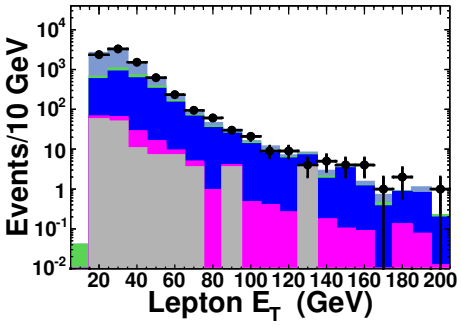

(b) The $E_{\rm T}$ of electrons and $p_{\rm T}$ of muons from $\ell\gamma\not\!\!E_{\rm T}$ events

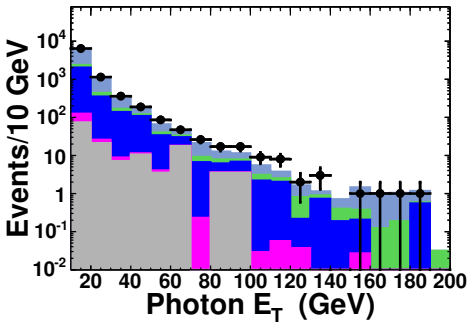

(c) $E_{\rm T}$ of the photons from $\ell\gamma\not\!\!E_{\rm T}$ events

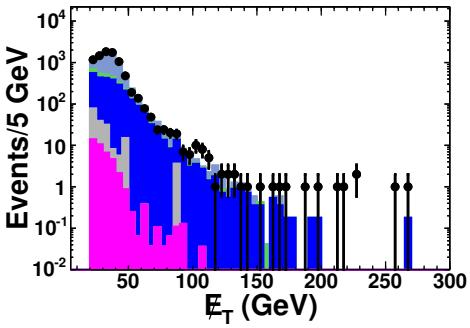

(d) $\not\!\!E_{\rm T}$ of events in the $\ell\gamma\not\!\!E_{\rm T}$ sample

Figure 7.3: Kinematic distributions for $\ell\gamma\not\!\!E_{\rm T}$ events in logarithmic scale a) the three-body transverse mass of $\ell\gamma\not\!\!E_{\rm T}$ system, b) the $E_{\rm T}$ of the leptons of the event, c) the $E_{\rm T}$ of the photon, and d) the missing transverse energy, $\not\!\!E_{\rm T}$. These are the same plots as in Figure 7.2 but in logarithmic scale.

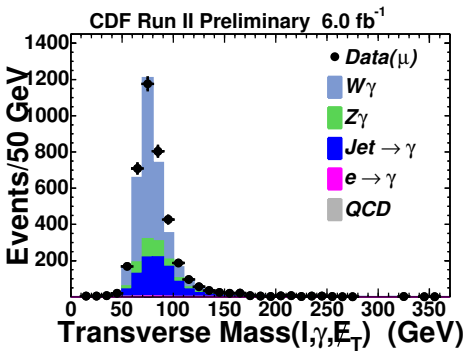

(a) Transverse Mass of the Muon, Photon, and $\not\!\!E_T$ object from $\mu\gamma\not\!\!E_T$ events

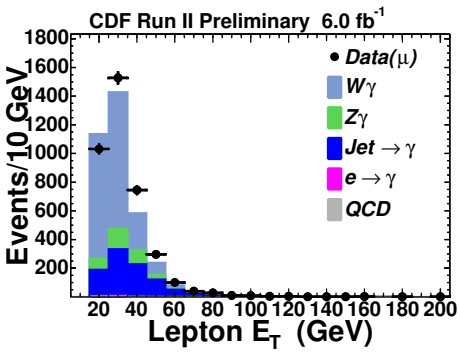

(b) The p_T of muons from $\mu\gamma\not\!\!E_T$ events

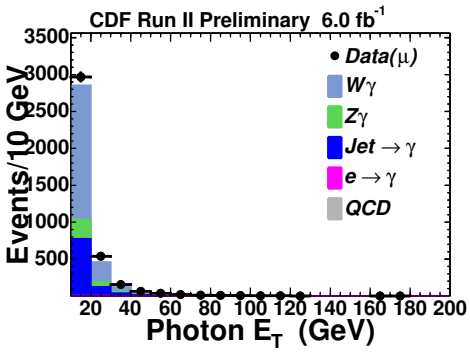

(c) E_T of the photons from $\mu\gamma\not\!\!E_T$ events

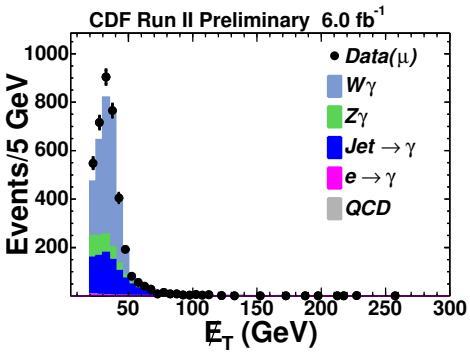

(d) $\not\!\!E_T$ of events in the $\mu\gamma\not\!\!E_T$ sample

Figure 7.4: Kinematic distributions for $\mu\gamma\not\!\!E_T$ events showing a) the three-body transverse mass of $\ell\gamma\not\!\!E_T$ system, b) the p_T of the muons of the event, c) the E_T of the photon, and d) the missing transverse energy, $\not\!\!E_T$.

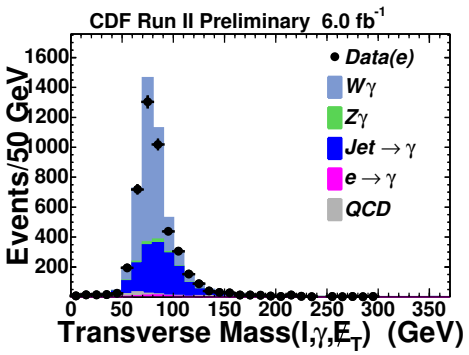

(a) Transverse Mass of the Electron, Photon, and $\not\!\!E_{\rm T}$ object from $e\gamma\not\!\!E_{\rm T}$ events

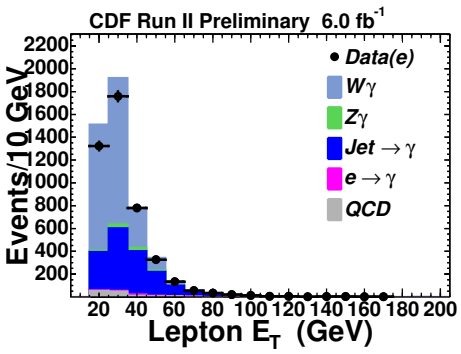

(b) The $E_{\rm T}$ of electrons from $e\gamma\not\!\!E_{\rm T}$ events

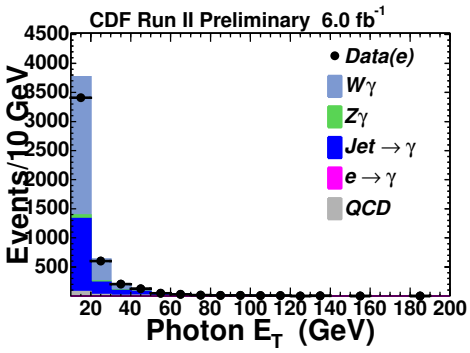

(c) $E_{\rm T}$ of the photons from $e\gamma\not\!\!E_{\rm T}$ events

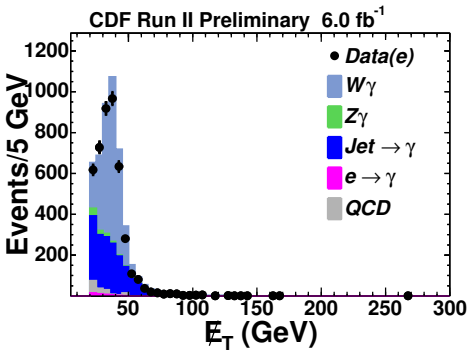

(d) $\not\!\!E_{\rm T}$ of events in the $e\gamma\not\!\!E_{\rm T}$ sample

Figure 7.5: Kinematic distributions for $e\gamma\not\!\!E_{\rm T}$ events a) the three-body transverse mass of $\ell\gamma\not\!\!E_{\rm T}$ system, b) the $E_{\rm T}$ of the leptons of the event, c) the $E_{\rm T}$ of the photon, and d) the missing transverse energy, $\not\!\!E_{\rm T}$.

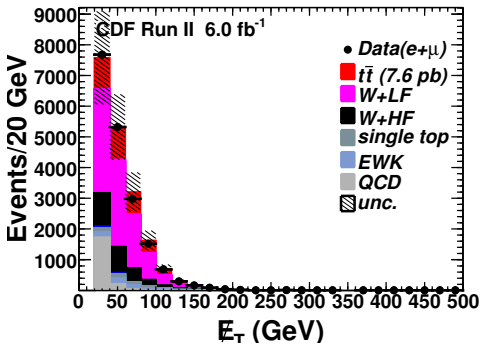

(a) $\not\!\!E_T$ of events in the pretagged $t\bar{t}$ sample

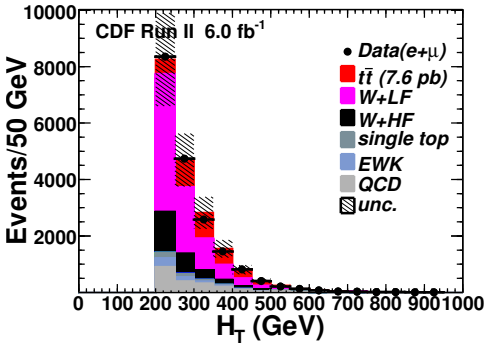

(b) H_T of events in the pretagged $t\bar{t}$ sample

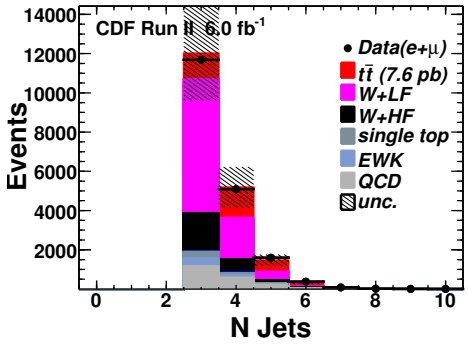

(c) N_{jets} of events in the pretagged $t\bar{t}$ sample

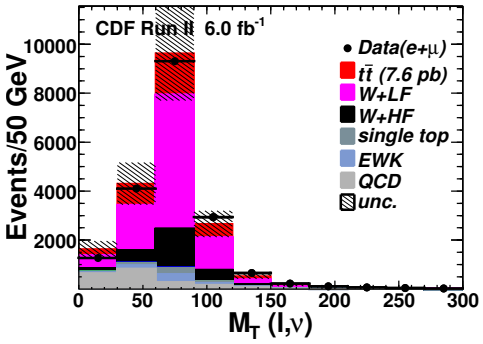

(d) M_T of the lepton and $\not\!\!E_T$ in the pretagged $t\bar{t}$ sample

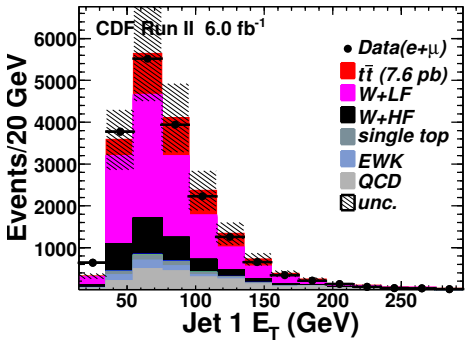

(e) E_T of the highest-energy jet in the pretagged $t\bar{t}$ sample

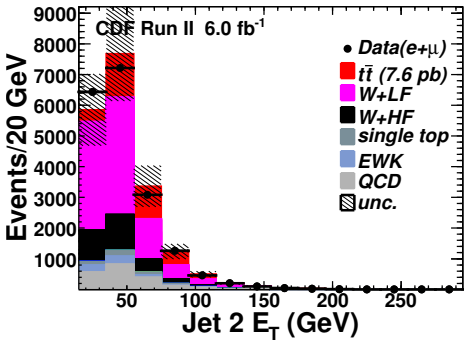

(f) E_T of the second highest energy jet in the pretagged $t\bar{t}$ sample

Figure 7.6: Kinematic distributions for pretagged $t\bar{t}$ events. We show a) the missing transverse energy ($\not\!\!E_T$), b) the total transverse energy (H_T), c) the total number of jets in the event, d) the transverse mass of the lepton and $\not\!\!E_T$, e) the E_T of the jet with the highest E_T, f) the E_T of the jet with the second highest E_T The k-factors due to heavy flavor content have a large uncertainty associated with them, and this drives the uncertainty on the histograms. The EWK histogram contains contributions from Z decays and diboson decays. The measured cross section of $t\bar{t}$ (7.6 pb) is used in the plots.

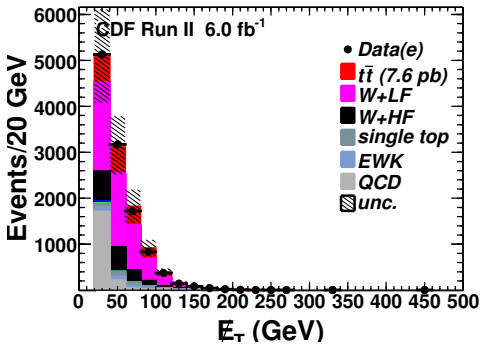

(a) $\not\!\!E_T$ of events in the pretagged $t\bar{t}(e)$ sample

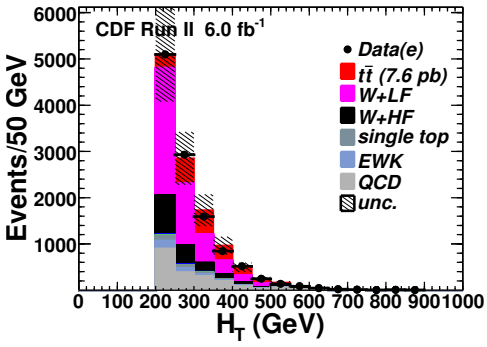

(b) H_T of events in the pretagged $t\bar{t}(e)$ sample

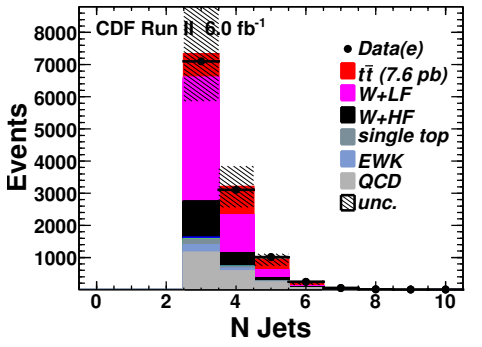

(c) N_{jets} of events in the pretagged $t\bar{t}(e)$ sample

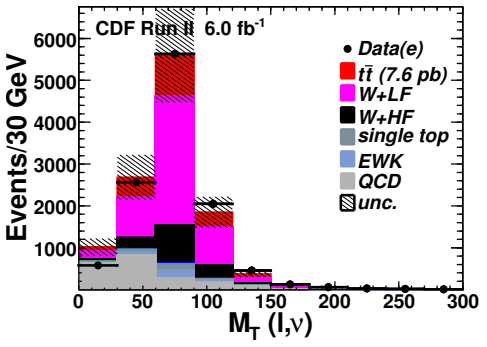

(d) M_T of the lepton and $\not\!\!E_T$ in the pretagged $t\bar{t}(e)$ sample

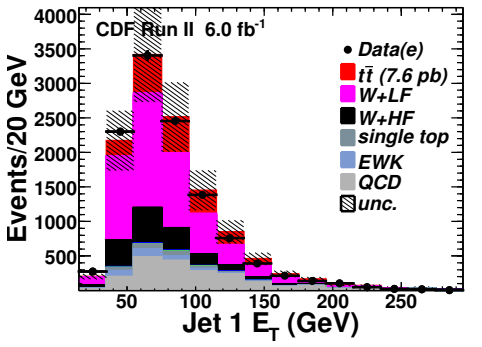

(e) E_T of the highest-energy jet in the pretagged $t\bar{t}(e)$ sample

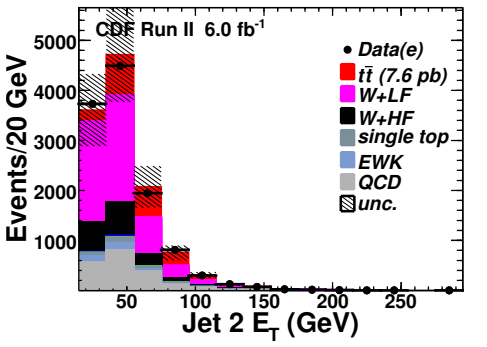

(f) E_T of the second highest energy jet in the pretagged $t\bar{t}(e)$ sample

Figure 7.7: Kinematic distributions of pretagged $t\bar{t}$ events from the electron stream. We show a) the missing transverse energy ($\not\!\!E_T$), b) the total transverse energy (H_T), c) the total number of jets in the event, d) the transverse mass of the lepton and $\not\!\!E_T$, e) the E_T of the jet with the highest E_T, f) the E_T of the jet with the second highest E_T The k-factors due to heavy flavor content have a large uncertainty associated with them, and this drives the uncertainty on the histograms. The EWK histogram contains contributions from Z decays and diboson decays. The measured cross section of $t\bar{t}$ (7.6 pb) is used in the plots.

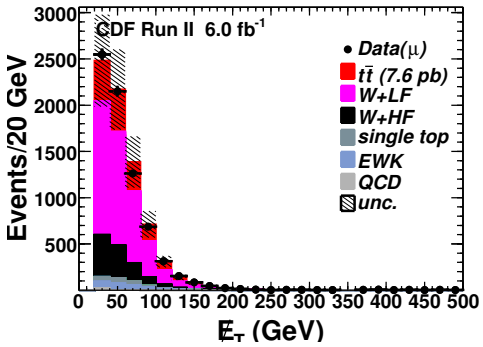

(a) $\not\!\!E_T$ of events in the pretagged $t\bar{t}(\mu)$ sample

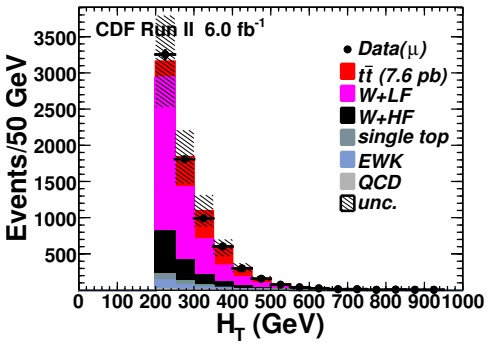

(b) H_T of events in the pretagged $t\bar{t}(\mu)$ sample

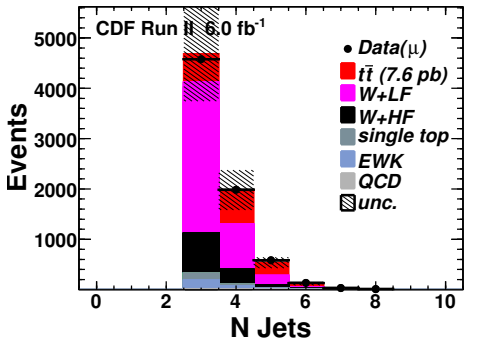

(c) N_{jets} of events in the pretagged $t\bar{t}(\mu)$ sample

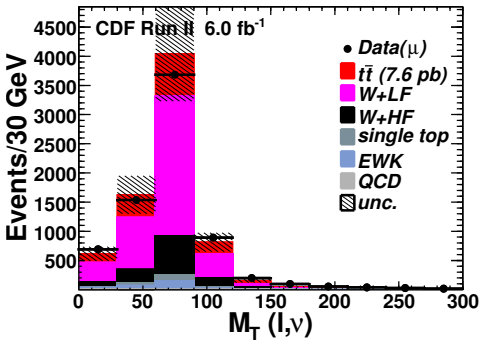

(d) M_T of the lepton and $\not\!\!E_T$ in the pretagged $t\bar{t}(\mu)$ sample

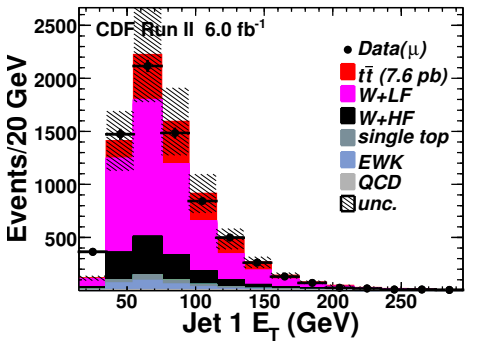

(e) E_T of the highest-energy jet in the pretagged $t\bar{t}(\mu)$ sample

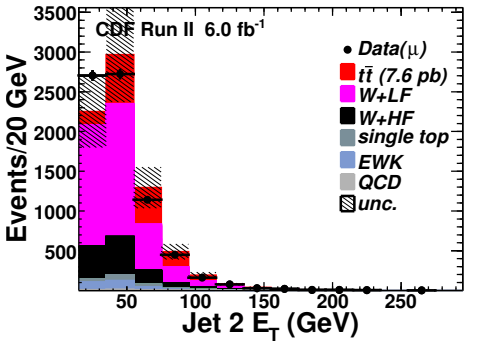

(f) E_T of the second highest energy jet in the pretagged $t\bar{t}(\mu)$ sample

Figure 7.8: Kinematic distributions of for pretagged $t\bar{t}$ events from muon stream. We show a) the missing transverse energy ($\not\!\!E_T$), b) the total transverse energy (H_T), c) the total number of jets in the event, d) the transverse mass of the lepton and $\not\!\!E_T$, e) the E_T of the jet with the highest E_T, f) the E_T of the jet with the second highest E_T The k-factors due to heavy flavor content have a large uncertainty associated with them, and this drives the uncertainty on the histograms. The EWK histogram contains contributions from Z decays and diboson decays. The measured cross section of $t\bar{t}$ (7.6 pb) is used in the plots.

8 Reducing Misidentified Photons Using The χ^2 of Photon Candidates

One of the variables we use to identify photons is based on the photon's shower shape in the CES. The shower is measured in two directions, along the strips and along the wires of the CES. In both cases, the shower shape is compared to the expected shower shape a photon should make in the CES. This predicted shape was measured using test-beam data. The shapes of the photon candidate, and the expected shower shape are compared using a χ^2 test. The χ^2 value of a photon candidate is the average of χ^2 values along the strip and wires of the CES.

While looking at distributions of $t\bar{t}\gamma$ MC and its data-driven backgrounds, the plot of the photon's χ^2 distribution looked particularly promising for removing some of the largest background contribution: jets misidentified as photons. In order to find the most effective cut value for the photon candidates, we use the $\ell\gamma\not\!\!E_{\rm T}$ (Section 7.2) distribution. We want to cut on a photon candidate's χ^2, and remove some of the jets misidentified as photons background while retaining most of the $W\gamma$ contribution.

The $\ell\gamma\not\!\!E_{\rm T}$ sample is not a true control sample for $t\bar{t}\gamma$ as it contains all of the $t\bar{t}\gamma$ signal events, however there are considerably more data points in the $\ell\gamma\not\!\!E_{\rm T}$ distribution. It is unlikely that any change in the selection criteria we choose from the $\ell\gamma\not\!\!E_{\rm T}$ distribution is due solely to the $t\bar{t}\gamma$ events. This is sometimes called a high-statistics control sample.

We isolate a sample of pure photons by requiring events with two same flavor leptons, and a photon that have a three-body invariant mass between 86 and 96 GeV; we call this sample $Z\gamma$ (Sec. 7.1). In this sample, there are nearly no backgrounds due to misidentified photons.

The control sample of $Z\gamma$ is a sample of real photons, the $\ell\gamma\not\!\!E_{\rm T}$ sample is a mixture of both real photons and jets misidentified as photons, and the photons from our jets misidentified as photons distributions from the $\ell\gamma\not\!\!E_{\rm T}$ sample are a sample of misidentified photons.

In Figure 8.1, we show a normalized χ distribution for observed photons for

various samples.We can see that 90% of most real photons (from the $Z\gamma$ sample) have a χ^2 value less than 10. The number of misidentified photons with a χ^2 less than 10 is about 70%.

We try to pin point a new lower χ^2 value to remove background, while preserving a large fraction of signal. We use a significance function to find this value.

Defining significance as:

$$Sig = \frac{S}{\sqrt{S+B}} \tag{8.1}$$

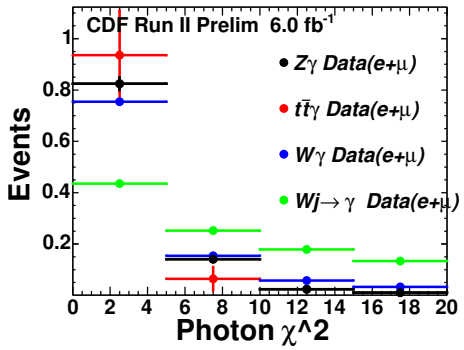

Figure 8.1: Spectrum of the photon's χ^2 distributions normalized to unity, for different samples

Where S is the signal of true $W\gamma$ events, as found by Monte Carlo, and B is backgrounds to the $\ell\gamma \not\!\!E_T$ signal such as jets misidentified as photons, and electrons misidentified as photons events. We found that the significance versus the χ^2 cut, did not peak between 0 and 20. We show the χ^2 distributions, and significance curves in Fig. 8.2, and there is no peak.

At this point we attempt a different approach: we use our samples as described earlier but we split the groups based on the photon's E_T. The lower energy scale had the photon's E_T between 10 and 25 GeV, and the higher energy scale had the photon's $E_T > 25$ GeV.

At low E_T, the χ^2 of the photon candidate should be smaller. Real photons should dominantly be arriving alone, but misidentified photons are more likely to come in a collimated pair, and hence have a worse χ^2 value.

We define efficiency and purity quantities typically used in describing the effi-

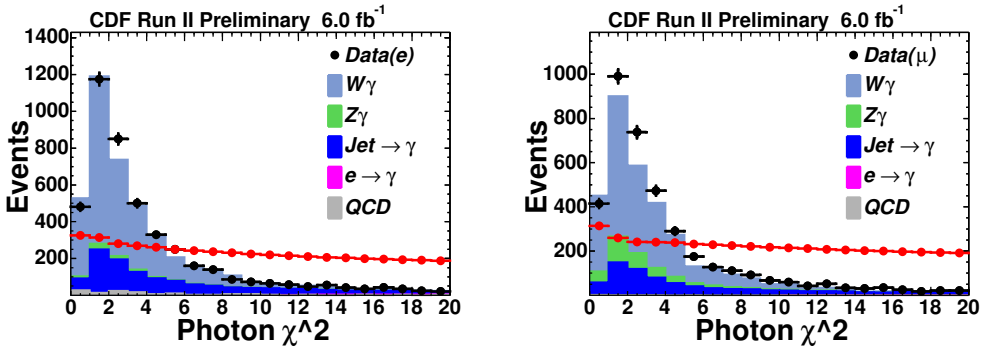

(a) $e\gamma\not{E}_{\mathrm{T}}$ (b) $\mu\gamma\not{E}_{\mathrm{T}}$

Figure 8.2: Spectrum of the photon's χ^2 distributions normalized by cross section and luminosity, for the $e\gamma\not{E}_{\mathrm{T}}$ (left) and $\mu\gamma\not{E}_{\mathrm{T}}$ (right) sample. The red crosses are proportional to the significance of the photon's χ^2; there is no peak in the curve for where to cut.

cacy of object selection. Since we have a nearly pure sample of photons from the $Z\gamma$ sample we use this to measure the efficiency of a proposed cut on χ^2. The efficiency is the fraction of low-$\mathrm{E_T}$ $Z\gamma$ event we accept based on the χ^2 cut.

To measure purity we make use of the $\ell\gamma\not{E}_{\mathrm{T}}$ sample, which has true photons from $W\gamma$ and misidentified photons from jets misidentified as photons samples. The purity of the sample is measured as the number of $W\gamma$ events relative to the number of accepted total $\ell\gamma\not{E}_{\mathrm{T}}$ events. For each cut value on the χ^2 value of the photon candidate we measure the acceptance of $W\gamma$ and use it to find the number of $W\gamma$ events.

To find an optimal place to cut we are willing to trade some efficiency for a higher purity sample. We know from Section 7.2, using the standard χ^2 cut of 20,clearly allows for some jets misidentified as photons events to be accepted as well. By varying the χ^2 cut, we plot the function of efficiency versus purity, shown in Figure 8.3(a).

The χ^2 value was changed in steps of 2 from 2 to the standard cut of 20. Figure 8.3(a) shows the efficiency versus the purity. It is obvious that we want both high purity and high efficiency, so we select the χ^2 value for a cut that has the efficiency and purity closest to the ordered pair (1,1) in Figure 8.3(a). This

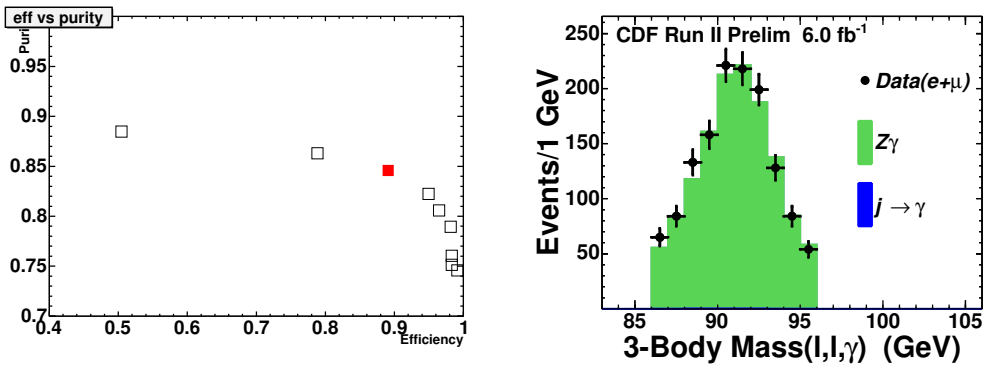

(a) $\ell\gamma\not{E}_{\rm T}$ (b) $Z\gamma$

Figure 8.3: Distribution of efficiency versus purity of a proposed χ^2 cut for photons with $E_T < 25$ GeV. The proposed cut starts at 2 and increases in steps of 2 to the standard cut of 20. The efficiency increases monotonically with increasing the χ^2 cut; and purity decreases monotonically. We choose to require χ^2 be less than 6 for lower energy photons. True photons were collected from a $Z\gamma$ decays (3 body mass nearly the Z-mass), and misidentified photons had isolation > 2. For each proposed χ^2 cut, we found the fraction of true photons and misidentified photons contained in a $W\gamma$ decay. The χ^2 cut goes up in steps of two from left to right and top to bottom.

corresponds to the value of 6 and is the colored marker in that figure. Using this information we require the χ^2 be less than 6, for photons with $E_T < 25$ GeV.

9 Systematic Uncertainties

A poorly modeled detector response can have an effect on each of our signal samples. This can systematically shift the measurements of the $t\bar{t}\gamma$ and $t\bar{t}$ cross sections.

After finding the uncertainties for each systematic uncertainty, the uncertainties are added in quadrature when independent, and linearly when correlated. Systematic uncertainties are included in the calculation of the total uncertainties for MC and data-driven backgrounds. The uncertainties in each background are carried through the analysis, and the results of the uncertainties on our cross-section measurements are calculated at the end. In the next few subsections we describe the uncertainties that arise in our analysis and present an estimate of the uncertainty for each source.

9.1 Jet Energy Scale

We measure jet energy in the calorimeters. However, there are known systematic effects between the energy we measure in the calorimeters, and what the actual energy of the jet was. To account for this, we apply a jet-energy (JES) systematic.

The energy of a jet can be mismeasured in several ways such as: response of the calorimeter to different particle types, non-linear response of the calorimeter, uninstrumented regions of the calorimeter, and energy radiated outside of the jet clustering algorithm [57]. Uncertainties for each of these effects is parameterized.

To find the total systematic effect of the JES on our measurement, each of these uncertainties is added together, and we find the shift on each of our MC samples and data-driven backgrounds, and on the data. The analysis is then carried through to completion, and we see a shift in the measurement of our cross sections of $t\bar{t}$, and $t\bar{t}\gamma$.

We shift the uncertainties of the JES both up and down one standard deviation away from their nominal positions, and to be conservative choose the larger difference on the cross-section measurements. We find the uncertainty on the cross-section measurements to be about 1%.

9.2 B-Jet Tagging

The efficiency of b-jet tagging is measured on a large set of dijet samples containing a low-p_T ($\sim$ 8 GeV) lepton. This sample enriched in heavy flavor. A scale factor is measured which relates the fraction of the efficiency of the tag rates observed in data compared to Monte Carlo. For the "loose" SecVtx tagger the scale factor is measured to be 0.95 ± 0.05. This uncertainty is applied to all MC samples where we look for a b-tag.

9.3 Mistags

A systematic uncertainty of 8% is used on the total amount of predicted mistagged events. This was the same amount quoted in a previous $t\bar{t}\gamma$ analysis [12].

The uncertainty in the number of mistagged events is due to several different factors. While we look for positively tagged events to identify heavy flavor, and negative tags to help discriminate against incorrectly tagged jets, there is error in these measurements. The distribution of L_{xy} is compared for data and MC and there are slight discrepancies in the fit.

We validate this 8% uncertainty using current data and the most up-to-date parameters on the mistag rate. The mistag rate is fluctuated both up and down one standard deviation, and the amount of events with a mistagged jet is found. We find that the uncertainty of 8% is slightly larger than found in the mistag matrix, but still consistent.

9.4 QCD Contamination

The QCD contamination is found using the antielectron method, which relies on the identification, and efficiencies of accepting antielectrons. The authors of the antielectron method have quoted a systematic uncertainty of 8% when using this method. This systematic uncertainty is applied only to the QCD measurements.

In Ref. [56], Cooper and Messina measure the amount of jets being misidentified as leptons and $\not\!\!E_T$ in $W^{\pm} \rightarrow e^{\pm}\nu + N_{jets}$ events. The authors find the uncertainty

by changing the value of $\not\!\!E_{\rm T}$ which they identify as signal, and the amount of jets in their signal events. The change in the amount of accepted QCD processes with jets misidentified as leptons and $\not\!\!E_{\rm T}$ is accounted for, and 8% covers the shift in these amounts.

9.5 Jets Misidentified as Photons

In modeling a tighter cut on a photon's χ^2 value, an $\ell\gamma\not\!\!E_{\rm T}$ sample was assembled. The largest contribution to this sample was from the SM $W\gamma$ process, but the second largest was due to jets misidentified as photons. A sample of both real and fake photons is assembled requiring: $\not\!\!E_{\rm T}$ greater than 20 GeV, an identified tight central lepton with track isolation less than 4 GeV, and a photon candidate which passes all photon cuts except for isolation requirements.

As in Section 5.1.1, we fit the isolation energy shape of the photon candidates with the isolation energy of electrons from $Z^0 \to e^+e^-$ decays as well as a straight line. This sample has a very large jets misidentified as photons contribution to the background, so the uncertainties we find are not statistics limited.

To find the uncertainty for this method, we varied the bounds of the isolation energy of the photon candidate between 38 and 58 GeV, and found that this had a rather large effect on the predicted amount of events with jets misidentified as photons. We also used a different polynomial shape as the background template of fake photons instead of the straight line.

Since the sample is so large, the shifts that we find in the expected amount of events with jets being misidentified as photons should be due almost entirely to systematic effects. We use a systematic uncertainty of 20% of the expected value, which corresponds to our largest deviation from the mean we observed while changing the parameters of the fitting functions.

9.6 Electron Misidentified as Photons

To model the amount of electrons misidentified as photons, a sample of $\rm Z^0 \to e^+e^-$ and $\rm Z^0 \to e{+}\text{“}\gamma\text{”}$ events are constructed. In the case of $\rm Z^0 \to e{+}\text{“}\gamma\text{”}$ an electron was

produced, emitted a photon, and the electron was lost.

The probability for an electron to fake a photon is parameterized based on the E_T spectrum of an electron. The probability takes a functional form, and each parameter in the function has a systematic uncertainty.

Each uncertainty in the functional form is fluctuated by a standard deviation and the shifts to the nominal measurement are added in quadrature. We find the total uncertainty on the predicted value of electrons misidentified as photons to be about 15%.

9.7 Lepton Identification

The electron identification systematic uncertainty is 1% and the muon identification systematic uncertainty is 2%. These values are combined in quadrature in the acceptance systematic uncertainty, and their values are shown in the uncertainty for the MC samples.

There is a systematic uncertainty of 1% introduced by modeling when requiring the vertex be within 60 cm of the origin of the detector.

9.8 Photon Identification

The photon identification uncertainty is 4% and this uncertainty is added in quadrature in the acceptance systematic uncertainty, as well as the uncertainty for MC samples with photons.

The 4% uncertainty comes from three sources: the photon energy scale, photon acceptance, and the photon isolation scale. The photon energy scale is modeled by comparing fully corrected energy distributions for data and MC. It is found that the data and MC agree up to a 1.5% uncertainty. Uncertainty in photon acceptance is included to cover a particular choice in parton density functions in Pythia MC, the uncertainty is found to be 3%. There is an uncertainty in the photon isolation scale of about 10% this uncertainty results in an additional 1% uncertainty in the acceptance of a photon. Adding these uncertainties in quadrature, one arrives at a 4% systematic uncertainty for photon identification [58].

9.9 Trigger Efficiency

Detector-specific corrections are applied to the MC in order to more accurately model the relative trigger efficiencies between CEM, CMUP, and CMX events. The uncertainty due to trigger efficiency is evaluated using Z events from data. There are two types of uncertainties that come from these corrections, trigger identification and trigger efficiencies. The resulting uncertainties are added in quadrature to the total systematic uncertainty.

9.10 Heavy Flavor Correction Factors for W+HF Samples

It has been found that the amount of b-tagged events found in a sample of lepton + $\not\!\!E_{\mathrm{T}}$ events differs strongly from the MC predictions at low jet multiplicity [48]. To compensate for this large difference an overall multiplicative factor is applied as a k-factor for the W+HF MC.

The k-factor is measured in the low jet multiplicity where W+HF should be the dominant contribution, and $t\bar{t}$ is very small. The uncertainty on the k-factor is quite large ($\sim$20%), and we propagate this uncertainty on each of the W+HF samples.

9.11 Luminosity Uncertainties

The uncertainty in our luminosity is derived from detector accuracy and the theoretical cross section for the inelastic $p\bar{p}$ collisions. The uncertainty on the luminosity is 6%, and we leave this systematic uncertainty uncombined with other uncertainties until the very end. The 6% uncertainty comes from a 4.4% uncertainty from the acceptance and operation of the luminosity monitor, and 4.0% from the uncertainty on the calculation of the total $p\bar{p}$ cross section.

10 Full Comparison of Data to Signal and Background Composition

In this section, we present our results for 6 fb^{-1}, we present each of our signal samples. We see excellent agreement across all three categories. We show the summation of all signal and background contributions to each of our signatures with the double counting contributions removed.

The contribution to double counting for each of the pairs of data-driven backgrounds can be found in Tables C.1, and C.2, in the Appendix C.

10.1 Results from the signature based search for $\ell\gamma\not{E}_{\text{T}}b$

The predicted and observed totals for the $\ell\gamma\not{E}_{\text{T}}b$ search are shown in Table 10.1. We observe 85 $\ell\gamma\not{E}_{\text{T}}b$ events compared to the expectation of 99.1 ± 9.3 events.

There is no significant discrepancy in the $\ell\gamma\not{E}_{\text{T}}b$ signature. Figure 10.1 shows the observed distribution summed over the $e\gamma\not{E}_{\text{T}}b$ and $\mu\gamma\not{E}_{\text{T}}b$ events in: a) the E_{T} of the lepton, b) the E_{T} of the photon, c) the number of jets distribution, d) the E_{T} of the b-jet, e) the missing transverse energy ($\not{E}_{\text{T}}$), and f) the transverse energy (H_{T}) of the event.

The predicted and observed kinematic distributions for $\mu\gamma\not{E}_{\text{T}}b$ are compared in Figure 10.2. The distributions for the $e\gamma\not{E}_{\text{T}}b$ signature are compared in Figure 10.3.

CDF Run II, 6.0 fb^{-1}			
Lepton + Photon + $\not\!\!E_{\rm T}$ + b Events, Isolated Leptons			
Standard Model Source	$e\gamma b\not\!\!E_{\rm T}$	$\mu\gamma b\not\!\!E_{\rm T}$	$(e+\mu)\gamma b\not\!\!E_{\rm T}$
$t\bar{t}\gamma$semileptonic	6.74 ± 1.24	5.91 ± 1.08	12.65 ± 2.29
$t\bar{t}\gamma$ dileptonic	3.90 ± 0.71	3.39 ± 0.62	7.29 ± 1.32
$W^{\pm}c\gamma$	2.29 ± 0.45	2.42 ± 0.47	4.71 ± 0.73
$W^{\pm}c\bar{c}\gamma$	0.25 ± 0.11	0.75 ± 0.22	1.00 ± 0.24
$W^{\pm}b\bar{b}\gamma$	1.92 ± 0.32	1.46 ± 0.27	3.38 ± 0.48
WZ	0.23 ± 0.10	0.09 ± 0.07	0.31 ± 0.12
WW	0.29 ± 0.07	0.26 ± 0.06	0.55 ± 0.10
Single Top (s-chan)	0.54 ± 0.24	0.46 ± 0.22	1.00 ± 0.34
Single Top (t-chan)	1.13 ± 0.45	0.83 ± 0.38	1.96 ± 0.61
$\tau \rightarrow \gamma$ fake	0.37 ± 0.11	0.37 ± 0.11	0.74 ± 0.17
Jet faking γ ($\ell j\not\!\!E_{\rm T}b, j \rightarrow \gamma$)	8.88 ± 2.57	5.28 ± 1.67	14.16 ± 3.85
Mistags	17.37 ± 1.71	12.02 ± 1.18	29.43 ± 2.75
QCD(Jets faking ℓ and $\not\!\!E_{\rm T}$)	14.39 ± 7.33	1.44 ± 0.73	15.83 ± 7.38
$ee\not\!\!E_{\rm T}b$, $e \rightarrow \gamma$	4.86 ± 0.71	–	4.86 ± 0.71
$\mu e\not\!\!E_{\rm T}b$, $e \rightarrow \gamma$	–	1.32 ± 0.23	1.32 ± 0.23
Total SM Prediction	63.2 ± 8.1	36.0 ± 2.6	99.1 ± 9.3
Observed in Data	51	34	85

Table 10.1: A comparison of the number of events predicted by the standard model (SM) and the observations for the $\ell\gamma\not\!\!E_{\rm T}b$ search. The SM predictions for this search are dominated by the $t\bar{t}\gamma$, and $W\gamma$+heavy flavor production. Other contributions come from misidentified leptons, photons, b-jets, or $\not\!\!E_{\rm T}$. MC samples have been scaled to 6.0 fb^{-1}. Data-driven backgrounds have been found in the method described in previous sections.

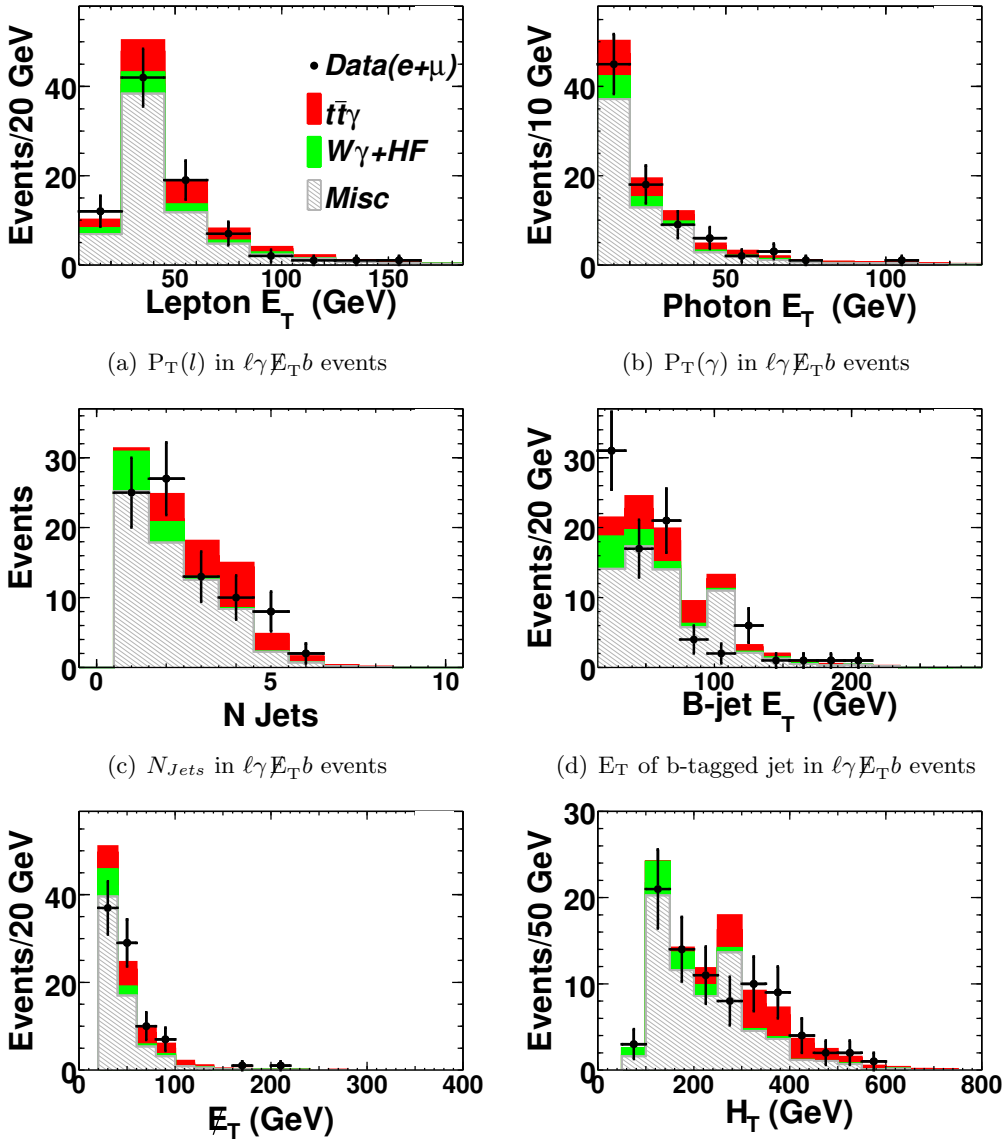

(a) $P_T(l)$ in $\ell\gamma \not{E}_T b$ events

(b) $P_T(\gamma)$ in $\ell\gamma \not{E}_T b$ events

(c) N_{Jets} in $\ell\gamma \not{E}_T b$ events

(d) E_T of b-tagged jet in $\ell\gamma \not{E}_T b$ events

(e) $\not{E}_T$ observed in $\ell\gamma \not{E}_T b$ events

(f) H_T observed in $\ell\gamma \not{E}_T b$ events

Figure 10.1: The following kinematic distributions for the $\ell\gamma \not{E}_T b$ sample are shown: a) the transverse energy (momentum) for electrons (muons), b) the transverse energy of the identified photon, c) the number of jets in the event, d) the transverse momentum of the identified b-jet, e) the missing transverse energy, f) the total transverse energy (H_T). The black dots are data, and the histograms show the expected SM contributions from radiative top decay ($t\bar{t}\gamma$), $W\gamma$ production with heavy flavor (HF), and Misc includes: WW, WZ, and single-top production as well as jets, τ leptons, electrons, and jets misidentified as photons, jets misidentified as leptons (QCD), and misidentified b-tags.

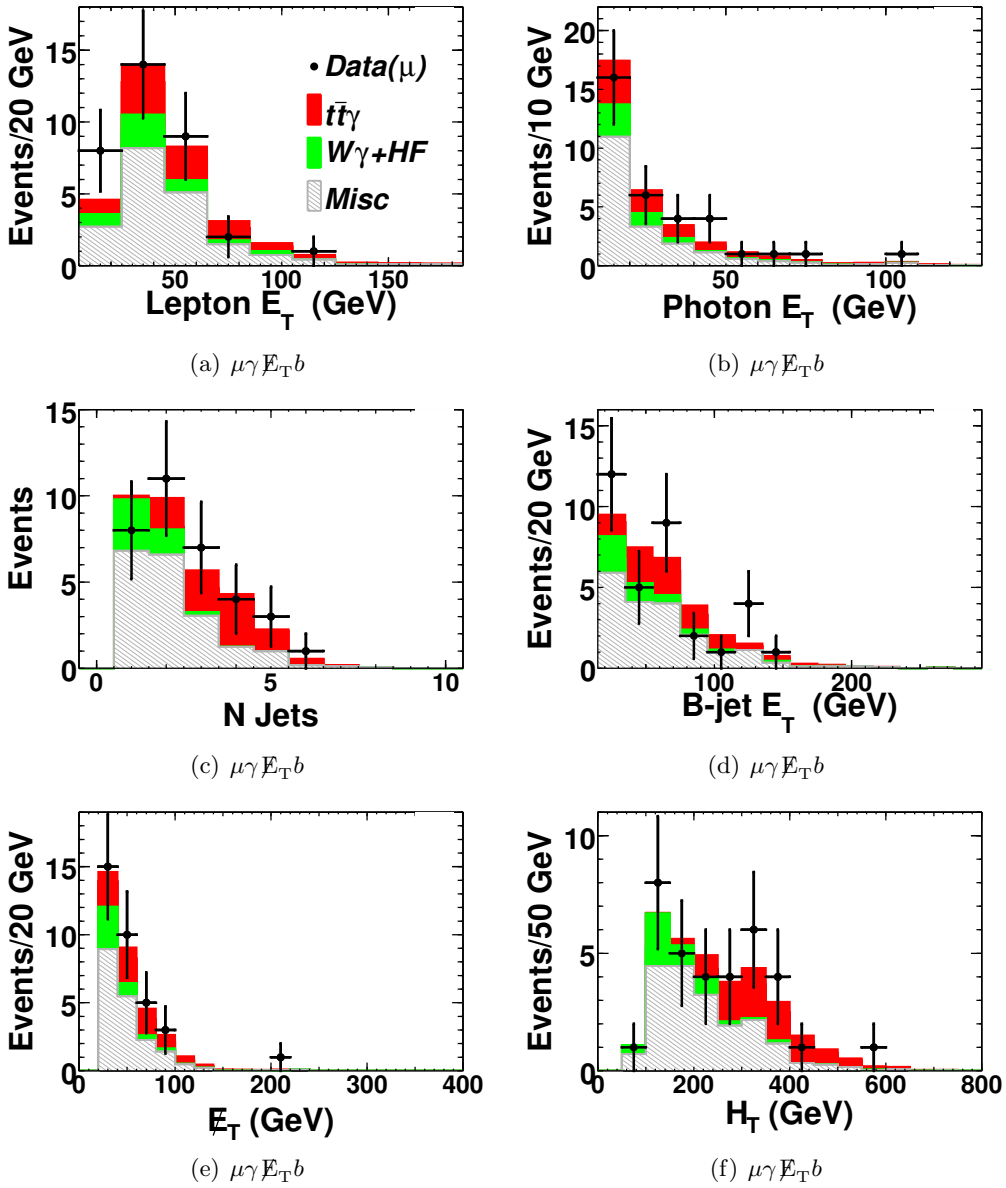

(a) $\mu\gamma\not{E}_{\mathrm{T}}b$ (b) $\mu\gamma\not{E}_{\mathrm{T}}b$

(c) $\mu\gamma\not{E}_{\mathrm{T}}b$ (d) $\mu\gamma\not{E}_{\mathrm{T}}b$

(e) $\mu\gamma\not{E}_{\mathrm{T}}b$ (f) $\mu\gamma\not{E}_{\mathrm{T}}b$

Figure 10.2: The following kinematic distributions for the $\mu\gamma\not{E}_{\mathrm{T}}b$ sample are shown: a) the transverse momentum muons, b) the transverse energy of the identified photon, c) the number of jets in the event, d) the transverse momentum of the identified b-jet, e) the missing transverse energy, f) the total transverse energy ($\mathrm{H_T}$). The black dots are data, and the histograms show the expected SM contributions from radiative top decay ($t\bar{t}\gamma$), $W\gamma$ production with heavy flavor (HF), and Misc includes: WW, WZ, and single-top production as well as jets, τ leptons, electrons, and jets misidentified as photons, jets misidentified as leptons (QCD), and misidentified b-tags.

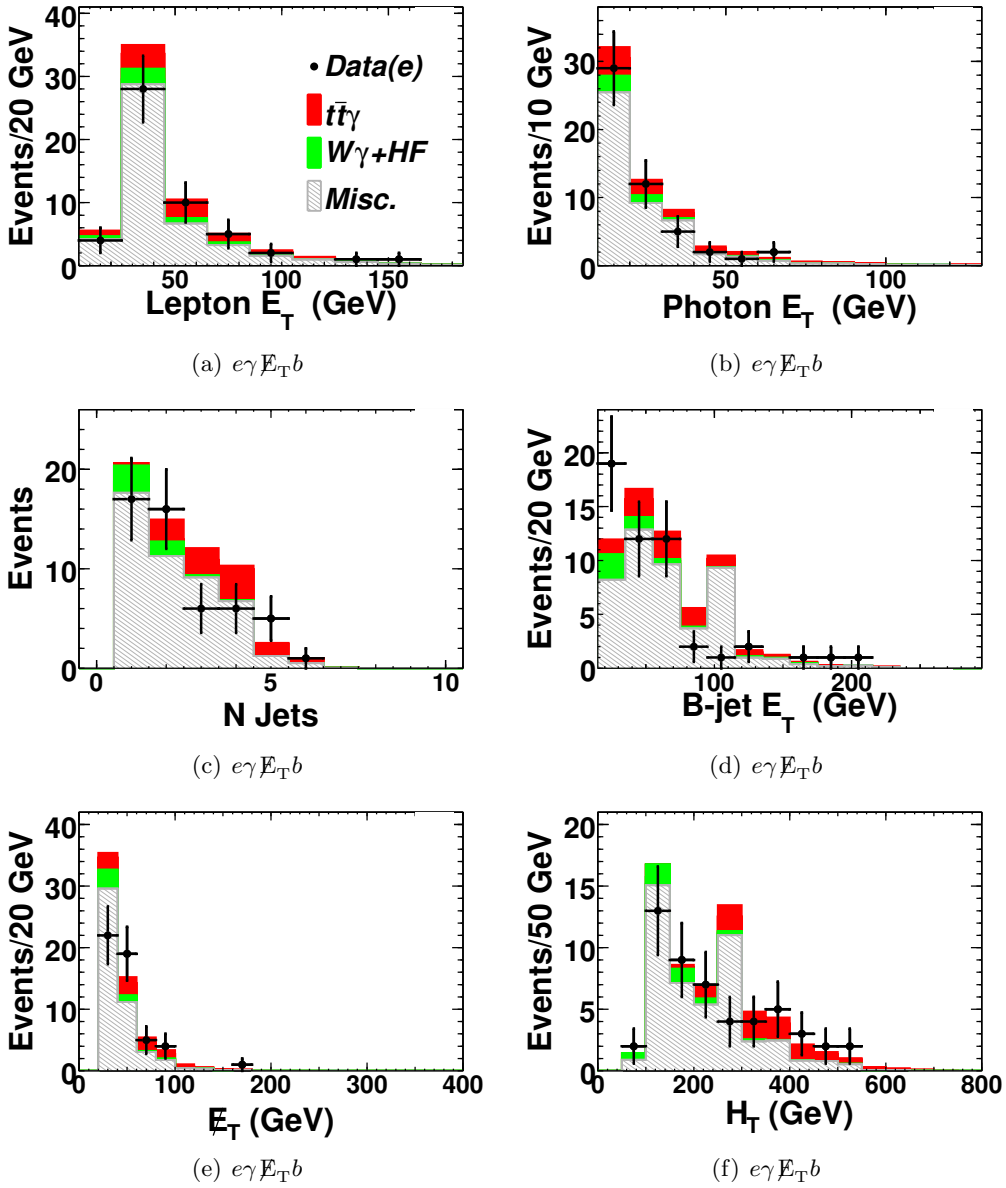

(a) $e\gamma\not{E}_{\mathrm{T}}b$ (b) $e\gamma\not{E}_{\mathrm{T}}b$

(c) $e\gamma\not{E}_{\mathrm{T}}b$ (d) $e\gamma\not{E}_{\mathrm{T}}b$

(e) $e\gamma\not{E}_{\mathrm{T}}b$ (f) $e\gamma\not{E}_{\mathrm{T}}b$

Figure 10.3: The following kinematic distributions for the $e\gamma\not{E}_{\mathrm{T}}b$ events are shown: a) the transverse energy for electrons, b) the transverse energy of the identified photon, c) the number of jets in the event, d) the transverse momentum of the identified b-jet, e) the missing transverse energy, f) the total transverse energy ($\mathrm{H_T}$). The black dots are data, and the histograms show the expected SM contributions from radiative top decay ($t\bar{t}\gamma$), $W\gamma$ production with heavy flavor (HF), and Misc includes: WW, WZ, and single-top production as well as jets, τ leptons, electrons, and jets misidentified as photons, jets misidentified as leptons (QCD), and misidentified b-tags.

10.2 Results for the $t\bar{t}\gamma$ Signature

We show in Figure 10.4 a signature event for $t\bar{t}\gamma$. This event has a photon which passes the χ^2 cut, two b-tagged jets, substantial $\not\!\!E_T$, and the H_T of the event is large at 206.8 GeV, as well as tight lepton with track isolation less than 4 GeV. This is precisely the type of signature that we would expect from a $t\bar{t}\gamma$ signal event.

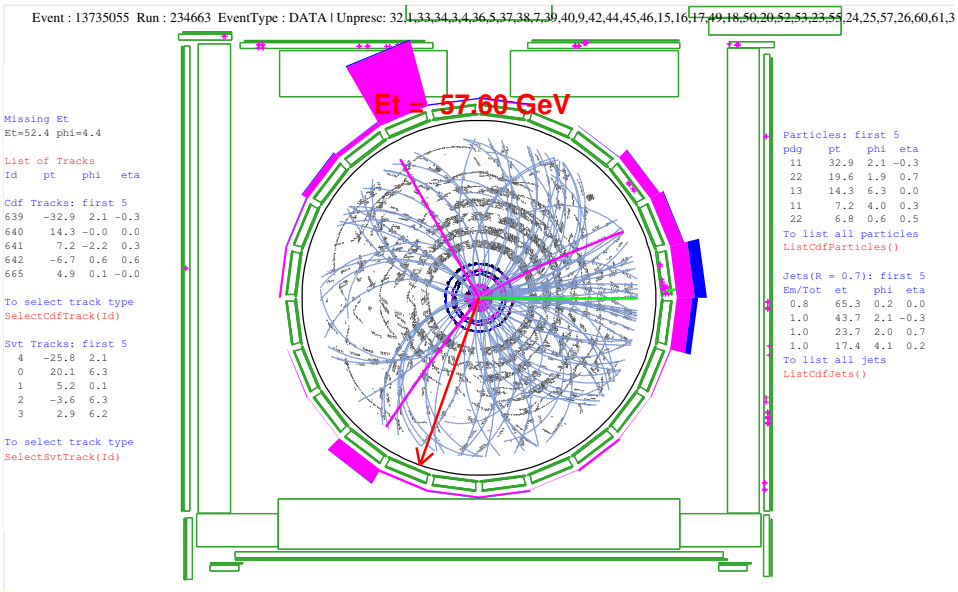

Figure 10.4: A high-p_T electron event (run 234663 event 13735055) with two b-tagged jets, high H_T, and electron track isolation less than 4 GeV. The H_T of the event is 206.8 GeV, and the $\not\!\!E_T$ is 56.8 GeV. There are 3 high p_T jets. The leading lepton p_T is 39.1 GeV, and the photon has a E_T of 18.7 GeV, and passes the χ^2 cut.

The predicted and observed totals for the $t\bar{t}\gamma$ search are shown in Table 10.2. We observed 30 $t\bar{t}\gamma$ events compared to an expectation of 26.9 ± 3.4 events.

Figure 10.5 shows the observed $t\bar{t}\gamma$ distributions of: a) the E_T of the lepton, b) the E_T of the photon, c) the number of jets distribution, d) the E_T of the b-jet e) the missing transverse energy ($\not\!\!E_T$), and f) the transverse energy (H_T) of the event.

The predicted and observed kinematic distributions for $t\bar{t}\gamma(\mu)$ events are compared in Figure 10.7. The distributions for the $t\bar{t}\gamma(e)$ events are compared in Figure 10.6.

CDF Run II, 6.0 fb^{-1}			
$t\bar{t}\gamma$, Isolated Leptons, Tight Chi2 on Photons			
Standard Model Source	$e\gamma b\not{E}_{\mathrm{T}}$	$\mu\gamma b\not{E}_{\mathrm{T}}$	$(e+\mu)\gamma b\not{E}_{\mathrm{T}}$
$t\bar{t}\gamma(semileptonic)$	5.98 ± 1.10	5.21 ± 0.97	11.19 ± 2.04
$t\bar{t}\gamma(dileptonic)$	1.47 ± 0.27	1.27 ± 0.24	2.74 ± 0.50
$W^{\pm}c\gamma$	0 ± 0.07	0 ± 0.07	0 ± 0.09
$W^{\pm}c\bar{c}\gamma$	0 ± 0.05	0.05 ± 0.05	0.05 ± 0.07
$W^{\pm}b\bar{b}\gamma$	0.15 ± 0.07	0.06 ± 0.05	0.21 ± 0.08
WZ	0.05 ± 0.05	0.05 ± 0.05	0.09 ± 0.06
WW	0.06 ± 0.03	0.06 ± 0.03	0.11 ± 0.03
Single Top (s-chan)	0.09 ± 0.10	0 ± 0.10	0.09 ± 0.13
Single Top (t-chan)	0.14 ± 0.14	0.13 ± 0.14	0.27 ± 0.19
$\tau \rightarrow \gamma$ fake	0.20 ± 0.08	0.10 ± 0.05	0.29 ± 0.09
Jet faking γ ($\ell j\not{E}_{\mathrm{T}}b, j \rightarrow \gamma$)	5.75 ± 1.76	1.79 ± 1.56	7.54 ± 2.53
Mistags	1.47 ± 0.37	1.02 ± 0.32	2.50 ± 0.51
QCD(Jets faking ℓ and $\not{E}_{\mathrm{T}}$)	0.38 ± 0.38	0.02 ± 0.020	0.40 ± 0.38
$ee\not{E}_{\mathrm{T}}b$, $e \rightarrow \gamma$	0.94 ± 0.19	–	0.94 ± 0.19
$\mu e\not{E}_{\mathrm{T}}b$, $e \rightarrow \gamma$	–	0.49 ± 0.11	0.49 ± 0.11
Total SM Prediction	$16.7 \pm 2.2(tot)$	$10.3 \pm 1.9(tot)$	$26.9 \pm 3.4(tot)$
Observed in Data	17	13	30

Table 10.2: A comparison of the number of events predicted by the standard model (SM) and the observations for the $t\bar{t}\gamma$ search. The SM predictions for this search are dominated by the $t\bar{t}\gamma$ production. Other contributions come from misidentified leptons, photons, b-jets, or $\not{E}_{\mathrm{T}}$. MC samples have been scaled to 6.0 fb^{-1}. All other Data-driven numbers have been measured in the manner described in earlier sections.

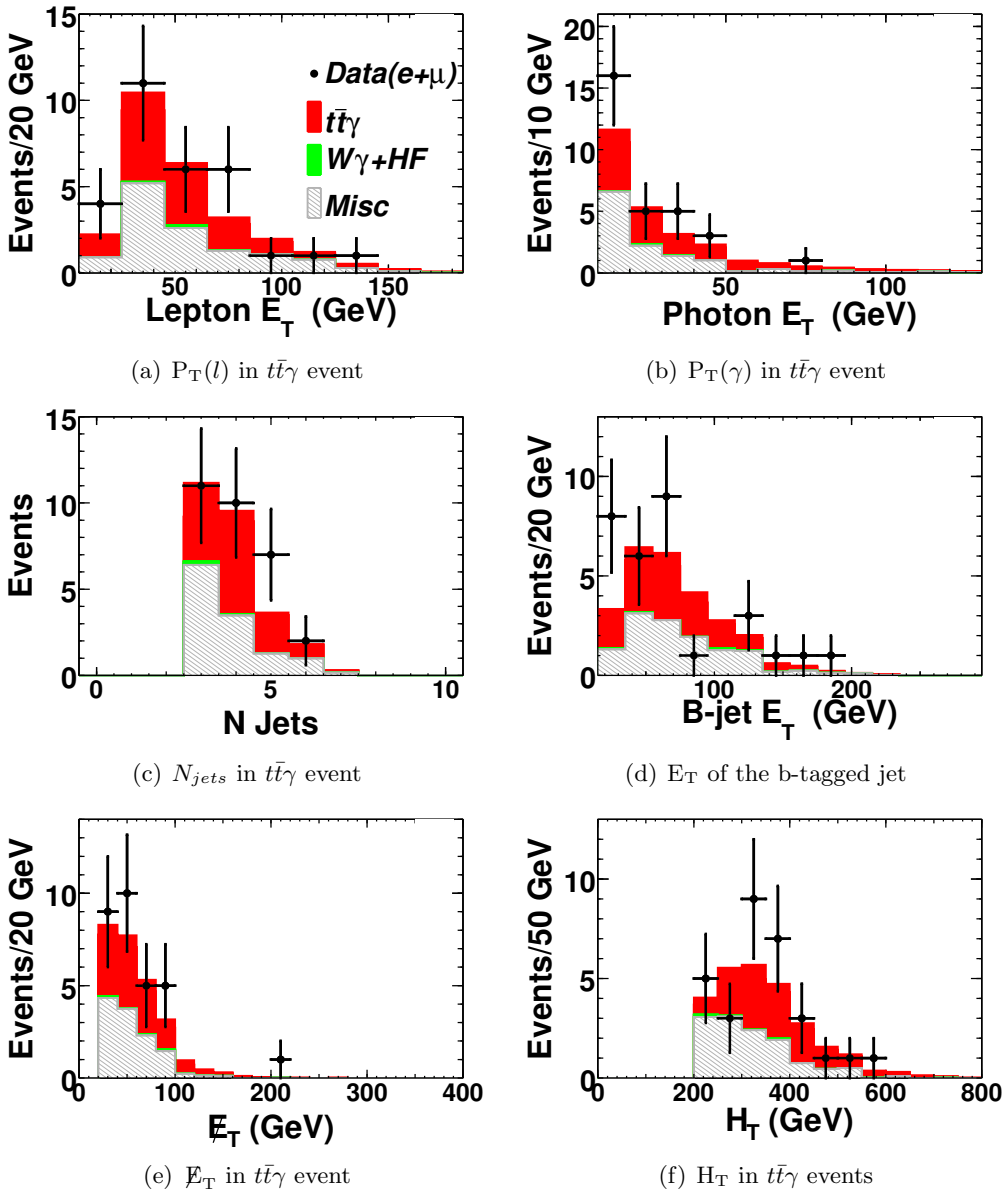

(a) $P_T(l)$ in $t\bar{t}\gamma$ event

(b) $P_T(\gamma)$ in $t\bar{t}\gamma$ event

(c) N_{jets} in $t\bar{t}\gamma$ event

(d) E_T of the b-tagged jet

(e) $\not{E}_T$ in $t\bar{t}\gamma$ event

(f) H_T in $t\bar{t}\gamma$ events

Figure 10.5: The following kinematic distributions for the $t\bar{t}\gamma$ sample are shown: a) the transverse energy (momentum) for electrons (muons), b) the transverse energy of the identified photon, c) the number of jets in the event, d) the transverse momentum of the identified b-jet, e) the missing transverse energy, f) the total transverse energy (H_T). The black dots are data, and the histograms show the expected SM contributions from radiative top decay ($t\bar{t}\gamma$), $W\gamma$ production with heavy flavor (HF), and Misc includes: WW, WZ, and single-top production as well as jets, τ leptons, electrons, and jets misidentified as photons, jets misidentified as leptons (QCD), and misidentified b-tags.

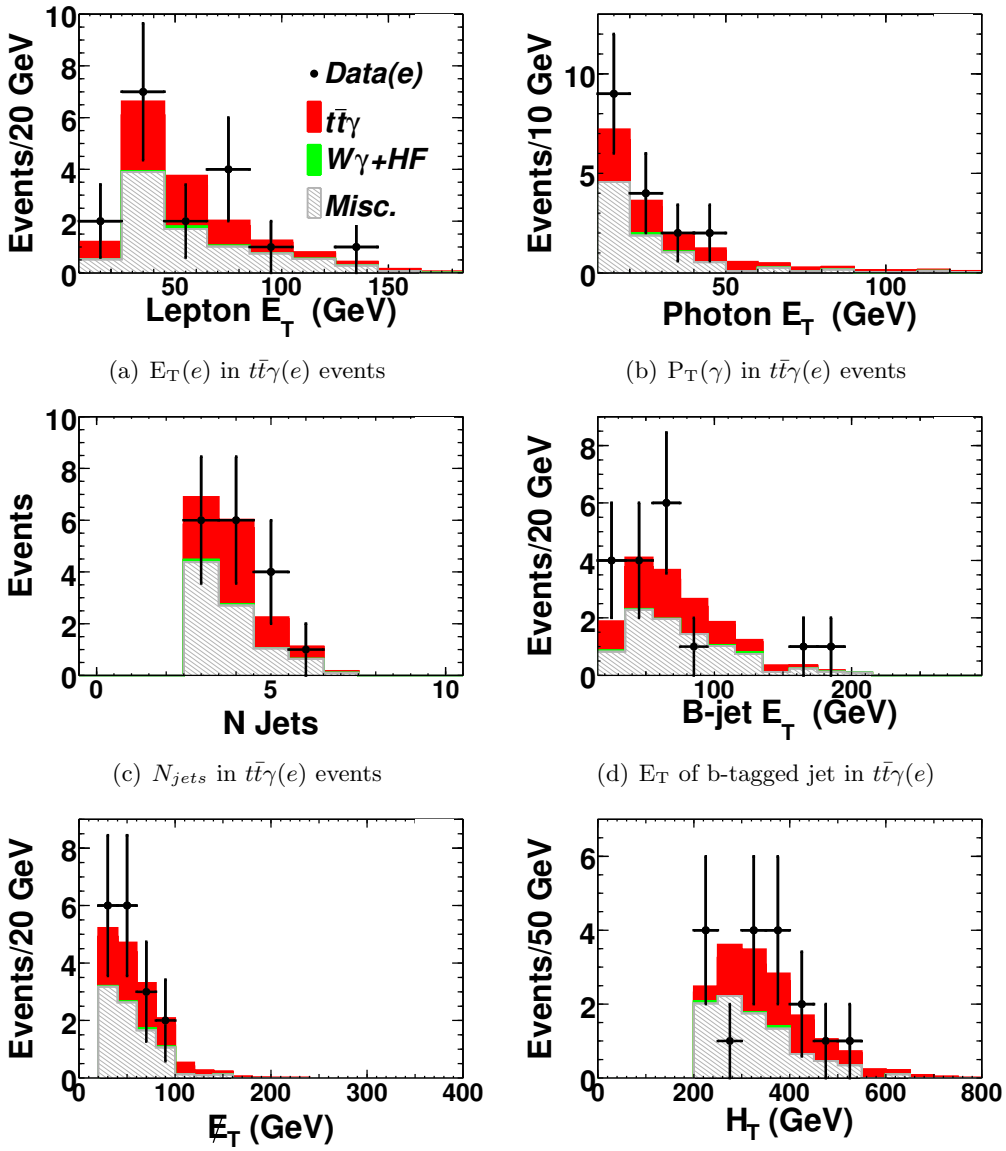

(a) $E_T(e)$ in $t\bar{t}\gamma(e)$ events

(b) $P_T(\gamma)$ in $t\bar{t}\gamma(e)$ events

(c) N_{jets} in $t\bar{t}\gamma(e)$ events

(d) E_T of b-tagged jet in $t\bar{t}\gamma(e)$

(e) $\not\!\!E_T$ observed in $t\bar{t}\gamma(e)$ events

(f) H_T observed in $t\bar{t}\gamma(e)$ events

Figure 10.6: The following kinematic distributions for $t\bar{t}\gamma$ (e-channel) events are shown: a) the transverse energy of the electron, b) the transverse energy of the identified photon, c) the number of jets in the event, d) the transverse momentum of the identified b-jet, e) the missing transverse energy, f) the total transverse energy (H_T). The black dots are data, and the histograms show the expected SM contributions from radiative top decay ($t\bar{t}\gamma$), $W\gamma$ production with heavy flavor (HF), and Misc includes: WW, WZ, and single-top production as well as jets, τ leptons, electrons, and jets misidentified as photons, jets misidentified as leptons (QCD), and misidentified b-tags.

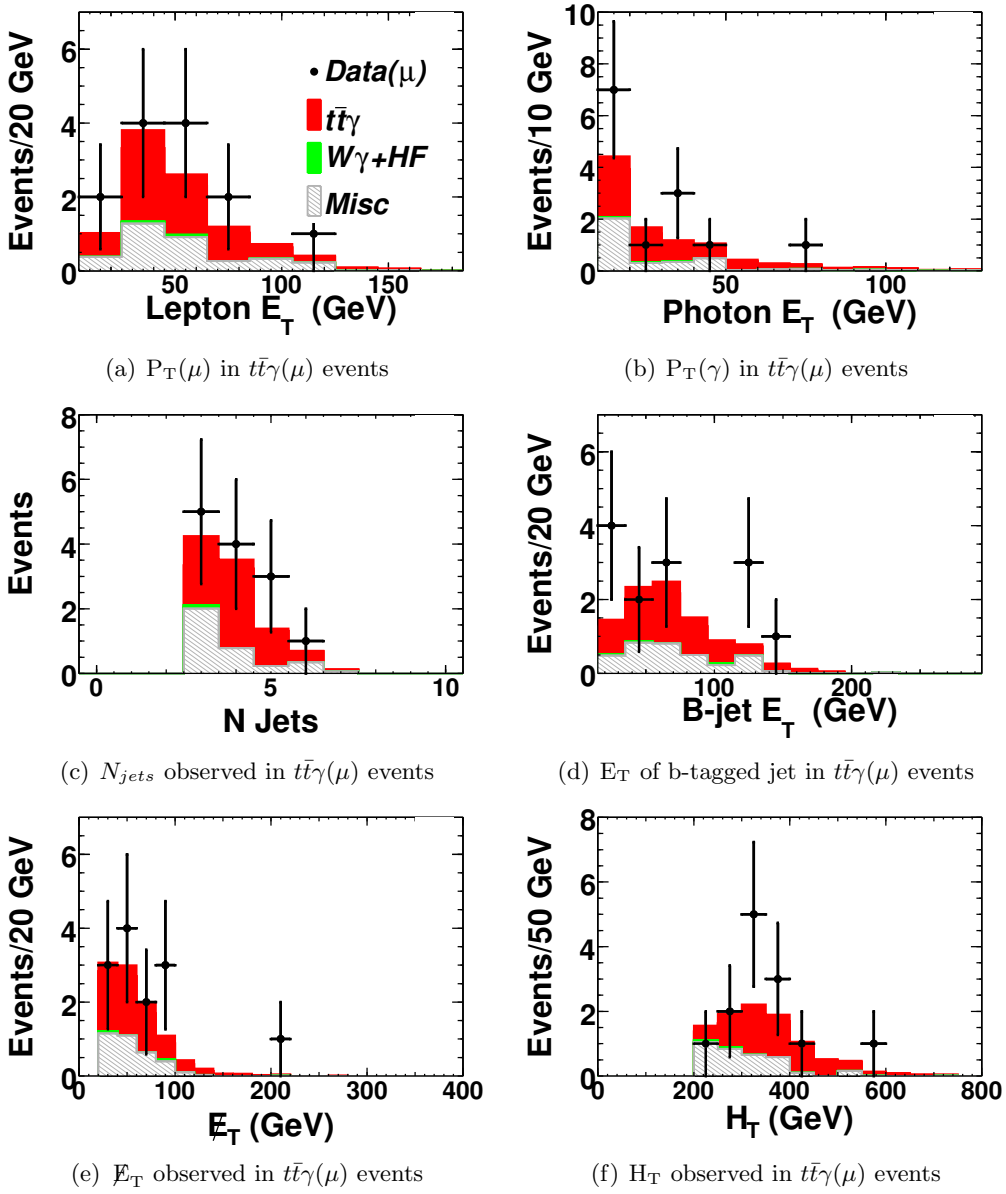

(a) $P_T(\mu)$ in $t\bar{t}\gamma(\mu)$ events

(b) $P_T(\gamma)$ in $t\bar{t}\gamma(\mu)$ events

(c) N_{jets} observed in $t\bar{t}\gamma(\mu)$ events

(d) E_T of b-tagged jet in $t\bar{t}\gamma(\mu)$ events

(e) $\not\!\!E_T$ observed in $t\bar{t}\gamma(\mu)$ events

(f) H_T observed in $t\bar{t}\gamma(\mu)$ events

Figure 10.7: The following kinematic distributions for the $t\bar{t}\gamma$ (μ-channel) events are shown: a) the transverse momentum, b) the transverse energy of the identified photon, c) the number of jets in the event, d) the transverse momentum of the identified b-jet, e) the missing transverse energy, f) the total transverse energy (H_T). The black dots are data, and the histograms show the expected SM contributions from radiative top decay ($t\bar{t}\gamma$), $W\gamma$ production with heavy flavor (HF), and Misc includes: WW, WZ, and single-top production as well as jets, τ leptons, electrons, and jets misidentified as photons, jets misidentified as leptons (QCD), and misidentified b-tags.

10.3 Results from the search for $t\bar{t}$

CDF Run II, 6.0 fb^{-1}			
$t\bar{t}$, Isolated Leptons, 3 or more jets, $H_T > 200$ GeV			
Standard Model Source	$eb\not{E}_T$	$\mu b\not{E}_T$	$(e+\mu)b\not{E}_T$
$t\bar{t}$	1420 ± 180	1080 ± 140	2500 ± 330
WW	29 ± 4	22 ± 3	51 ± 7
WZ	8.6 ± 1.1	6.5 ± 0.9	15.1 ± 2.0
ZZ	1.3 ± 0.2	1.0 ± 0.1	2.3 ± 0.3
$W^{\pm}b\bar{b}$ (inclusive)	203 ± 34	146 ± 24	348 ± 58
$W^{\pm}c\bar{c}$ (inclusive)	127 ± 23	94 ± 17	221 ± 40
$W^{\pm}c$ (inclusive)	85 ± 13	61 ± 9	147 ± 23
Single top (s-channel)	76 ± 10	59 ± 8	135 ± 18
Single top (t-channel)	66 ± 9	50 ± 7	116 ± 16
$Z \to ll + b\bar{b}$	31 ± 3	22 ± 2	53 ± 5
$Z \to \tau\tau$	6 ± 8	9 ± 8	14 ± 11
Mistags	358 ± 29	214 ± 17	572 ± 46
QCD (jets faking l and $\not{E}_T$)	222 ± 38	20 ± 3	240 ± 40
Total SM Prediction	2630 ± 196	1790 ± 146	4420 ± 340
Observed in Data	2720	1709	4429

Table 10.3: A comparison of the number of events predicted by the standard model (SM) and the observations for the $t\bar{t}$ search. The SM predictions for this search are dominated by the $t\bar{t}$ production. Other contributions come from jets misidentified as leptons, and light flavored jets mistakenly b-tagged. MC samples have been scaled to 6.0 fb^{-1}. All other data-driven numbers have been measured in the manner described in earlier sections.

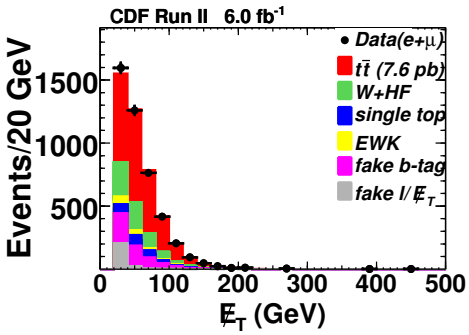

(a) $\not\!\!E_T$ observed in $t\bar{t}$ events

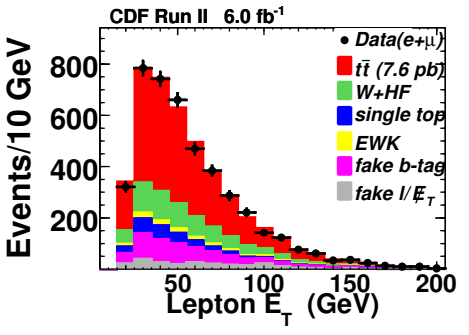

(b) E_T (p_T) of the e (μ) in $t\bar{t}$ events

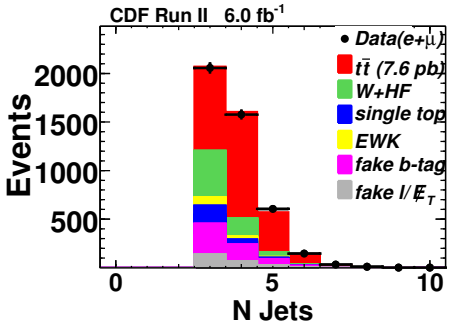

(c) N_{jets} in $t\bar{t}$ events

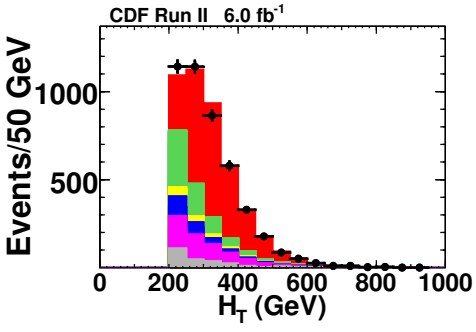

(d) H_T observed in $t\bar{t}$ events

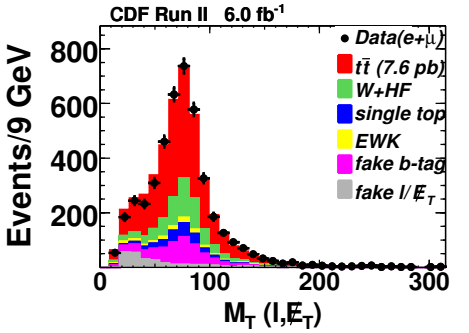

(e) M_T of the lepton and $\not\!\!E_T$ in $t\bar{t}$ events

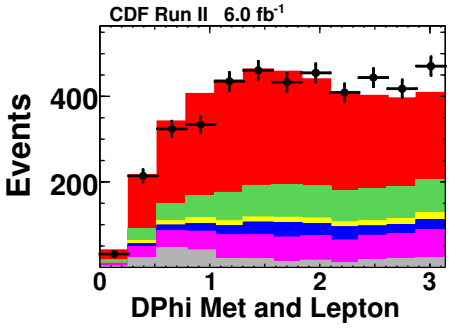

(f) Difference in ϕ between the lepton and $\not\!\!E_T$ in $t\bar{t}$ events

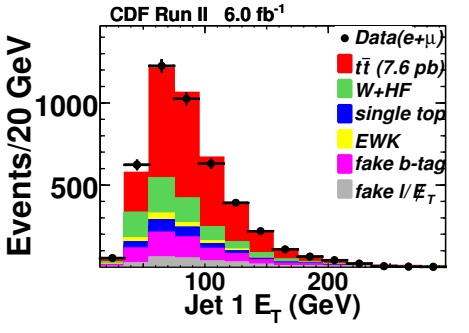

(g) E_T of the highest E_T jet in $t\bar{t}$ events

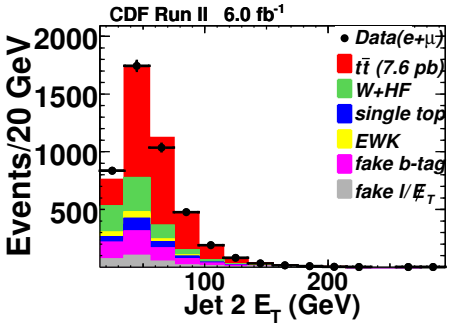

(h) E_T of the second highest E_T jet in $t\bar{t}$ events

Figure 10.8: Kinematic distributions for $t\bar{t}$ events

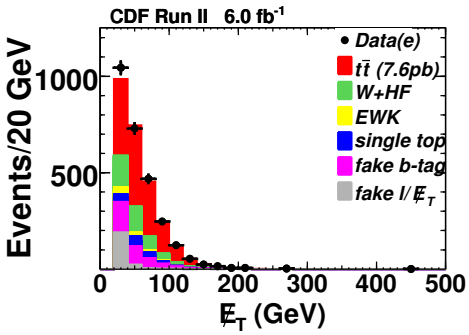

(a) $\not\!\!E_T$ observed in $t\bar{t}(e)$ events

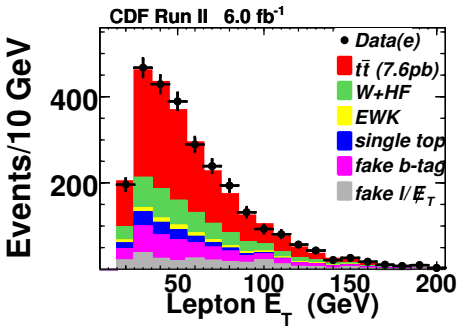

(b) $E_T(e)$ in $t\bar{t}(e)$ events

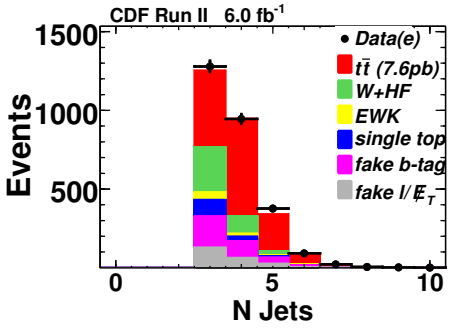

(c) N_{jets} in $t\bar{t}(e)$ events

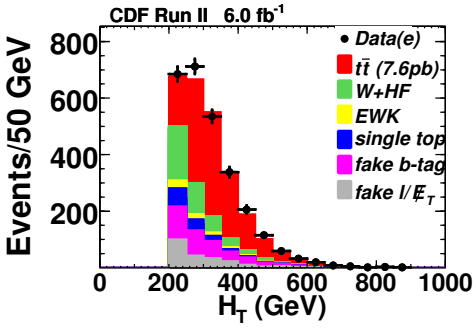

(d) H_T observed in $t\bar{t}(e)$ events

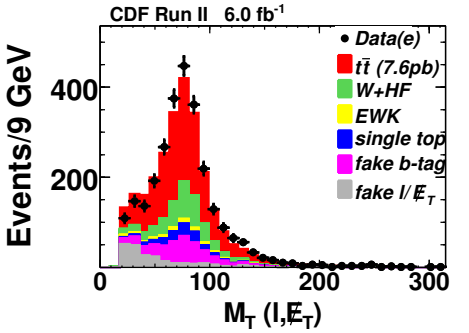

(e) M_T of the e and $\not\!\!E_T$ in $t\bar{t}(e)$ events

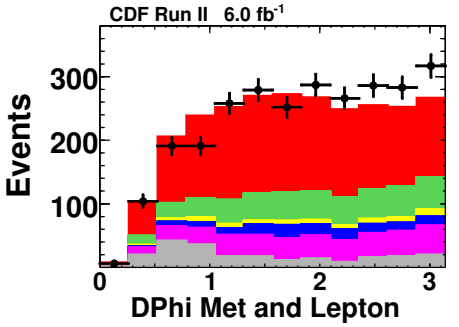

(f) Difference in ϕ between the e and $\not\!\!E_T$ in $t\bar{t}(e)$ events

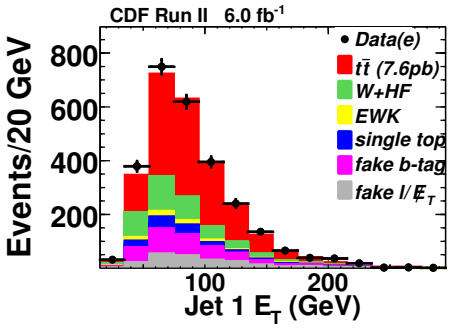

(g) E_T of the highest E_T jet in $t\bar{t}(e)$ events

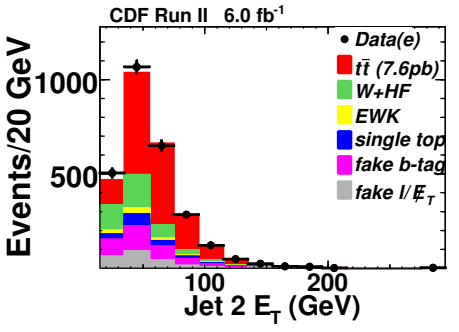

(h) E_T of the second highest E_T jet in $t\bar{t}(e)$ events

Figure 10.9: Kinematic distributions for $t\bar{t}$ (e-channel) events

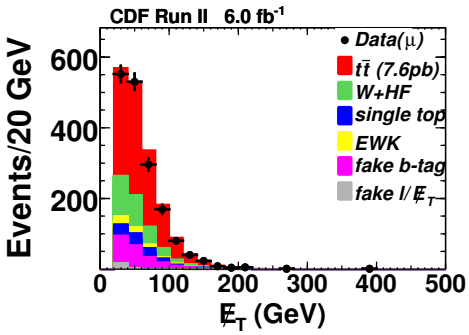

(a) $\not\!\!E_T$ observed in $t\bar{t}(\mu)$ events

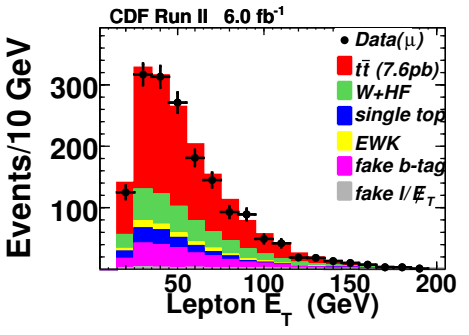

(b) $P_T(\mu)$ in $t\bar{t}(\mu)$ events

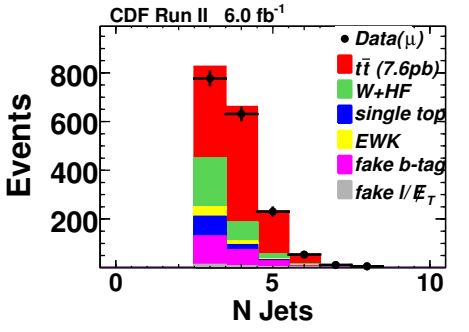

(c) N_{jets} in $t\bar{t}(\mu)$ events

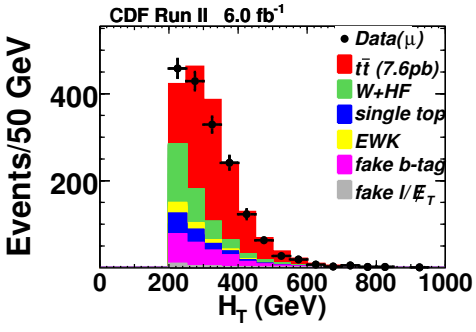

(d) H_T observed in $t\bar{t}(\mu)$ events

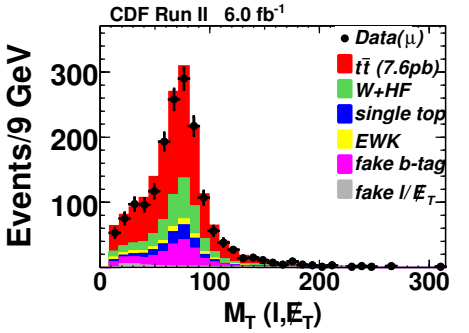

(e) M_T of the μ and $\not\!\!E_T$ in $t\bar{t}(\mu)$ events

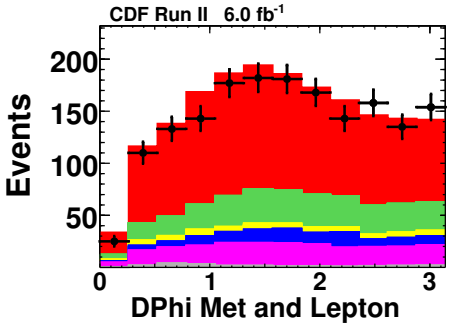

(f) Difference in ϕ between the μ and $\not\!\!E_T$ in $t\bar{t}(\mu)$ events

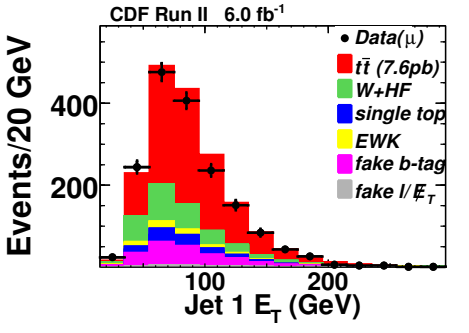

(g) E_T of the highest E_T jet in $t\bar{t}(\mu)$ events

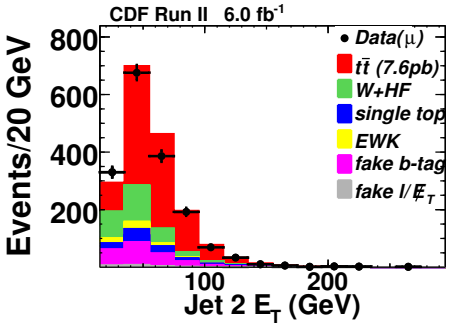

(h) E_T of the second highest E_T jet in $t\bar{t}(\mu)$ events

Figure 10.10: Kinematic distributions for $t\bar{t}$ (μ-channel) events

11 Conclusions

In this thesis, we presented a search for anomalous production of the signature $\ell+\gamma$+b-jet+$\not\!\!E_{\rm T}$ and a search for $t\bar{t}+\gamma$ events produced in $p\bar{p}$ collisions at $\sqrt{s} = 1.96$ TeV using data taken with the CDF detector during Run II at the Tevatron. In the $\ell\gamma\not\!\!E_{\rm T}b$ signature, we search for physics beyond the SM and do not see any significant deviations from predictions. However the $t\bar{t}\gamma$ process is fully predicted, but no experiment has seen evidence of it. By tightening our selection on the $\ell\gamma\not\!\!E_{\rm T}b$ signature we are able to search for an incredibly rare, yet fully predicted, physics process. Both of these signatures provide a test of the SM.

In searching for the the $\ell\gamma\not\!\!E_{\rm T}b$ signature, we did not see a large deviation from SM predictions. In the $\ell\gamma\not\!\!E_{\rm T}b$ signal sample, we observed 85 events, compared to the prediction of 99.1 ± 9.3 events. The dominant uncertainty in this signal is due to the QCD contribution to the $\ell\gamma\not\!\!E_{\rm T}b$ signal events. The largest discrepancy seems to be due to the predicted amount of QCD; this discrepancy is due to statistical effects, and will likely be resolved with more luminosity.

The QCD contribution is found by summing antielectron events with $\not\!\!E_{\rm T} > 20$ GeV. Examining these distributions more closely, there are two events with $\not\!\!E_{\rm T}$ just above the 20 GeV threshold. Had there been only one such event, the predicted number of events would have dropped by nearly 4 events. Our data would then be within one standard deviation of our predictions.

In the $t\bar{t}\gamma$ search, we use a LO generator (MadGraph) and find the LO leptonic $t\bar{t}\gamma$ cross section to be 0.094 pb. We then correct the LO calculation for NLO effects by multiplying by a k-factor $= \sigma_{NLO}/\sigma_{LO} = 0.977$ [59]. The SM estimate for the leptonic production cross section of $t\bar{t}\gamma$ is then found to be 0.092 pb. We use the branching ratio of W$\rightarrow l\nu$ (0.324) and find the production cross section of $t\bar{t}\gamma$, $\sigma_{t\bar{t}\gamma}$ = 0.17 pb[5]. The theoretical production cross section of $t\bar{t}$ at the Tevatron is found to be $7.08^{+0.00+0.36}_{-0.32-0.27}$ pb [60]. Using the ratio of these theoretical cross sections, we

[5]We know the total $t\bar{t}\gamma$ cross section is the sum of the hadronic, dileptonic, and semileptonic cross sections. Once produced, each W boson has a 0.324 chance of producing leptons. The probability of at least one W boson decaying leptonically is then $1 - 0.676^2 = 0.543$

compute the ratio of $t\bar{t}\gamma$ to $t\bar{t}$ to be $0.024\ ^{+0.012}_{-0.014}$.

We measured the semileptonic $t\bar{t}\gamma$ cross section

$$\sigma_{t\bar{t}\gamma} = \frac{(30\pm5.47)-(13.0\pm2.6)}{6.0\text{fb}^{-1}(0.0286\pm0.0031)} =$$
$$0.10 \pm 0.03(\text{stat.}) \pm 0.02(\text{sys.}) \pm 0.01(\text{lum.})\text{pb}$$

and the measured cross section compares well with the SM estimate. We have left uncombined the statistical (stat.), systematic (sys.) and luminosity (lum.) uncertainties. Using the branching ratio of W$\rightarrow l\nu = 0.324$, we find the $t\bar{t}\gamma$ production cross section to be:

$$\sigma_{t\bar{t}\gamma} = 0.18 \pm 0.08 \text{ pb}.$$

We also measured the $t\bar{t}$ production cross section

$$\sigma_{t\bar{t}} = \frac{(4429\pm66.55)-(1916.16\pm28.58\pm96.26)}{6.0\text{fb}^{-1}(0.05497\pm0.0046)} =$$
$$7.62 \pm 0.20 \text{ (stat.)} \pm 0.68(\text{sys.}) \pm 0.46(\text{lum.})\text{pb}$$

where we have left the statistical, systematic, and luminosity uncertainties uncombined.

Finally we compute the ratio between the production cross sections of $t\bar{t}\gamma$ and $t\bar{t}$ to be:

$$\Re = 0.024 \pm 0.009. \tag{11.1}$$

Our measurements agree well with theoretical predictions as well as previous similar measurements of similar signatures.

We observe 30 events in the $t\bar{t}\gamma$ signal sample. The predicted number of background (i.e. without $t\bar{t}\gamma$ events) events is 13.0$\pm$ 2.6 events. The probability of the backgrounds alone yielding 30 or more events is 0.0016 or 3.0 standard deviations on a Gaussian distribution. Three standard deviations is a point at which we may claim to have seen evidence of this process. This is the first evidence of associated production of $t\bar{t}$ with an electroweak gauge boson. The next benchmark for $t\bar{t}\gamma$ will

occur when the probability corresponds to five standard deviations, which is roughly 1 in a million; at this point we would claim that the $t\bar{t}\gamma$ process has been observed.

The Tevatron experiments will stop performing $p\bar{p}$ collisions in October of 2011. It is unlikely CDF will observe the $t\bar{t}\gamma$ process before the Tevatron shuts down. In an attempt to predict future measurements of the $t\bar{t}\gamma$ process, we extrapolate the current running conditions, and event yields up to the end of the running of the Tevatron.

In 2010, the CDF detector acquired nearly 2 fb^{-1} of data. Assuming this rate continues, by shutdown the CDF detector will have recorded 8.6 fb^{-1} of data. Further assuming that the rate of observed events and predictions grows linearly with the luminosity, and that the uncertainties behave as expected, we predict that CDF will observe 42.5 events, and the SM non-$t\bar{t}\gamma$ backgrounds will be about 18.4 ± 4.0 events. The probability of the backgrounds alone causing 42.5 events is 0.00066 or 3.2 standard deviations. With these results the precision of the cross-section or ratio measurements will not be largely changed.

Suppose for one final $t\bar{t}\gamma$ measurement at Tevatron, CDF and D0 were to combine their results for the $t\bar{t}\gamma$ signal sample after shutdown, and the rates of signal and backgrounds continued at CDF observed rates. Under these assumptions, the combination would observe 86.4 signal events and the SM non-$t\bar{t}\gamma$ backgrounds would be about 36.7 ± 5.6 events. The probability of the backgrounds alone yielding 86.4 signal events is 7.2×10^{-5} or 4.7 standard deviations. With some improvements, and perhaps a few additional unexpected signal events, a five standard deviation result could be seen at the Tevatron after shutdown.

This search will have a new life at the LHC. There are many interesting properties left to measure about the top quark and its couplings to the electroweak bosons Z^0 and γ. Detailed parameters associated with these couplings cannot be measured at the Tevatron. The dominant production of $t\bar{t}$, at the Tevatron, is quark-antiquark annihilation; initial state radiation limits the sensitivity of $t\bar{t}\gamma$ production to anomalous quark couplings. Furthermore, the $t\bar{t}+Z^0$ cross section is approximately 20 times smaller than that of the $t\bar{t}\gamma$ process. The future of experiments

with $t\bar{t}$+X, where X is an electroweak boson, is at the LHC.

Design parameters should allow the LHC to eventually accumulate 300 fb^{-1} of data. At 300 fb^{-1} of luminosity, the LHC experiments will easily be able to measure the $t\bar{t}\gamma$ cross section, and most likely observe the $t\bar{t}\gamma$ process. Further, ATLAS and CMS should be able to probe the $t\bar{t}\gamma$ coupling with a precision of about 4-7% per experiment [61]. With 300 fb^{-1} of data collected at the LHC, the process $t\bar{t}$+Z^0 is likely to be measured and the associated couplings of the Z^0 boson to the top quark will allow an even deeper probe of the SM.

While nature did not provide an exciting and significant excess in any of the searches we have performed, we have demonstrated evidence for a process with a rate lower than that of a Higgs boson with a mass between 120 and 140 GeV/c^2, which is no small feat. The LHC will find the selection criteria in this analysis useful for similar searches.

12 Acknowledgments

We are grateful to Uli Baur for invaluable help with our analysis and help for generating MC processes, and help finding theoretical predictions of both the $t\bar{t}$ and the $t\bar{t}\gamma$ cross sections for the Tevatron. We thank Tim Steltzer, Steve Mrenna, and Fabio Maltoni for their support and development for MadGraph and Pythia and Soushi Tsuno for help with our MC. Alexander Paramonov helped us to get started on the TTGNtuple. We thank Tom Schwarz for his valuable insights in helping us improve the $t\bar{t}$ sample. We thank Ray Culbertson for his many contributions. We would also like to thank our CDF collaborators for their many contributions.

A Comparisons of Signal Events from 1.9 fb^{-1} to 6.0 fb^{-1}

In this section we present tables showing the run and event numbers, and various kinematic featrues of signal events found in a previous $t\bar{t}\gamma$ analysis [12], and what we find in our analysis of 6.0 fb^{-1}.

A.1 Comparison of Standard Signatures Between UCNtuple and the TTGNtuple.

We have made the following cross-checks against UCNtuple to verify the TTGNtupler code, for data periods: bhel0h, bhmu0h, bhel0d, and bhmu0d:

- Have compared number of dilepton events in both electron and muon data streams
- Checked further across all six combinations of CMX, CMUP and stubless muons
- Checked for Z's decaying to both central electrons, or one central and one plug electron
- Compared number of dilepton and photon events
- Compared number of lepton, photon, and $\not\!\!E_{\text{T}}$ events

For the first 1.78 fb^{-1} we made further comparisons

- Repeated comparisons mentioned above
- Checked the run and event numbers of all $\ell\gamma\not\!\!E_{\text{T}}b$ events

We have compared event yields obtained in the UCNtuple and in the TTGNtupler for the first 1.78 fb^{-1}, and results are shown in Tables A.1. The errors in the tables are only statistical, and do not take into consideration any systematic effects.

We see very good agreement between the TTGNtuple which is built on top of the STNtuple, and results from the UCNtuple. It is important to note that

there were differences between how the event parameters were calculated between the two data formats, such as event vertex and b-tagging which can change event parameters.

Next we compared $\ell\gamma\not{E}_{\rm T}b$ signal events observed in the UCNtuple code, and those observed in the TTGNtuple code. We observed that there was one additional signal event (run 185594, event 1009158) in the same range, and this was due to a change in the b-tagging prescription between the ntupling.

Dataset	Number of Zs	Number of W's	Number of lg$\not{E}_{\rm T}$	Number of llg
TTG (μ)	31.43 ± 0.13	474.78 ± 0.52	0.72 ± 0.020	0.19 ± 0.010
UC (μ)	31.43 ± 0.13	474.95 ± 0.52	0.74 ± 0.020	0.19 ± 0.010
TTG (e)	31.91 ± 0.13	700.59 ± 0.63	0.83 ± 0.022	0.27 ± 0.012
UC (e)	31.86 ± 0.13	695.52 ± 0.63	0.83 ± 0.022	0.27 ± 0.012

Table A.1: TTGntuple vs UCntuple comparison for Muon events. The luminosity was found using the good run list v17 with em mu and silicon. We see decent agreement between TTG and UC ntuples with a disagreement of 2%. Using the good run list and the SAM lumi script we find the luminosity to be 1.78 pb^{-1}

A.2 List Of Lepton-Photon-$\not{E}_{\rm T}$-B Events (1.9 fb^{-1})

run/event	$P_T(\ell)$	$\not{E}_{\rm T}$	M($\ell\not{E}_{\rm T}$)	$P_T(\gamma)$	M($W\gamma$)	H_T	$P_T(\ell\gamma)$	M($\ell\gamma$)	jets	b tags
196879/3659187	22.03	44.62	44.46	40.89	77.91	272.77	62.83	21.71	4	1
196892/77507	37.88	41.17	74.72	14.71	89.41	138.17	52.04	43.56	1	1
197321/1409712	27.36	57.74	51.78	20.42	62.56	323.96	46.91	18.62	5	1
193396/1050006	39.31	86.54	56.02	12.25	74.13	349.52	35.89	37.30	4	2
207488/2477561	73.01	89.01	6.43	13.62	23.96	413.75	84.99	17.48	4	2
209850/2864478	40.56	59.57	70.66	62.93	159.08	259.32	73.28	85.57	2	1
222835/7771229	66.94	21.69	41.06	35.33	109.30	243.99	40.11	94.72	3	1
223494/10133378	30.90	28.91	56.38	10.34	63.60	91.90	39.49	12.23	1	1
227377/11344663	53.97	29.02	78.48	10.23	86.21	116.46	63.48	24.03	1	1
231294/19688018	28.33	21.17	5.52	10.38	26.43	117.61	34.20	22.50	2	1
232226/1187677	37.45	23.52	59.19	32.60	86.34	134.06	55.72	68.69	1	1
233110/55577	88.95	29.68	96.10	10.04	105.16	187.45	90.74	39.83	1	1
233798/1492655	51.20	29.35	59.20	43.12	123.08	206.84	30.16	89.42	3	1
234663/13735055	39.13	56.83	81.25	18.65	100.18	206.77	57.63	29.17	3	2
236965/6459811	44.66	44.31	62.77	27.05	84.38	200.71	45.36	66.81	2	1
237478/34732412	28.46	28.07	7.68	27.26	28.46	219.67	53.49	20.93	3	1

Table A.2: List Of $e\gamma\not{E}_{\rm T}b$ Events

run/event	$P_T(\ell)$	$\not\!\!E_{\rm T}$	M($\ell\not\!\!E_{\rm T}$)	$P_T(\gamma)$	M($W\gamma$)	H_T	$P_T(\ell\gamma)$	M($\ell\gamma$)	jets	b tags
160591/847583	70.10	23.20	26.48	11.11	28.70	282.57	80.61	12.99	5	1
155996/1456579	27.42	31.06	51.75	21.88	74.81	107.33	46.60	26.19	1	1
197287/7739046	48.69	82.20	21.88	37.14	78.33	385.24	77.19	63.27	3	1
199620/711826	46.02	27.41	70.38	107.97	158.19	321.51	61.95	182.40	2	1
195343/9039070	27.59	53.02	68.64	45.81	97.28	213.05	67.14	37.49	3	1
206828/3127590	122.91	45.52	50.90	17.39	81.35	353.99	132.36	49.65	3	2
209532/76676	26.49	65.50	15.64	28.99	92.49	194.06	19.15	52.09	1	1
209819/2062462	46.11	72.74	7.19	16.51	17.70	342.24	61.45	15.28	3	1
209862/445276	37.65	47.25	55.31	13.75	84.58	332.52	31.44	47.38	3	1
218692/305924	22.25	32.01	49.37	46.57	94.67	162.16	34.96	59.28	3	1
221201/7636658	68.58	47.08	67.79	12.87	98.84	367.00	55.75	60.49	6	1
221723/9869061	22.44	98.04	19.44	13.77	67.72	351.00	27.08	32.02	5	3

Table A.3: List Of $\mu\gamma\not\!\!E_{\rm T}b$ Events

A.3 List Of Lepton-Photon-$\not\!\!E_{\rm T}$-B Events (6.0 fb^{-1})

run/event	$P_T(\ell)$	$\not\!\!E_{\rm T}$	M($\ell\not\!\!E_{\rm T}$)	$P_T(\gamma)$	M($W\gamma$)	H_T	$P_T(\ell\gamma)$	M($\ell\gamma$)	jets	b tags
263189/1635317	39.74	38.57	75.97	10.49	83.78	110.43	42.65	27.82	1	1
185594/10091587	21.29	65.06	21.75	24.79	40.69	311.21	38.38	25.49	5	1
155996/1456579	27.42	31.08	51.74	21.85	74.79	107.69	46.57	26.22	1	1
160591/847583	70.10	23.20	26.47	11.11	28.70	281.76	80.61	12.99	5	1
195343/9039070	27.60	56.14	70.29	45.80	99.10	231.93	67.15	37.50	4	1
199620/711826	46.12	27.29	70.30	107.92	158.23	319.82	61.81	182.59	2	1
197287/7739046	48.57	82.11	21.80	37.12	78.21	383.10	77.06	63.27	3	1
209532/76676	26.52	65.53	15.62	29.06	92.65	193.33	19.19	52.18	1	1
209819/2062462	46.00	73.28	7.00	16.58	17.74	342.23	61.42	15.29	3	1
209862/445276	37.61	46.95	54.76	13.77	84.19	331.10	31.40	47.39	3	1
221723/9869061	22.46	97.88	19.48	13.77	67.71	349.34	27.10	32.03	5	3
218692/305924	22.30	31.96	49.43	46.57	94.65	161.31	34.94	59.35	3	1
221201/7636658	68.83	46.78	68.40	12.87	99.18	364.37	56.00	60.59	6	1
206828/3127590	122.94	45.41	51.14	17.39	81.53	351.44	132.39	49.65	3	2
239906/2521891	41.39	46.19	67.07	16.23	82.95	160.93	56.79	10.48	1	1
242648/1139872	45.10	46.95	80.16	69.34	140.79	238.57	109.91	32.37	1	1
244676/30558295	29.19	77.72	95.16	14.14	104.16	369.97	16.43	44.77	2	1
255090/1491384	20.29	42.65	41.39	11.35	50.82	137.75	17.06	26.65	2	1
255674/9652682	45.31	20.07	53.72	11.71	68.81	121.59	47.68	42.39	2	1
256581/55740	47.98	38.95	53.25	26.00	68.43	197.60	73.81	18.10	2	1
259189/993053	37.31	57.58	10.24	48.52	13.50	291.92	85.78	26.55	2	1
259673/16312239	47.70	37.26	81.68	12.39	95.23	323.45	53.18	43.62	4	1
265582/12252209	32.12	26.13	56.23	19.05	69.38	104.63	43.72	41.03	1	1
263877/861995	44.24	47.81	91.43	42.76	130.49	247.39	79.45	52.59	2	1
273941/7990271	21.17	70.39	77.07	52.12	131.18	284.96	59.52	48.85	2	1
274454/7114423	24.19	29.61	47.98	20.65	64.74	98.01	13.60	44.06	1	1
275267/4787467	39.85	31.02	56.11	15.51	63.64	147.91	54.00	12.26	3	1
283848/715117	20.17	32.65	50.75	30.64	76.43	109.73	46.81	32.76	1	1
289019/7952256	37.09	32.15	27.84	38.52	71.42	286.37	66.74	51.16	3	1
284145/12389851	31.64	37.53	63.29	13.64	79.60	179.06	19.87	42.52	2	1
286649/5942921	43.26	210.92	76.95	34.25	131.46	571.63	75.13	20.86	4	1
288288/8522938	22.08	44.30	35.14	20.17	51.00	206.80	42.16	16.75	2	1
287885/14307179	57.71	84.15	68.38	77.37	139.62	424.14	129.68	86.05	4	1

Table A.4: List Of $\mu\gamma\not\!\!E_{\rm T}b$ Events 6.0 fb^{-1}

run/event	$P_T(\ell)$	$\not\!\!E_{\rm T}$	M($\ell\not\!\!E_{\rm T}$)	$P_T(\gamma)$	M($W\gamma$)	H_T	$P_T(\ell\gamma)$	M($\ell\gamma$)	jets	b tags
193396/1050006	39.38	86.47	56.79	12.25	74.80	346.89	35.78	37.50	4	2
196879/3659187	22.04	44.71	44.11	40.90	77.80	274.41	62.81	21.91	4	1
196892/77507	37.90	41.19	74.61	14.71	89.34	137.60	52.02	43.70	1	1
197321/1409712	27.42	57.40	52.19	20.42	62.95	317.91	46.92	18.80	5	1
207488/2477561	72.99	88.74	6.03	13.62	23.77	407.81	85.00	17.43	4	2
209850/2864478	40.82	59.96	71.55	63.23	160.01	259.54	74.03	85.82	2	1
222835/7771229	67.22	21.63	41.27	35.33	109.62	244.20	40.14	95.00	3	1
223494/10133378	31.02	28.91	56.39	10.29	63.55	92.02	39.61	12.07	1	1
227377/11344663	54.19	28.99	78.55	10.19	86.25	116.81	63.64	24.09	1	1
231294/19688018	28.60	21.24	5.47	10.36	26.58	117.93	34.39	22.70	2	1
232226/1187677	37.98	23.49	59.55	32.92	87.14	135.11	56.10	69.77	1	1
233110/55577	90.28	28.85	92.70	10.08	101.89	215.32	92.05	40.28	2	1
233798/1492655	51.39	29.22	59.58	43.12	123.16	205.91	30.65	89.46	3	1
234663/13735055	39.28	56.87	81.10	18.65	100.08	207.33	57.75	29.31	3	2
236965/6459811	44.86	44.27	62.64	27.05	84.28	199.48	45.70	66.82	2	1
237478/34732412	28.62	27.99	7.77	27.25	27.93	217.81	53.78	20.57	3	1
238452/3001418	21.55	48.73	44.27	16.98	61.87	165.09	38.36	25.50	2	1
239853/6663393	60.92	46.39	69.29	21.24	89.48	368.03	60.51	58.17	2	1
243070/9866427	40.65	31.55	70.92	20.12	86.62	114.74	60.76	24.33	1	1
244485/6641451	23.71	69.29	51.48	27.54	67.42	307.21	50.43	17.69	3	1
255142/9581948	82.39	54.96	86.00	14.02	94.93	371.09	87.70	43.18	4	1
256076/323194	33.47	25.44	43.28	35.10	69.87	273.04	41.47	57.16	2	1
259929/17566118	29.34	27.90	49.42	11.32	65.89	527.85	21.03	40.07	5	1
263572/787882	40.23	46.51	86.51	19.58	105.22	125.87	56.99	25.17	1	1
263597/15412402	146.08	34.09	137.83	64.59	187.73	407.35	190.66	92.39	2	1
265865/2447364	57.02	85.64	139.50	21.21	158.91	241.44	63.60	50.25	2	1
266209/10796672	72.17	43.15	61.83	12.39	65.34	383.59	83.63	19.46	6	1
266618/2186795	91.69	50.40	132.51	13.75	151.17	401.23	78.46	73.94	3	1
267393/4100968	30.35	51.29	76.49	17.69	97.48	186.86	47.48	33.58	2	1
268356/2385623	35.51	63.74	71.46	23.53	107.44	178.61	52.33	27.68	1	1
268906/7480455	26.86	37.55	38.89	11.63	55.36	117.35	19.86	32.96	2	1
270000/10044710	31.03	53.26	67.28	14.86	92.22	153.25	34.37	31.81	2	1
270063/20707930	21.65	31.81	52.49	20.03	68.72	95.24	22.20	39.99	1	1
270140/651228	75.88	30.36	92.27	13.51	102.12	179.87	82.37	50.79	1	1
270434/8460797	60.57	61.68	114.47	25.16	146.26	320.34	61.08	60.77	4	1
273747/7624925	53.84	41.04	67.50	22.66	83.87	196.29	75.95	22.05	1	1
275728/4876317	64.15	41.17	76.86	30.98	129.09	177.44	51.82	90.94	1	1
275804/18282441	36.67	27.67	63.50	14.83	76.66	398.56	36.32	44.16	5	1
277505/3178590	32.92	64.37	54.22	12.73	58.62	210.24	40.01	32.67	2	1
284145/13516440	39.14	31.87	70.41	16.19	85.08	111.84	50.47	22.96	1	1
284548/13105874	136.03	30.76	19.61	12.88	36.16	388.59	146.01	29.66	4	1
285112/1499977	25.29	40.22	54.76	10.54	69.57	105.05	33.35	13.16	1	1
285220/11443424	25.62	39.89	60.48	18.87	81.55	297.76	43.84	9.22	2	1
285353/523667	32.77	34.52	56.43	11.29	70.42	116.21	41.11	16.48	1	1
285569/3068625	34.34	21.94	39.49	13.01	52.38	102.84	32.84	34.15	1	1
285851/8166809	26.19	61.52	79.48	34.65	122.32	470.84	59.61	40.83	5	2
286665/2186117	44.33	42.40	76.44	11.00	83.03	157.53	53.10	19.44	2	1
287396/3664026	31.43	53.51	81.97	18.71	95.25	132.23	15.04	47.87	1	1
288485/7268797	63.18	85.57	93.40	50.36	121.71	478.02	113.38	32.66	2	2
288886/8553454	45.46	38.82	75.89	20.84	103.50	125.71	44.74	56.01	1	1
289107/4996702	50.59	166.98	83.38	13.26	86.42	516.79	59.70	23.52	5	2

Table A.5: List Of $e\gamma\not\!\!E_{\rm T}b$ Events 6.0 fb^{-1}

B Stripping the STNtuple into a TTGNtuple

The stripped TTGNtuple begins with stripping the StNtuple to events which contain at least one loose lepton, or an antielectron.

We then further strip the TTGNtuple requiring one of the following groups of objects must be in an event:

- a tight lepton and a loose lepton
- tight photon and loose lepton
- loose lepton and met > 15
- antielectron + a photon
- antielectron + a bjet
- met > 15 and bjet > 0
- met > 15 and a tight photon
- loose lepton and a bjet
- bjet and a photon.

B.1 TTGNtupler package

The TTGNtupler package is an ntupler built on top of the Stntuple framework using its classes and methods to access information about the data.

When first running the package over the Stntuples we produce TTGNtuples on the CDF CAF and saved them on the UChicago Clusters. We show the initial number of events in the Stntuple as well as the amount of events which have at least one loose lepton or one antielectron.

Dataset	Stntuple	N Events	N Stripped	Begin Run	End Run	int.lumi (pb)
bhel0d	bhelbd	26,499,561	3,338,119	138425	186598	520
bhel0h	bhelbh	19,813,851	2,831,808	191208	203799	460
bhel0i	bhelbi	28,940,435	3,958,586	203819	228596	730
bhel0i, bhel0j	bhelbij	11,588,610	1,483,459	228664	233111	290
bhel0j	bhelbj	32,259,040	3,964,960	233133	246231	760
bhel0k	bhelbk	37,161,882	2,917,732	252836	261005	380
bhel0m	bhelbm	194,285,076	11,635,876	261119	289197	3430
bhel0p	bhelbp	26,811,506	1,741,178	289273	291025	450
bhmu0d	bhmubd	6,629,080	785,803	138425	186598	520
bhmu0h	bhmubh	5,740,083	629,063	191208	203799	460
bhmu0i	bhmubi	8,853,061	972,538	203819	228596	730
bhel0i, bhel0j	bhelbij	4,712,958	452,395	228664	233111	290
bhmu0j	bhmubj	12,578,391	1,216,406	233133	246231	760
bhmu0k	bhmubk	32,847,648	1,620,320	252836	261005	380
bhmu0m	bhmubm	127,623,660	6,150,455	261119	289197	3430
bhmu0p	bhmubp	10,885,737	647,755	289273	291025	450

Table B.1: Results of isolating events with at least one loose lepton or antielectron from raw Stntuples

Dataset	TTG Location (UC diskspace)	Stripped Location (Yale diskspace)
bhelbd	/cdf/s13/auerbach/cafTest/bhelbd/	/group/cdf/data/auerbach/benbhelbdNEW.11/
bhelbh	/cdf/s9/auerbach/cafTest/bhelbh/	/group/cdf/data/auerbach/benbhelbhNEW.11/
bhelbi	/cdf/s9/auerbach/cafTest/bhelbi/	/group/cdf/data/auerbach/benbhelbiNEW.11/
bhelbi, bhelbj	/cdf/s13/auerbach/cafTest/bhelij/	/group/cdf/data/auerbach/benbhelbij.11/
bhelbj	/cdf/s9/auerbach/cafTest/bhelbj/	/group/cdf/data/auerbach/benbhelbjNEW.11/
bhelbk	/cdf/s9/auerbach/cafTest/bhelbk/	/group/cdf/data/auerbach/benbhelbkNEW.11/
bhelbm	/cdf/s9/auerbach/cafTest/bhelbm/	/group/cdf/data/auerbach/benbhelbmh.11/ /group/cdf/data/auerbach/benbhelbmlow.11/
bhelbm	/cdf/s9/auerbach/cafTest/newbhelbm/	/group/cdf/data/auerbach/newelbm.11/
bhmubd	/cdf/s13/auerbach/cafTest/bhmubd/	/group/cdf/data/auerbach/benbhmubdNEW.13/
bhmubh	/cdf/s9/auerbach/cafTest/bhmubh/	/group/cdf/data/auerbach/benbhmubhNEW.13/
bhmubi	/cdf/s9/auerbach/cafTest/bhmubi/	/group/cdf/data/auerbach/benbhmubiNEW.13/
bhmubi, bhmubj	/cdf/s13/auerbach/cafTest/bhmuij/	/group/cdf/data/auerbach/benbhmubij.13/
bhmubj	/cdf/s9/auerbach/cafTest/bhmubj/	/group/cdf/data/auerbach/benbhmubjNEW.13/
bhmubk	/cdf/s9/auerbach/cafTest/bhmubk/	/group/cdf/data/auerbach/benbhmubkNEW.13/
bhmubm	/cdf/s9/auerbach/cafTest/bhmubm/	/group/cdf/data/auerbach/benbhmubmNEW.13/
bhmubm	/cdf/s9/auerbach/cafTest/newbhmubm/	/group/cdf/data/auerbach/newmubm.13/

Table B.2: Location of the TTGntuples processed on the CDF CAF, and then transferred to the University of Chicago machines.

C Total Amount of Double Counting for $\ell\gamma \not\!\!E_{\rm T} b$ and $t\bar{t}\gamma$ Signals

In this section we show two tables that show the total amount of double counting from each of the six pairs of data-driven background samples.

CDF Run II Preliminary, 6.0fb^{-1}			
Lepton + Photon + $\not\!\!E_{\rm T}$ + b Events, Isolated Leptons			
Double Counting Source	$e\gamma b\not\!\!E_{\rm T}$	$\mu\gamma b\not\!\!E_{\rm T}$	$(e+\mu)\gamma b\not\!\!E_{\rm T}$
Jets Faking Photons and Electrons Faking Photons	0.0085	0	0.00850
Jets Faking Photons and Mistags	3.92	1.90	5.820
Jets Faking Photons and QCD	0	0	0
Electrons Faking Photons and QCD	0	0	0
Mistags and QCD	0.18	0.0032	0.180
Mistags and electrons faking photons	0.25	0.10	0.35
Total amount of Double Counting	4.36	2.00	6.360

Table C.1: This table shows the predicted amount of double counting between two data- driven backgrounds for the $\ell\gamma\not\!\!E_{\rm T}b$ signal

CDF Run II Preliminary, 6.0fb^{-1}			
$t\bar{t}\gamma$, Isolated Leptons, Tighter Chi2 Cut on Photons			
Double Counting Source	$e\gamma b\not\!\!E_{\rm T}$	$\mu\gamma b\not\!\!E_{\rm T}$	$(e+\mu)\gamma b\not\!\!E_{\rm T}$
Jets Faking Photons and Electrons faking Photons	0.0085	0	0.00850
Jets Faking Photons and Mistags	0.29	0.15	0.440
Jets Faking Photons and QCD	0	0	0
Electrons Faking Photons and QCD	0	0	0
Mistags and QCD	0	0	0
Mistags and electrons faking photons	0.039	0.031	0.070
Total amount of Double Counting	0.34	0.18	0.520

Table C.2: This table shows the predicted amount of double counting between two data- driven backgrounds for the $t\bar{t}\gamma$ signal

D Full Requirements Used for MadGraph MC Sets

In this subsection we present a table showing the full list of event parameters that were used to generate the MadGraph MC samples.

```
#*********************************************************************
# Minimum pt's                                                       *
#*********************************************************************
  6  = ptj ! minimum pt for the jets
  6  = ptb ! minimum pt for the b
  6  = pta ! minimum pt for the photons
  6  = ptl ! minimum pt for the charged leptons
#*********************************************************************
```

```
# Maximum rapidity                                                    *
#*********************************************************************
 4.0  = etaj ! max rap for the jets
 4.0  = etab ! max rap for the b
 2.0  = etaa ! max rap for the photons
 4.0  = etal ! max rap for the charged leptons
#*********************************************************************
# Minimum DeltaR distance                                             *
#*********************************************************************
 0.4 = drjj ! distance between jets
 0.4   = drbb ! distance between b's
 0.4 = drll ! distance between leptons
 0.4 = draa ! distance between gammas
 0.4   = drbj ! distance between b and jet
 0.4 = draj ! distance between gamma and jet
 0.4 = drjl ! distance between jet and lepton
 0.4   = drab ! distance between gamma and b
 0.4   = drbl ! distance between b and lepton
 0.4 = dral ! distance between gamma and lepton
#*********************************************************************
# Minimum invariant mass for pairs                                    *
#*********************************************************************
 0  = mmjj ! min invariant mass of a jet pair
 10  = mmbb ! min invariant mass of a b pair
 0  = mmaa ! min invariant mass of gamma gamma pair
 10  = mmll ! min invariant mass of l+l- (same flavour) lepton pair
#*********************************************************************
```

E SM MC Samples Used for $t\bar{t}$ Analysis

In this short section we merely list the SM MC dataset names and cross sections used to analyze the $t\bar{t}$ signal and its backgrounds. The full list is presented below in Table E.1.

DataSet	Common Name	Cross Section (pb)
$t\bar{t}$	tt0s75	6.7
W→eν+$b\bar{b}$+0p	bt0s0w	2.98
W→eν+$b\bar{b}$+1p	bt0s1w	0.888
W→eν+$b\bar{b}$+≥2p	bt0s2w	0.287
W→ $\mu\nu$+$b\bar{b}$+0p	bt0s5w	2.98
W→ $\mu\nu$+$b\bar{b}$+1p	bt0s6w	0.888
W→ $\mu\nu$+$b\bar{b}$+≥2p	bt0s7w	0.287
W→eν+$c\bar{c}$+0p	ct0s0w	5.00
W→eν+$c\bar{c}$+1p	ct0s1w	1.79
W→eν+$c\bar{c}$+≥2p	ct0s2w	0.628
W→ $\mu\nu$+$c\bar{c}$+0p	ct0s5w	5.00
W→ $\mu\nu$+$c\bar{c}$+1p	ct0s6w	1.79
W→ $\mu\nu$+$c\bar{c}$+≥2p	ct0s7w	0.628
W→eν+c+0p	st0sw0	17.1
W→eν+c+1p	st0sw1	3.39
W→eν+c+2p	st0sw2	0.507
W→eν+c+≥3p	st0sw3	0.083
W→ $\mu\nu$+c+0p	bt0s0w	17.1
W→ $\mu\nu$+c+1p	bt0s1w	3.39
W→ $\mu\nu$+c+2p	bt0s2w	0.507
W→ $\mu\nu$+c+≥3p	bt0s2w	0.083
Single Top (s-channel)	st0s00	0.88
Single Top (t-channel)	st0s01	1.98
WW	ihhs1a	12.4
WZ	jhhs1a	3.7
ZZ	khhs1a	1.4
Z→ $\tau\tau$ +0p	zt0st3	158
Z→ $\tau\tau$ +1p	zt0st4	21.5
Z→ $\tau\tau$ +≥2p	zt0st2	4.14
Z→ ee+$b\bar{b}$ +0p	zt0sb0	0.511
Z→ ee+$b\bar{b}$ +1p	zt0sb1	0.134
Z→ ee+$b\bar{b}$ +≥2p	zt0sb2	0.0385
Z→ $\mu\mu$+$b\bar{b}$ +0p	zt0sb5	0.511
Z→ $\mu\mu$+$b\bar{b}$ +1p	zt0sb6	0.134
Z→ $\mu\mu$+$b\bar{b}$ +≥2p	zt0sb7	0.0385

Table E.1: Monte Carlo samples used for $t\bar{t}$ sample.

References

[1] J. J. Aubert et al. Experimental Observation of a Heavy Particle J. *Phys. Rev. Lett.*, 33(23):1404–1406, Dec 1974.

[2] J. E. Augustin et al. Discovery of a Narrow Resonance in e^+e^- Annihilation. *Phys. Rev. Lett.*, 33(23):1406–1408, Dec 1974.

[3] S. W. Herb et al. Observation of a Dimuon Resonance at 9.5 GeV in 400-GeV Proton-Nucleus Collisions. *Phys. Rev. Lett.*, 39(5):252–255, Aug 1977.

[4] F. Abe et al. Observation of Top Quark Production in $\mathrm{p\bar{p}}$ Collisions with the Collider Detector at Fermilab. *Phys. Rev. Lett.*, 74(14):2626–2631, Apr 1995.

[5] G. Karagiorgi et al. Leptonic CP Violation Studies at MiniBooNE in the (3+2) Sterile Neutrino Oscillation Hypothesis. *Phys. Rev. D*, 75(1):013011, Jan 2007.

[6] S.L. Glashow, Nucl. Phys. **22** 588, (1961); S. Weinberg, Phys. Rev. Lett. **19** 1264, (1967); A. Salam, Proc. 8th Nobel Symposium, Stockholm, (1979).

[7] Michael E. Peskin and Daniel V. Schroeder. *An Introduction to Quantum Field Theory*. Westview Press, 1995.

[8] Benjamin W. Lee, C. Quigg, and H. B. Thacker. Weak interactions at very high energies: The role of the higgs-boson mass. *Phys. Rev. D*, 16(5):1519–1531, Sep 1977.

[9] T. Aaltonen et al. Top Quark Mass Measurement in the $lepton + jets$ Channel Using a Matrix Element Method and in situ Jet Energy Calibration. *Phys. Rev. Lett.*, 105(25):252001, Dec 2010.

[10] U. Baur et al. Physics at Future Hadron Colliders. *eConf*, C010630:E4001, 2001.

[11] U. Baur, A. Juste, L. H. Orr, and D. Rainwater. Probing Electroweak Top Quark Couplings at Hadron Colliders. *Phys. Rev.*, D71:054013, 2005.

[12] T. Aaltonen *et al.* Searching the $\ell\gamma\not\!\!E_{\mathrm{T}}$ + b-quark for Radiative Top Quark Decay and Non-Standard-Model Processes. *Phys. Rev. D. 80, 011102 (2009)*, 2009.

[13] G.D. Kribs S.P. Martin S. Ambrosanio, G.L. Kane and S. Mrenna. *Phys. Rev. D*, **55**.

[14] CDF Collaboration. Search for New Physics in Lepton + Photon + X Events with 305-pb^{-1} of $\mathrm{p\bar{p}}$ Collisions at $\sqrt{s} = 1.96$ TeV. 2006.

[15] Christopher S. Hill. Operational Experience and Performance of the CDFII Silicon Detector. *Nucl. Instrum. Meth.*, A530:1–6, 2004.

[16] A. Sill. CDF Run II Silicon Tracking Projects. *Nucl. Instrum. Meth.*, A447:1–8, 2000.

[17] Anthony A. Affolder et al. Intermediate Silicon Layers Detector for the CDF Experiment. *Nucl. Instrum. Meth.*, A453:84–88, 2000.

[18] T. Affolder et al. *Nuc. Instrum. Meth.*, A526:249, 2004.

[19] S. Kuhlman et al. *Nucl.Instrum.Meth.*, A518:39–41, 2004.

[20] S. Bertolucci et al. The CDF Central and Endwall Hadron Calorimeter. *Nucl. Instrum. and Meth. A*, 267(2-3):301 – 314, 1988.

[21] P. Melese G. Apillinari, K. Goulianos and M. Lindgren. *Nucl.Instrum.Meth.*, A412:515–526, 1998.

[22] I. Zaljubovskyh et al. Design and Construction of New Central and Forward Muon Counters for CDF-II. *Nucl.Instrum.Meth.*, A538:358–371, 2005.

[23] A. Ruiz et al. A Time-of-Flight Detector in CDF-II. *Nuc. Instrum. Meth.*, A518:605–608, 2004.

[24] D. Acosta et al. *Nucl. Instrum. Meth.*, A461:540–544, 2001.

[25] R. Downing et al. *Nucl.Instrum.Meth*, A570:36–50, 2007.

[26] A. Abulencia *et al.* Search for New Physics in Lepton+Photon+X Events with 929 pb^{-1} of $\mathrm{p\bar{p}}$ Collisions at $\sqrt{s} = 1.96$ TeV . *Phys. Rev. D*, 75:112001, 2007.

[27] P. Onyisi and the UC CDF Physics Group. The ucntuple is described on the web page:. http://hep.uchicago.edu/cdf/flatntuple, 2004.

[28] Victoria Martin. High pt Muons, Recommended Cuts and Efficiencies for Release 5.3.1. CDF Note 7031, CDF, 2005.

[29] Victoria Martin. High-Pt Muon ID Cuts and Efficiencies for use with 5.3.1 Data and 5.3.3 MC. CDF Note 7367, CDF, 2005.

[30] Larry Nodulman. Curvature corrections for 5.3.1. CDF Note 6971, CDF, 2004.

[31] Anyes Taffard. Run II Cosmic Ray Tagger. CDF Note 6100, CDF, 2003.

[32] Anyes Taffard. Run II Cosmic Ray Tagger Perfomances. CDF Note 6255, CDF, 2003.

[33] Lauren Beitler. Talk given to the W+Jets Meeting, Oct. 10, 2003.

[34] C. Hill, J. Incandela, and C. Mills. Electron identification in offline release 5.3. CDF Note 7309, CDF, 2005.

[35] Henry Frisch Andrei Loginov. Search for Lepton + Photon + X. CDF Note 7550, CDF, 2005.

[36] Andrei Loginov, Irina Shreyber, Henry Frisch. A Signature-Based Search for Anomalous Lepton+Photon+MET+b-jet Production and SM ttbar+photon Production in 2 fb^{-1} with the CDF-II Detector. CDF Note 9272, CDF, 2008.

[37] Tim Nelson, Rick Snider, David Stuart. Forward Electron Tracking with the PhoenixMods Package. CDF Note 6278, CDF, 2003.

[38] See http://www-cdf.fnal.gov/internal/physics/joint_physics/instructions/electron_cuts.html.

[39] F. Abe et al. Measurement of the Ratio σB(p$\bar{\text{p}}$ →W→eν)/σB(p$\bar{\text{p}}$ → Z^0 →ee) in p$\bar{\text{p}}$ Collisions at $\sqrt{s}$ =1800 GeV. *Phys. Rev. D*, 52(5):2624–2655, Sep 1995.

[40] P.J. Wilson. Calorimeter Isolation and Lateral Shower Leakage for Photons and Electrons. CDF Note 4170, CDF, 1997.

[41] A. Bhatti et al. Determination of the Jet Energy Scale at the Collider Detector at Fermilab. *Nucl. Inst. and Meth. A*, 566(2):375 – 412, 2006.

[42] D. Acosta et al. Measurement of the $t\bar{t}$ Production Cross Section in p$\bar{\text{p}}$ Collisions at $\sqrt{s} = 1.96\,TeV$ Using Lepton + Jets Events with Secondary Vertex b - tagging. *Phys. Rev. D*, 71(5):052003, Mar 2005.

[43] T. AAltonen et al. Measurement of the Ratio $\sigma_{t\bar{t}}$ / $\sigma_{Z/\gamma^* \to ll}$ and Precise Extraction of the $t\bar{t}$ Cross Section. *Phys. Rev. Lett*, **105**(1):012001, Jun 2010.

[44] T. Stelzer and W. F. Long. Madgraph. *Comput.Phys.Commun.*, 357(81), 1994.

[45] S. Tsuno, A.S. Thompson. A CDF-interface module for Les Houches Accords. CDF Note 6333, CDF, 2003.

[46] S. Mrenna. *Comput. Phys. Commun.*, 101, 1997.

[47] UC CDF Physics Group. The ucntuple sets are listed on the web page:. http://hep.uchicago.edu/cdf/datasets/, 2004.

[48] A. Ivanov, T. Schwarz, C. Plager, E. S. Kennedy, G. Giurgiu, P. Maksimovic, M. Mathis, S. Rappoccio, and M. Mangano. Simultaneous Top and W + Heavy Flavor Cross Section Measurement. CDF Note 9866, CDF, 2010.

[49] T. Schwarz A. Ivanov and R.Erbacher. Calibration of Heavy-Flavor Content in W + Jets Data. CDF Note 9403, CDF, 2008.

[50] R.Culbertson, A.Pronko, Shin-Shan Eiko Yu. The Probability of an Electron Faking an Isolated Prompt Photon in CEM . CDF Note 8220, CDF, 2006.

[51] I.Shreyber, A.Loginov, and H.Frisch. A Search for Anomalous Production of the Signature $\ell + \gamma + b - quark + \not{E}_{\text{T}}$ and a Search for Standard Model $t\bar{t} + \gamma$ Production in 929 pb^{-1}. CDF Note 9335, CDF, 2008.

[52] C.Lester, J.Deng, A.Goshaw, B.Heinemann, A.Nagano, and T.Phillips. Measurement of the Rate of Jets Faking Central Isolated Photons Using 1fb^{-1} of Data. CDF Note 9033, CDF, 2007.

[53] See http://www-cdf.fnal.gov/internal/people/links/ThomasJunk/mistag/mistag4100invpb.html.

[54] S.Grinstein, J.Guimaraes da Costa, D. Sherman. SecVtx Mistag Asymmetry for Winter 2007. CDF Note 8626, CDF, 2007.

[55] Franklin et al. Method 2 Backgrounds for 1.12/fb Lepton+Jets Analyses. Cdf note.

[56] B.Cooper, A. Messina. Estimation of the Background to $W^{\pm} \to e^{\pm}\nu + N$ Jet Events. CDF Note 7760, CDF, 2005.

[57] A. Bhatti et al. Determination of the Jet Energy Scale at the Collider Detector at Fermilab. *Nucl. Instrum. Meth.*, A566:375–412, 2006.

[58] R. Culbertson, C .Deluca, S. Grinstein, M. Martinez, and S.S. Yu. Measurement of the Inclusive and Isolated Prompt Photon Cross Section at CDF. Cdf note.

[59] Duan Peng-Fei et al. QCD Corrections to Associated Production of $t\bar{t}\gamma$ at Hadron Colliders. *arXiv*, hep-ph/0907.1324, 2009.

[60] N. Kidonakis. Top Quark Pair and Single Top Production at Tevatron and LHC energies. *arXiv*, hep-ph/1008.2460, 2010.

[61] U. Baur, A. Juste, L. H. Orr, and D. Rainwater. Probing electroweak top quark couplings at hadron colliders. *Phys. Rev. D*, 71(5):054013, Mar 2005.